Silicon detectors

Marco Bomben

APC & UPC

Outline

- Main applications, motivations and history
- Semiconductors physics
- Silicon radiation detectors
- Timing with silicon detectors
- Perspectives

Yes, but who are you?

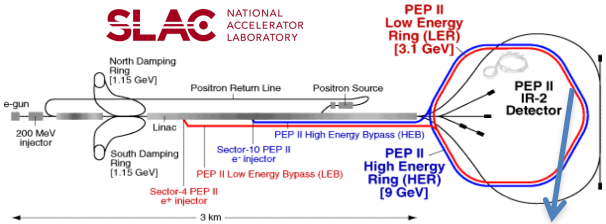

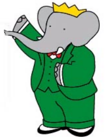

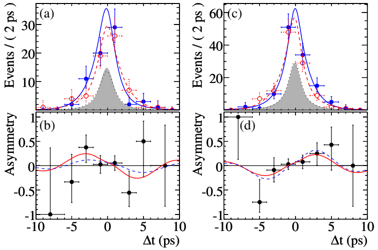

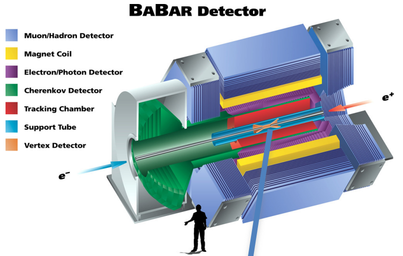

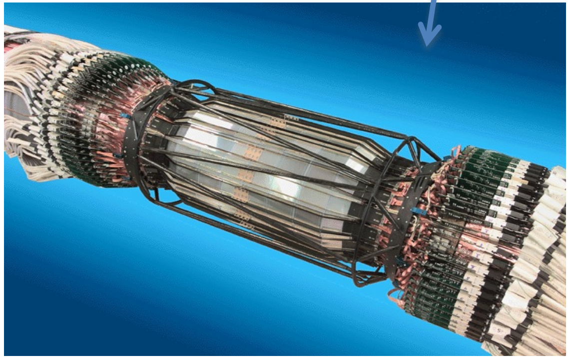

Yes, but who are you?

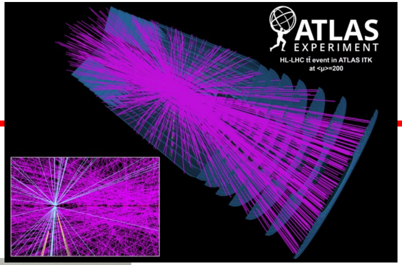

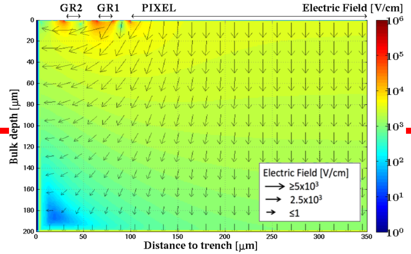

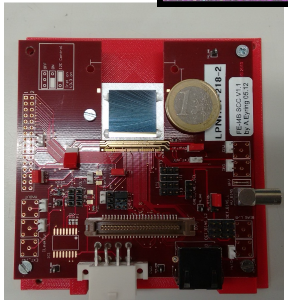

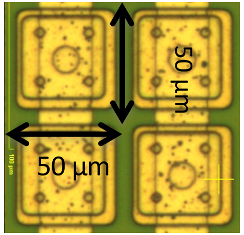

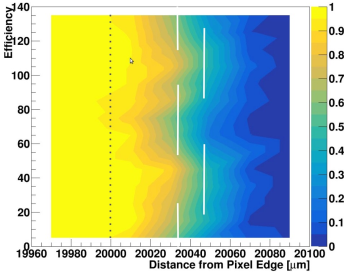

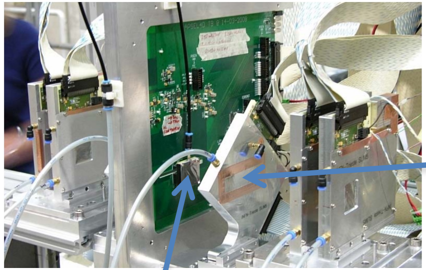

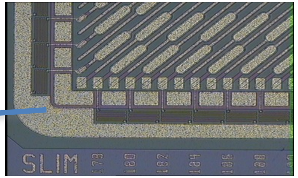

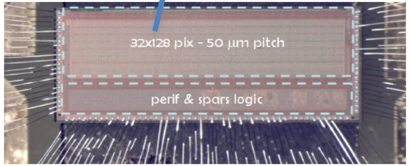

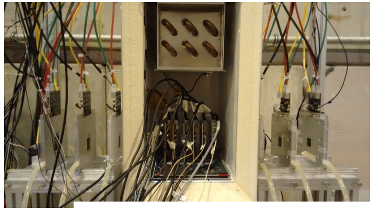

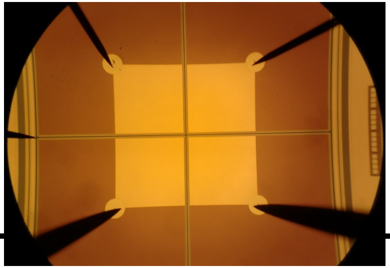

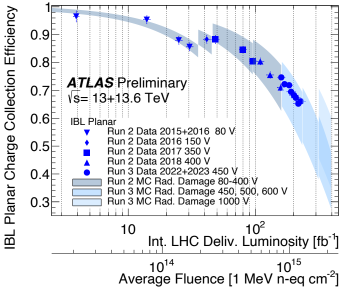

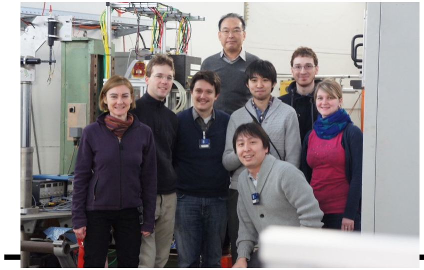

Acknowlegments

Thanks to: I. Abt, V. Bonvicini, G. Calderini, S. Holland, M. Krammer, M. Moll, P. Wells, W. Riegler and more

- You can find great lectures here: http://www.hephy.at/fileadmin/user_upload/Lehre/Unterlagen/Praktikum/Halbleiterdetektoren.pdf
- And here: http://wwwusers.ts.infn.it/~bonvicin/Dottorandi08.pdf

References

- H. Spieler, Semiconductor Detector Systems, Oxford Science Publications, 2005

See also: http://www-physics.lbl.gov/~spieler/

- G. Lutz, Semiconductor Radiation Detectors: Device Physics , Springer (July 11, 2007)
- S.Sze, Physics of Semiconductor Devices, J.Wiley, 1981

- H. F.-W. Sadrozinski, Applications of Silicon Detectors, IEEE Trans. Nucl. Sci. Vol. 48 n.4 pp.933 –940, 2001.
- F. Hartmann, Silicon tracking detectors in high-energy physics, Nucl. Instr. and Meth. A666 (2012) 25-46
- D. Renker and E. Lorenz, Advances in solid state photon detectors, 2009 JINST 4 P04004

- PDG

Outline

- Main applications, motivations and history
- Semiconductors physics
- Silicon radiation detectors
- Timing with silicon detectors
- Perspectives

Before solid state detectors: gas detectors

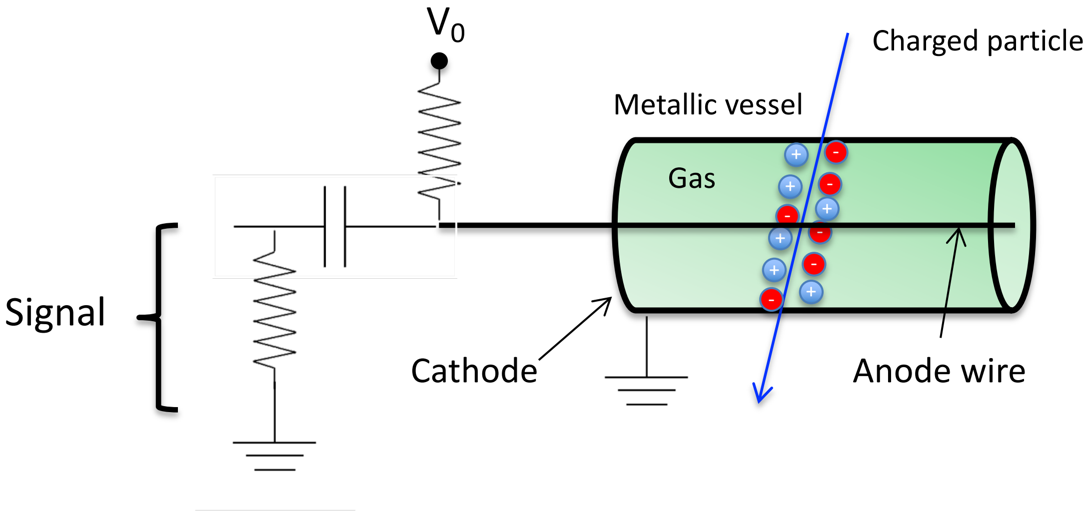

A voltage difference is applied between a central wire (”anode”) and the metallic vessel containing the gas (“cathode”, at ground).

Signal is readout from the anode

This basic model is a good representation for the three original gas detectors, i.e. the ionisation chamber, the proportional counter and the Geiger-Müller counter

The basics of a silicon detector

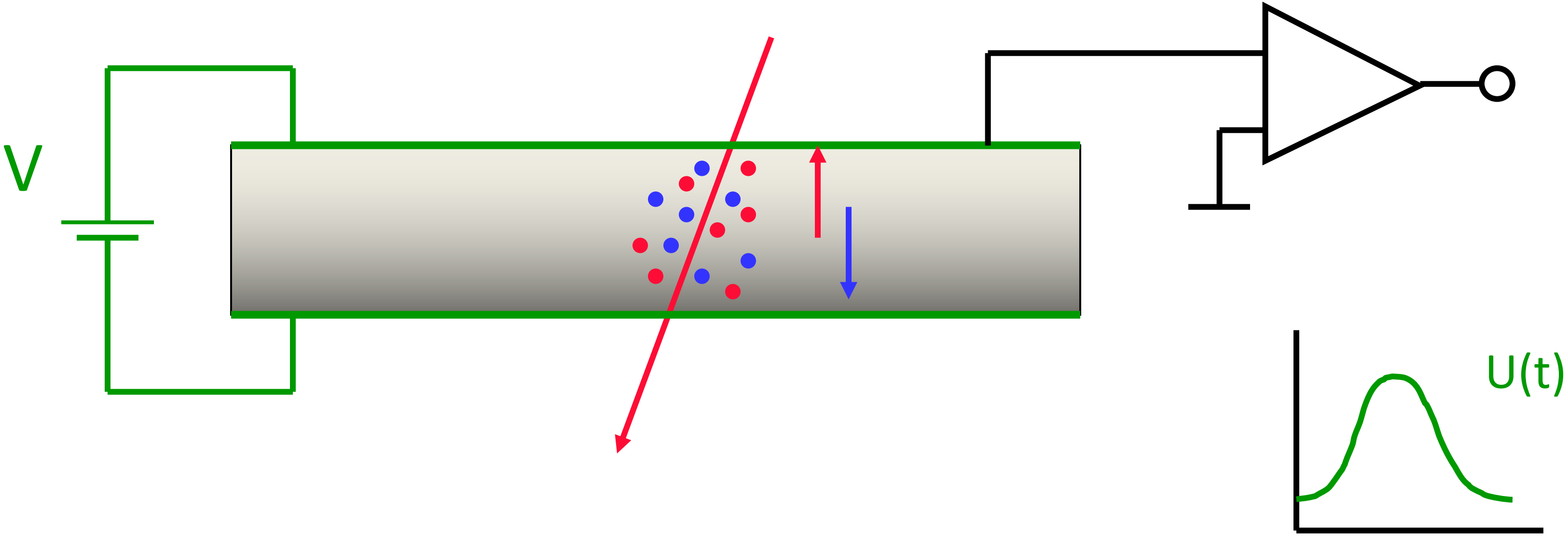

A solid state ionization chamber

Signal given by the drift of charges (electrons and holes) under the effect of the electric field

The signal is then amplified and shaped

Main applications

- γ spectroscopy with high energy resolution (10 keV – few MeV range)

- Vertex and tracking detectors with high spatial resolution

- Energy measurements of charged particles (few MeV) and Particle ID via dE/dx (multiple layers)

Why?

- ✓ Only few eV per electron-hole pair
- ✓ Use microchip technology; structures with sub μm precision can be produced at low cost; read-out electronics can be directly bonded to detector
- ✓ high density compared to gases - need only thin layers
- ✓ Solid material, no need for vessel/cryostat

Principle of operation

In semiconductors at T > 0 K few electrons populate the conduction band, and few holes are present in the valence band

Radiation can provide energy to an electron in valence band to be promoted to conduction band. At the same time a hole is created in valence band

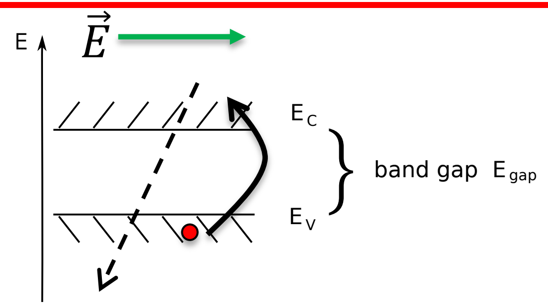

Principle of operation

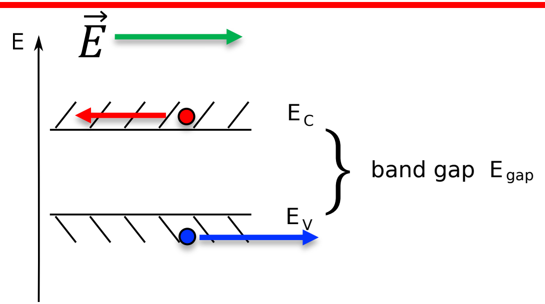

In semiconductors at T > 0 K few electrons populate the conduction band, and few holes are present in the valence band

Radiation can provide energy to an electron in valence band to be promoted to conduction band. At the same time a hole is created in valence band

The detector is polarised, so the charge carriers move under the effect of the electric field

A current appears in my detector circuit

Outline

- Main applications, motivations and history
- Semiconductors physics
- Silicon radiation detectors
- Timing with silicon detectors
- Perspectives

What is a semiconductor?

- In an isolated atom the electrons have only discrete energy levels. In solid state material the atomic levels merge to energy bands.
- In metals the conduction and the valence band overlap,
- whereas in isolators and semiconductors these levels are separated by an energy gap (band gap).
- In semiconductors this gap is large (compared to kT ~ 1/40 eV)

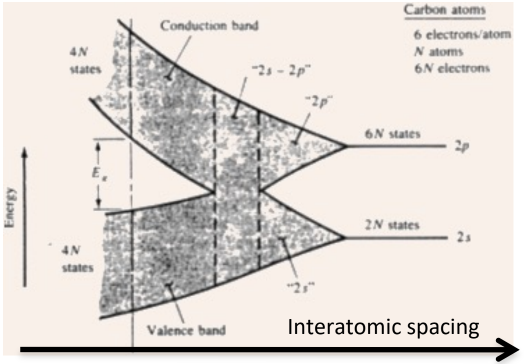

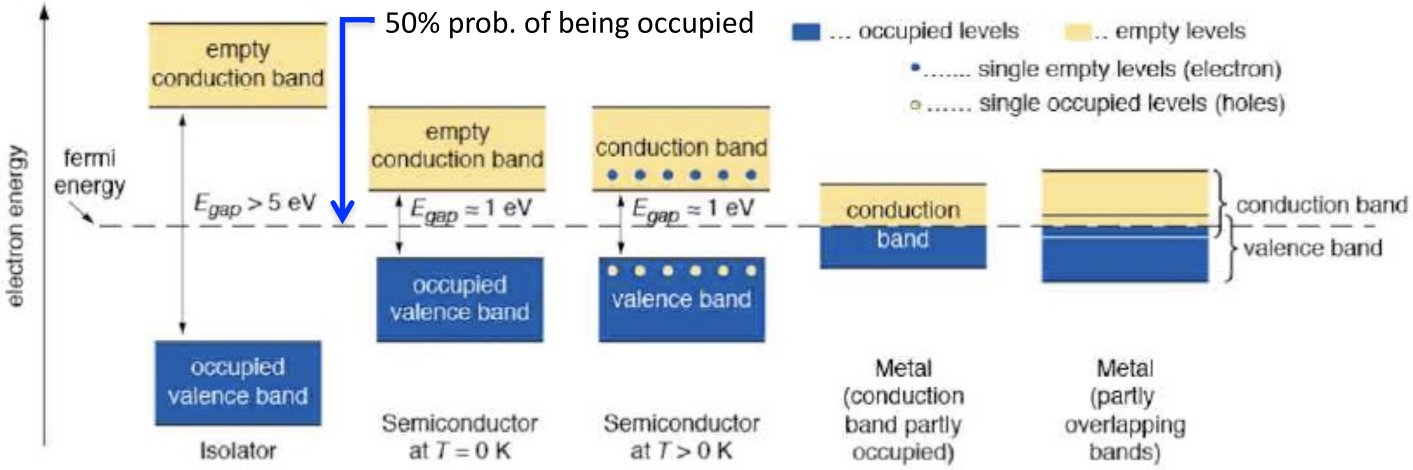

A few semiconductors used in research

Germanium: Used in nuclear physics, due to small band gap (0.66 eV) needs cooling (usually done with liquid nitrogen at 77 K)

Silicon: Standard material for vertex and tracking detectors in high energy physics, can be operated at room temperature, synergies with micro electronics industry.

Diamond (CVD or single crystal): Large band gap (6 eV), requires no depletion zone, very radiation hard, drawback is a low signal and high cost

Compound semiconductors: GaAs (faster than Si, no good insulating layer), CdTe (large Z, hence efficient for photodection);

Indirect vs direct semiconductors

[Sze]

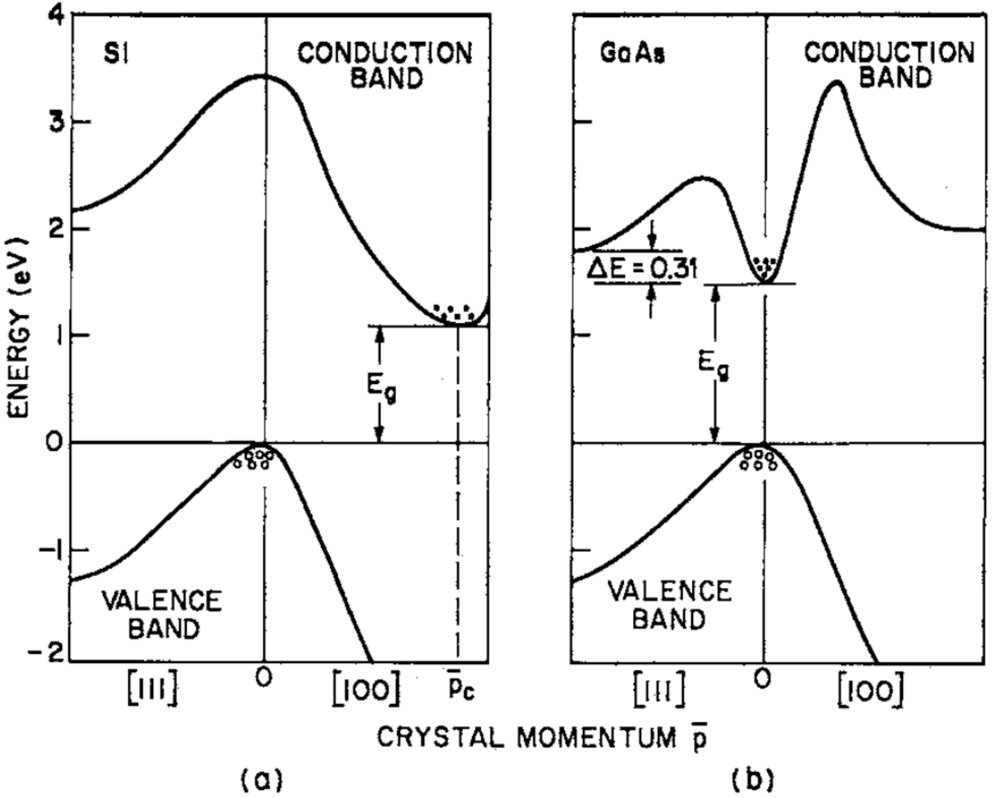

In Si (and Ge) a photon is not enough to create electron-hole pairs since it carries ~ 0 crystal momentum

Phonons are necessary

Important aspect for photon detection (and even more for photon emission)

Some properties of Semiconductors

Table 8.2 Properties of silicon, germanium, gallium arsenide, cadmium telluride and diamond. D = diamond lattice, ZB = zinc blende lattice, temperature dependent quantities given at 300 K.

Property	Si	Ge	GaAs	CdTe	Diamond
atomic number (Z)	14	32	31/33	48/52	6
atom mass (u)	28.09	72.60	72.32	120.0	12.01
density ρ (g/cm^3)	2.328	5.327	5.32	5.85	3.51
crystal structure	D	D	ZB	ZB	D
lattice constant (Å)	5.431	5.646	5.653	6.48	3.57
semiconductor type	indirect	indirect	direct	direct	indirect
band gap E_G (eV)	1.12	0.66	1.424	1.44	5.5
intr. carrier density (cm^{-3})	1.01×10^{10}	2.4×10^{13}	2.1×10^{6}	10^7	≈ 0
resistivity (Ω cm)	2.3×10^{5}	47	10^8	10^9	$\approx 10^{16}$
dielectric constant (ϵ)	11.9	16	13.1	10.2	5.7
radiation length X_0 (cm)	9.36	2.30	2.29	1.52	12.15
average energy for (e/h) creation (eV)	3.65	2.96	4.2	4.43	13.1
thermal conductivity ($\frac{W}{cmK}$)	1.48	0.6	0.55	0.06	>18
mobility ($\frac{cm^2}{Vs}$)					
electrons μ_n	1450	3900	8500	1050	≈1800
holes μ_h	500	1800	400	90	≈2300
lifetime					
electrons τ_e	>100 µs	∼ms	1–10 ns	0.1–2 µs	≈100 ns
holes τ_h	>100 µs	∼ms	20 ns	0.1–1 µs	≈50 ns

Bond model of semiconductors

Example of column IV elemental semiconductor (2dim projection)

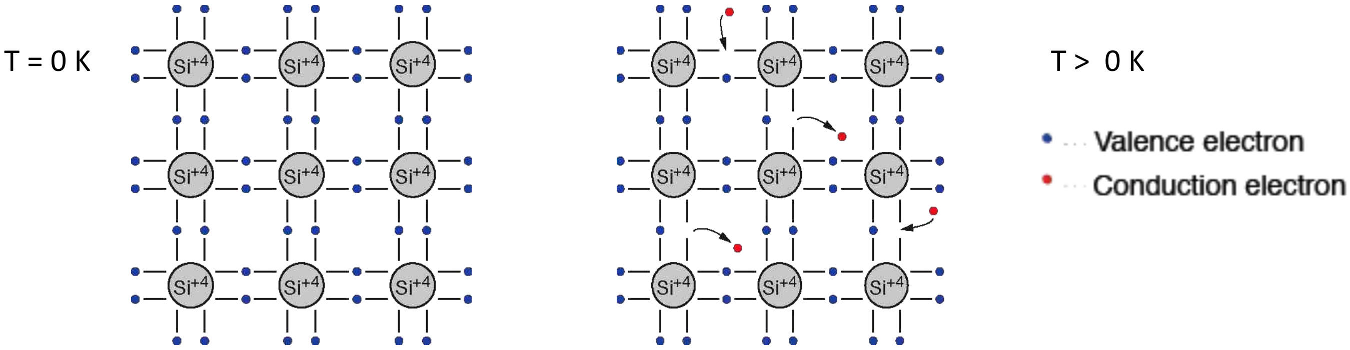

Each atom has 4 closest neighbors, the 4 electrons in the outer shell are shared and form covalent bonds.

At low temperature all electrons are bound

At higher temperature thermal vibrations break some of the bonds ➔ free e- (n) cause conductivity (electron conduction)

The remaining open bonds attract other e- ➔ The "holes" (p) change position (hole conduction)

Intrinsic carrier concentration $n_{i:}$ $n = p = n_i$ ~ 1.0×10^{10} cm^{-3} (T=300K)

Transport of charge carriers

Transport of charge carriers in a semiconductor: diffusion and drift

Diffusion: proportional to the gradient of the carrier density
Drift: proportional to the applied electric field

$$\boxed{\begin{aligned}\vec{J}_n &= \vec{J}_{n,drift} + \vec{J}_{n,diff} = q\left(\mu_n n \vec{E} + D_n \nabla n\right) \\ \vec{J}_p &= \vec{J}_{p,drift} + \vec{J}_{p,diff} = q\left(\mu_p p \vec{E} - D_p \nabla p\right)\end{aligned}}$$

D: diffusion coefficient [cm²/s]
μ: mobility [cm²/(Vs)]

Einstein's equation

$$D_n = \frac{kT}{q}\mu_n$$

$$D_p = \frac{kT}{q}\mu_p$$

$$\boxed{\vec{v}_{drift} = \mu \vec{E}}$$

Valid at low/moderate fields; for large fields (>~ 5x10^3 V/cm) the carriers velocities saturates (Si: v ~ 10^7 cm/s) ➔ **10-30 ns collection time in 100-300 μm**

μ depends on doping and temperature.
For intrinsic silicon: μ_n~ 1350 cm²/(Vs), μ_p ~ 450 cm²/(Vs)

Estimate SNR in an intrinsic silicon detector

Let's make a simple calculation for silicon:

Mean ionization energy $I_0 = 3.62$ eV, mean energy loss per flight path $dE/dx = 3.87$ MeV/cm, intrinsic charge carrier density at $T = 300$ K $n_i = 1.45 \cdot 10^{10}$ cm^{-3}.

Assuming a detector with a thickness of $d = 300\ \mu$m and an area of $A = 1$ cm^2.

$\boxed{\rightarrow \text{Signal of a mip in such a detector:}}$

$$\frac{dE/dx \cdot d}{I_0} = \frac{3.87 \cdot 10^6 \,\mathrm{eV/cm} \cdot 0.03\,\mathrm{cm}}{3.62\,\mathrm{eV}} \boxed{\approx 3.2 \cdot 10^4 \ \mathrm{e^- h^+ - pairs}}$$

$\boxed{\rightarrow \text{Intrinsic charge carrier in the same volume}}$ ($T = 300$ K):

$$n_i\, d\, A = 1.45 \cdot 10^{10}\,\mathrm{cm}^{-3} \cdot 0.03\,\mathrm{cm} \cdot 1\,\mathrm{cm}^2 \boxed{\approx 4.35 \cdot 10^8 \ \mathrm{e^- h^+ - pairs}}$$

→ Number of thermal created e⁻h⁺-pairs are four orders of magnitude larger than signal!!!

Have to remove the charge carrier!

$\boxed{\rightarrow \text{Depletion zone in reverse biased pn junctions}}$

N-doping

Doping with an element 5 atom (e.g. P, As, Sb). The 5th valence electron is weakly bound.

The doping atom is called donor
The released conduction electron leaves a positively charged ion

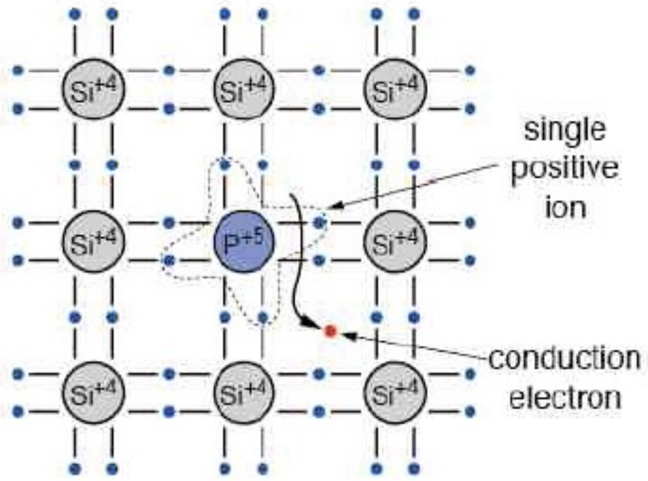

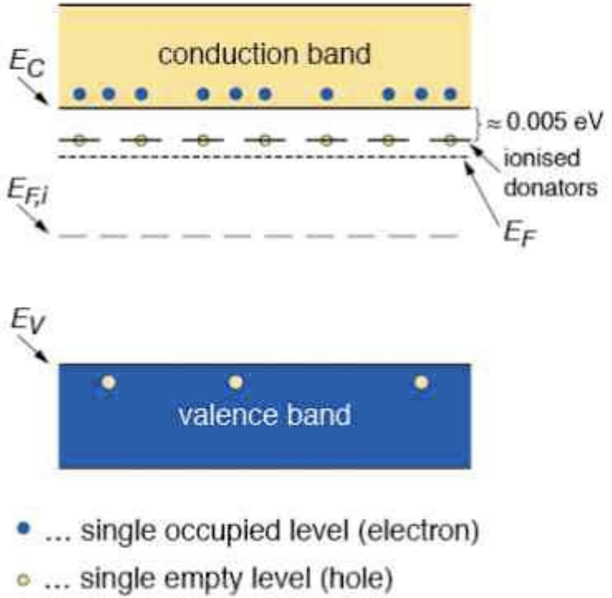

Electrons (holes) are called majority (minority) carriers.

P-doping

Doping with an element 3 atom (e.g. B, Al, Ga, In). One valence bond remains open

The doping atom is called acceptor
The acceptor atom in the lattice is negatively charged

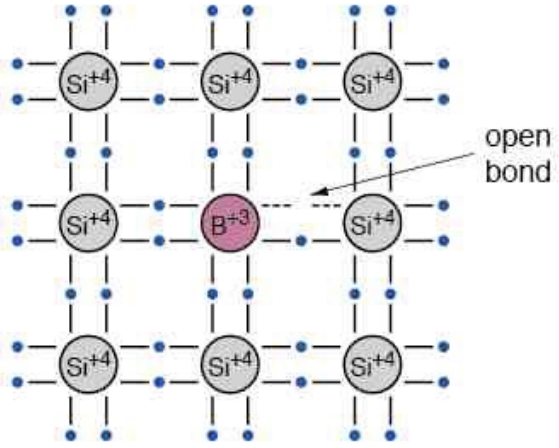

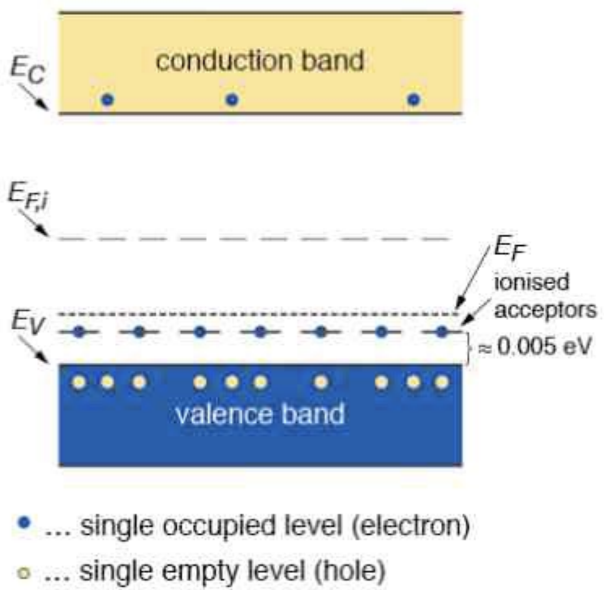

Holes (electrons) are called majority (minority) carriers.

The p-n junction

At n-type and p-type interface: diffusion of surplus carries to the other material until thermal equilibrium is reached.
The remaining ions create a space charge and an electric field stopping further diffusion.
The stable space charge region is free of charge carries: the depletion zone.

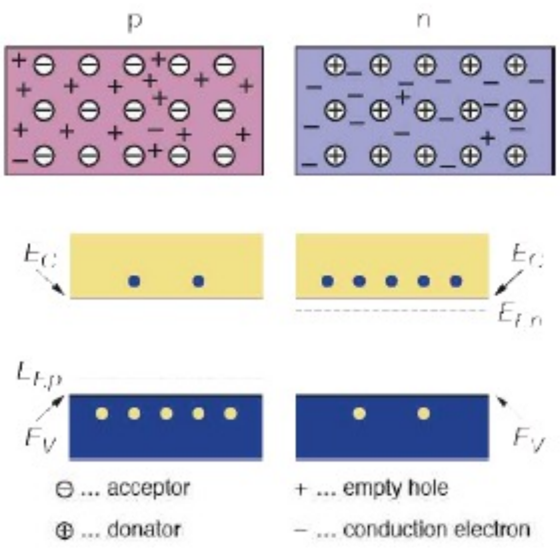

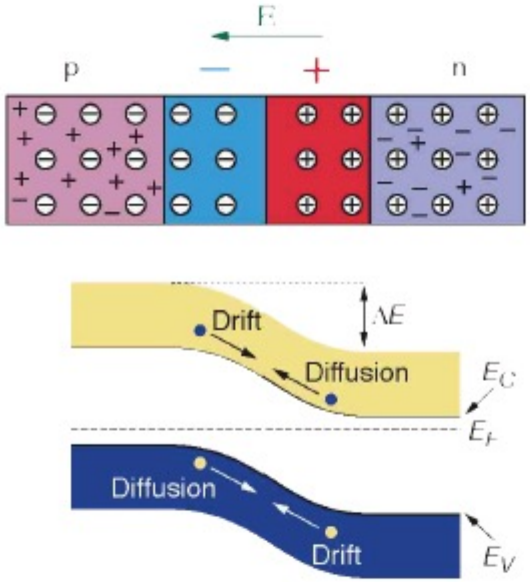

The p-n junction – forward and reverse bias

Applying a forward bias voltage *V*,
e- and holes are refilled to the depletion zone.
The depletion zone becomes narrower

p-n junction in forward bias

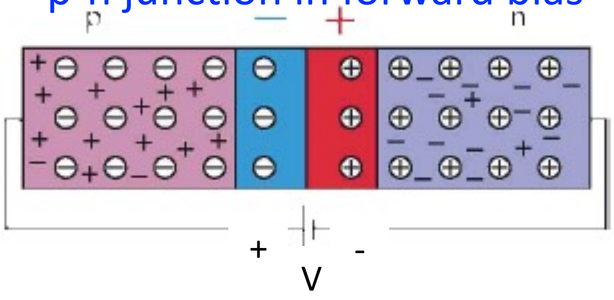

That's not what we want!

Applying a reverse bias voltage *V*,
e- and holes are pulled out of the depletion zone.
The depletion zone becomes larger.

p-n junction in reverse bias

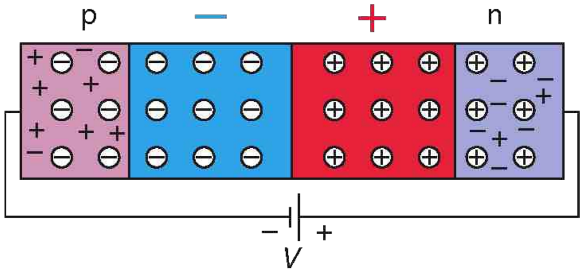

That's the way we operate our semiconductor detectors!

Electrical characteristics of p-n junction

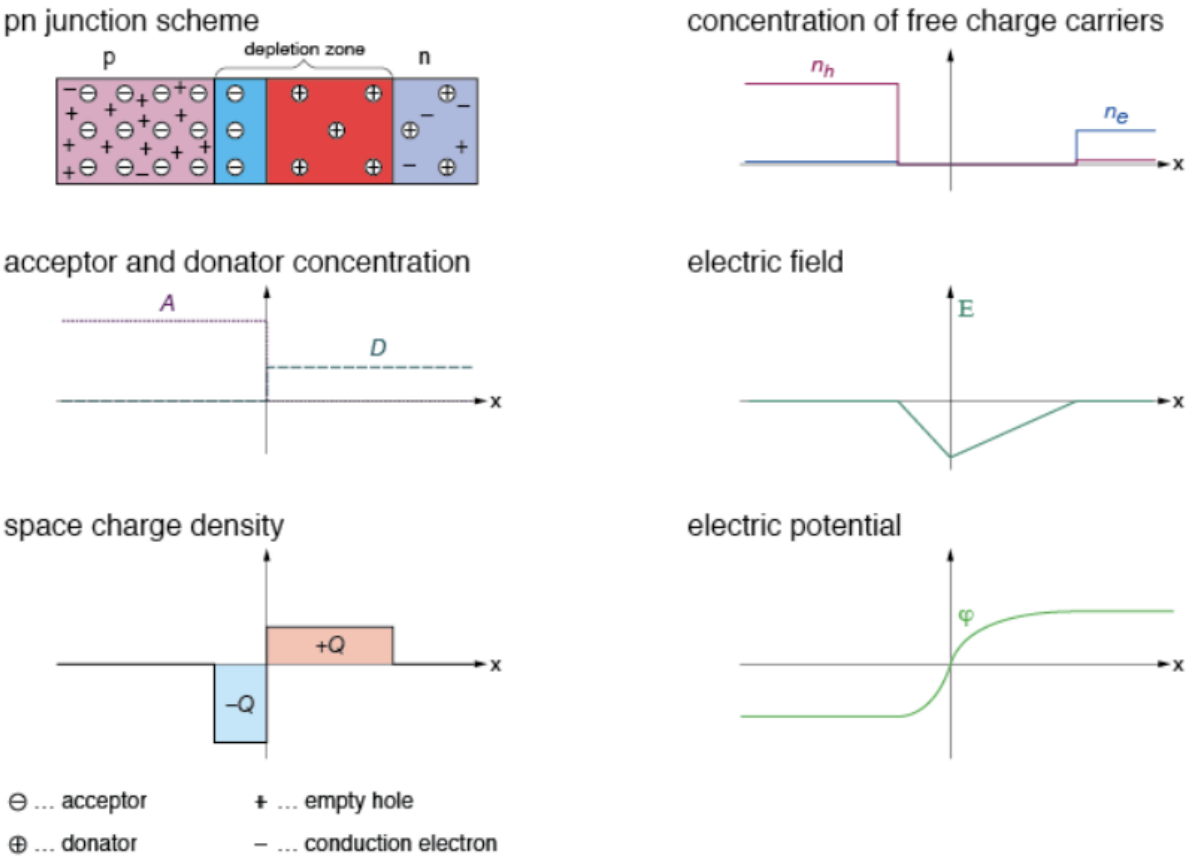

[Eckstein]

P-n junction – width of the depletion zone

Example of a typical p^+-n junction in a silicon detector:

Effective doping concentration $N_a = 10^{15}$ cm^{-3} in p+ region and $N_d = 10^{12}$ cm^{-3} in n bulk.

Without external voltage:

$$W_p = 0.02\ \mu m$$
$$W_n = 23\ \mu m$$

Applying a reverse bias voltage of 100 V:

$$W_p = 0.4\ \mu m$$
$$W_n = 363\ \mu m$$

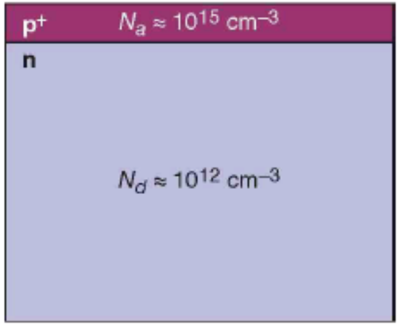

p^+n junction

Width of depletion zone in n bulk:

$$\boxed{W \approx \sqrt{2\varepsilon_0\varepsilon_r\mu\rho|V|}} \quad \text{with} \quad \rho = \frac{1}{e\mu N_{eff}}$$

V ... External voltage
ρ ... specific resistivity
μ ... mobility of majority charge carriers
N_{eff} ... effective doping concentration

CV analysis: observables

C^{-2} vs V

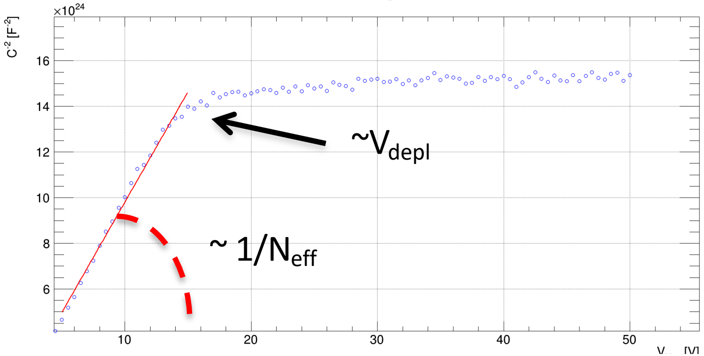

$$C = \frac{A\epsilon_0\epsilon_{sc}}{w}\sqrt{\frac{V_{depl}}{V}} = A\sqrt{\frac{qN_{eff}\epsilon_0\epsilon_{sc}}{2}\frac{1}{V}}$$

$$N_{eff} = 2\frac{\left(\frac{d(C^{-2})}{dV}\right)^{-1}}{q\epsilon_0\epsilon_{sc}A^2}$$

log10(C) vs log10(V)

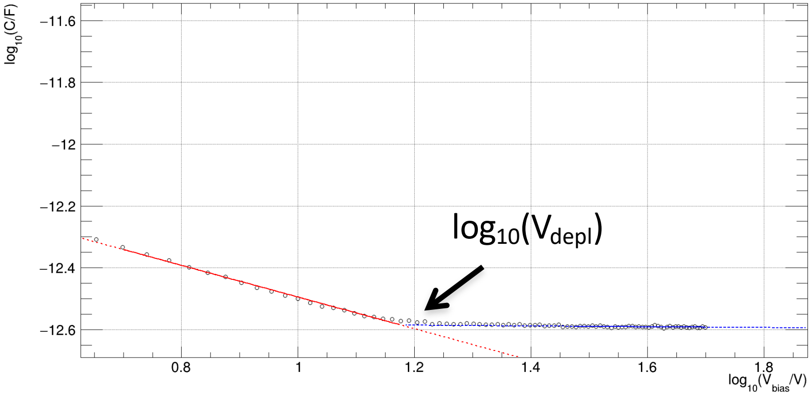

Depletion voltage: howto

- By definition, differential capacitance is the change in charge (Q) in a device in response to a change in voltage (V):

$$C=\Delta Q/\Delta V$$

- One general practical way to implement this is to apply a small AC ($\upsilon \sim 10^2 - 10^6$ Hz) voltage signal (millivolt range) to the device under test, and then measure the resulting current. Integrate the current over time to derive Q and then calculate C from Q and V.
- C-V measurements in a semiconductor device are made using two simultaneous voltage sources: an applied AC voltage signal (dVac) and a DC voltage (Vdc) that is swept in time, as illustrated in the next slide.

Voltage ramp for CV analysis

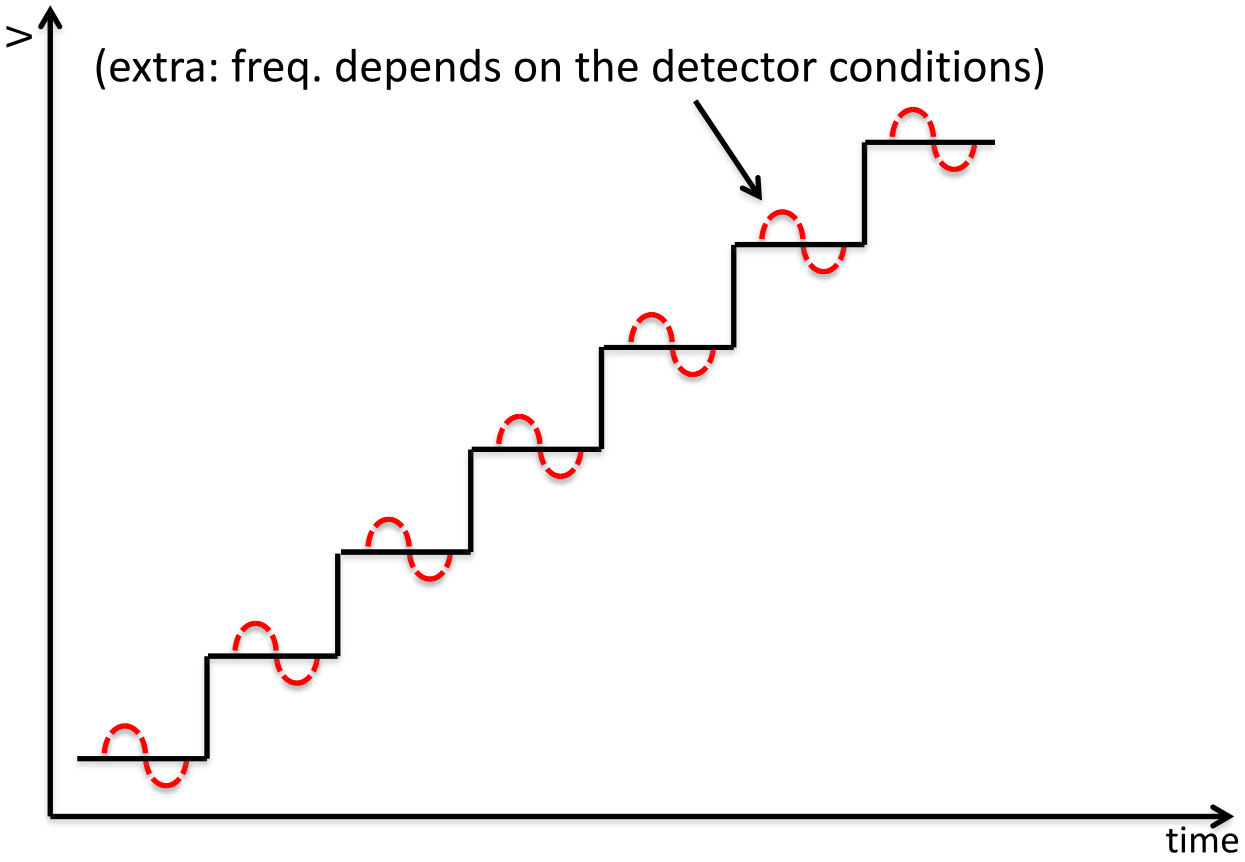

Connections for CV analysis

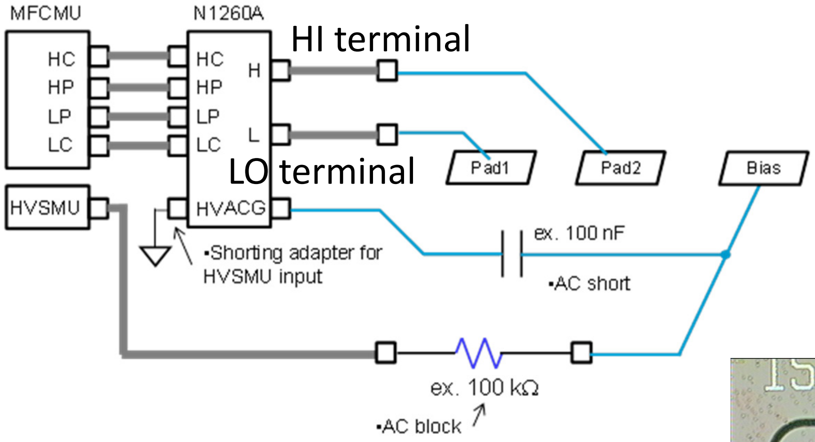

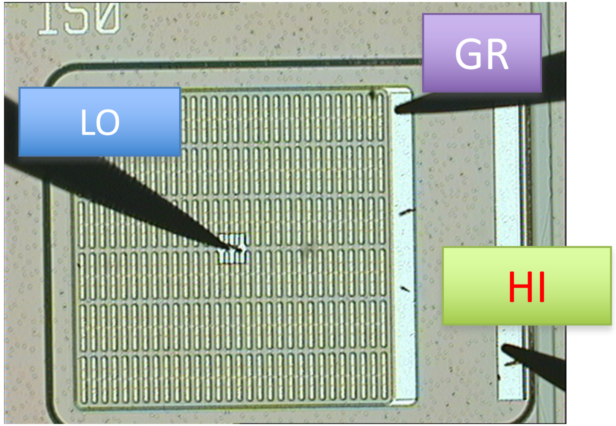

P-n junction – Current voltage characteristics

Typical current-voltage of a p-n junction (diode): exponential current increase in forward bias, small saturation in reverse bias.

Ideal diode equation: $$I = I_0 \cdot \left[\exp\left(\frac{eV}{kT}\right) - 1\right]$$

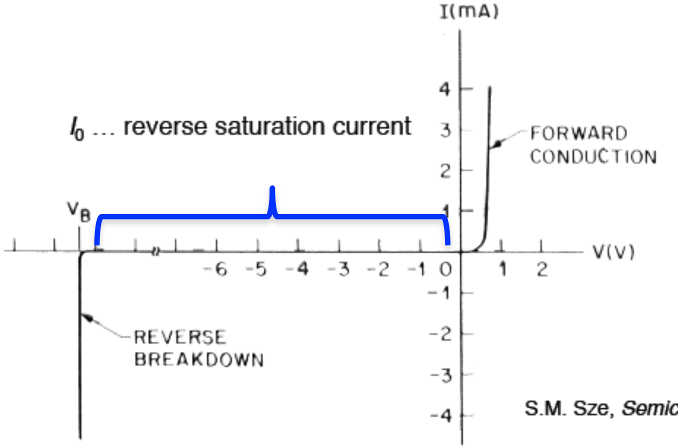

P-n junction – Current voltage characteristics

Typical current-voltage of a p-n junction (diode): exponential current increase in forward bias, small saturation in reverse bias.

Ideal diode equation: $\boxed{I = I_0 \cdot \left[\exp\left(\frac{eV}{kT}\right) - 1\right]}$

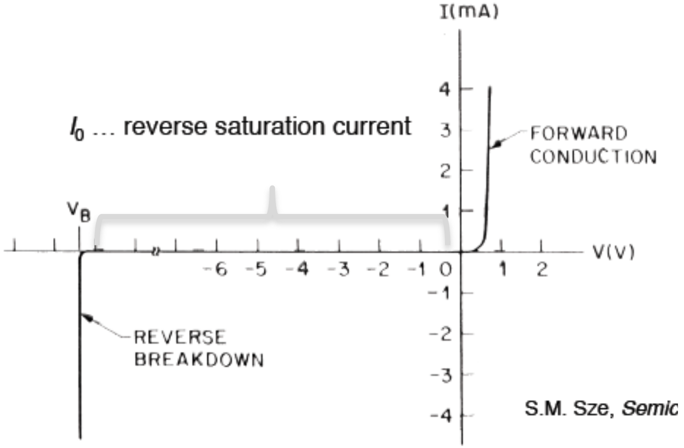

Leakage current origin:
thermally generated carriers

In reverse bias:
extra contribution
from bulk generated current

Generation lifetime

Detector volume

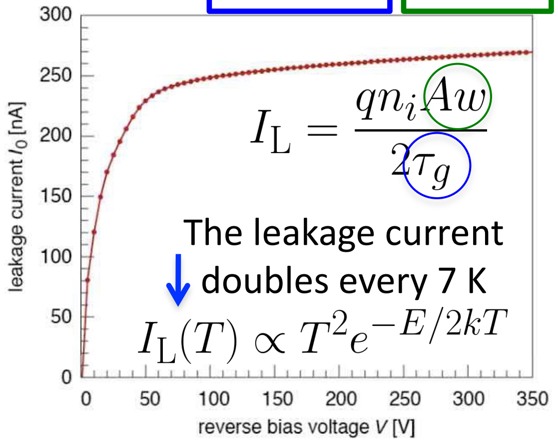

$$I_\mathrm{L} = \frac{q n_i A w}{2\tau_g}$$

The leakage current
↓ doubles every 7 K

$$I_\mathrm{L}(T) \propto T^2 e^{-E/2kT}$$

IV in real life

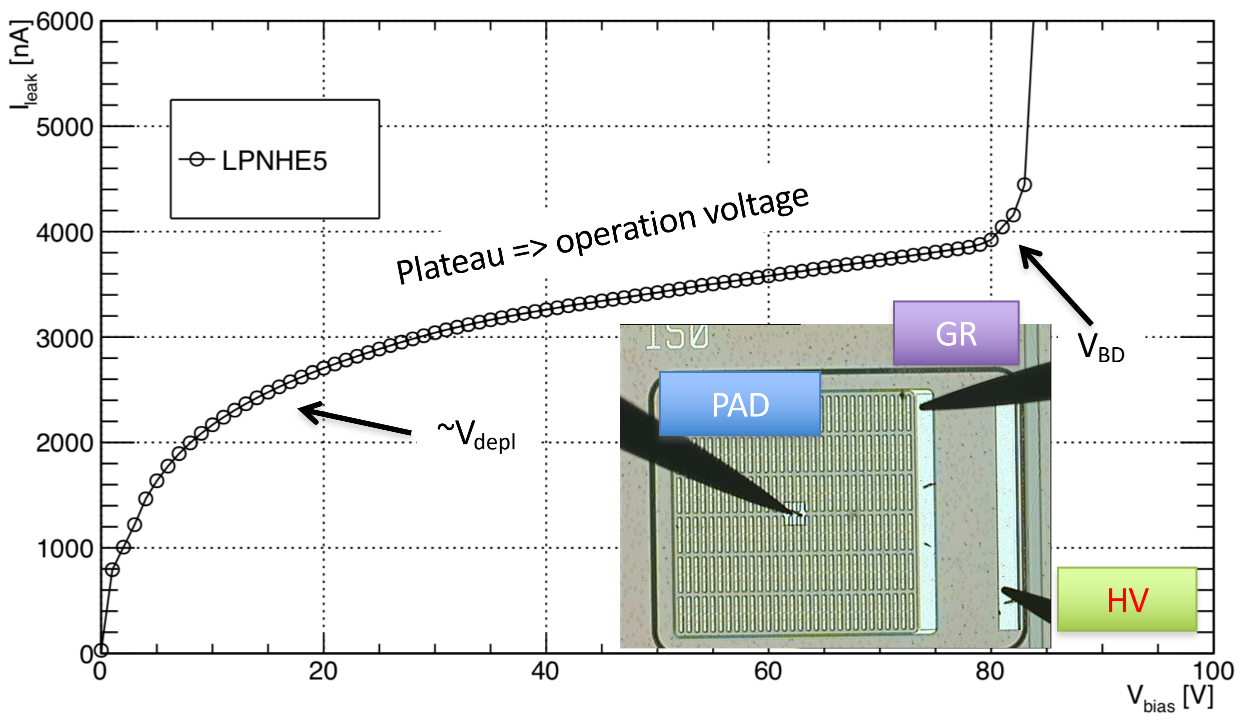

Examples of p-n junction diodes

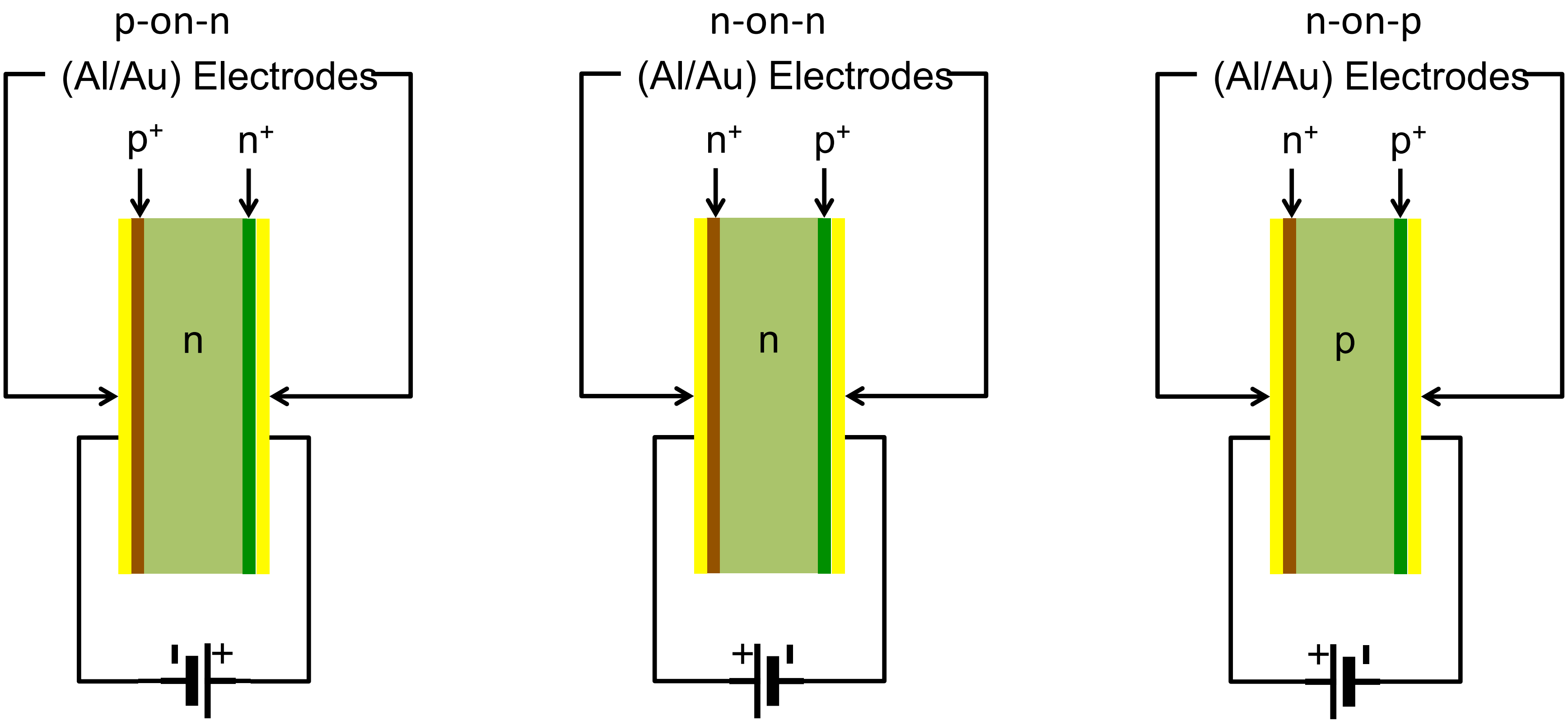

Examples of p-n junction diodes

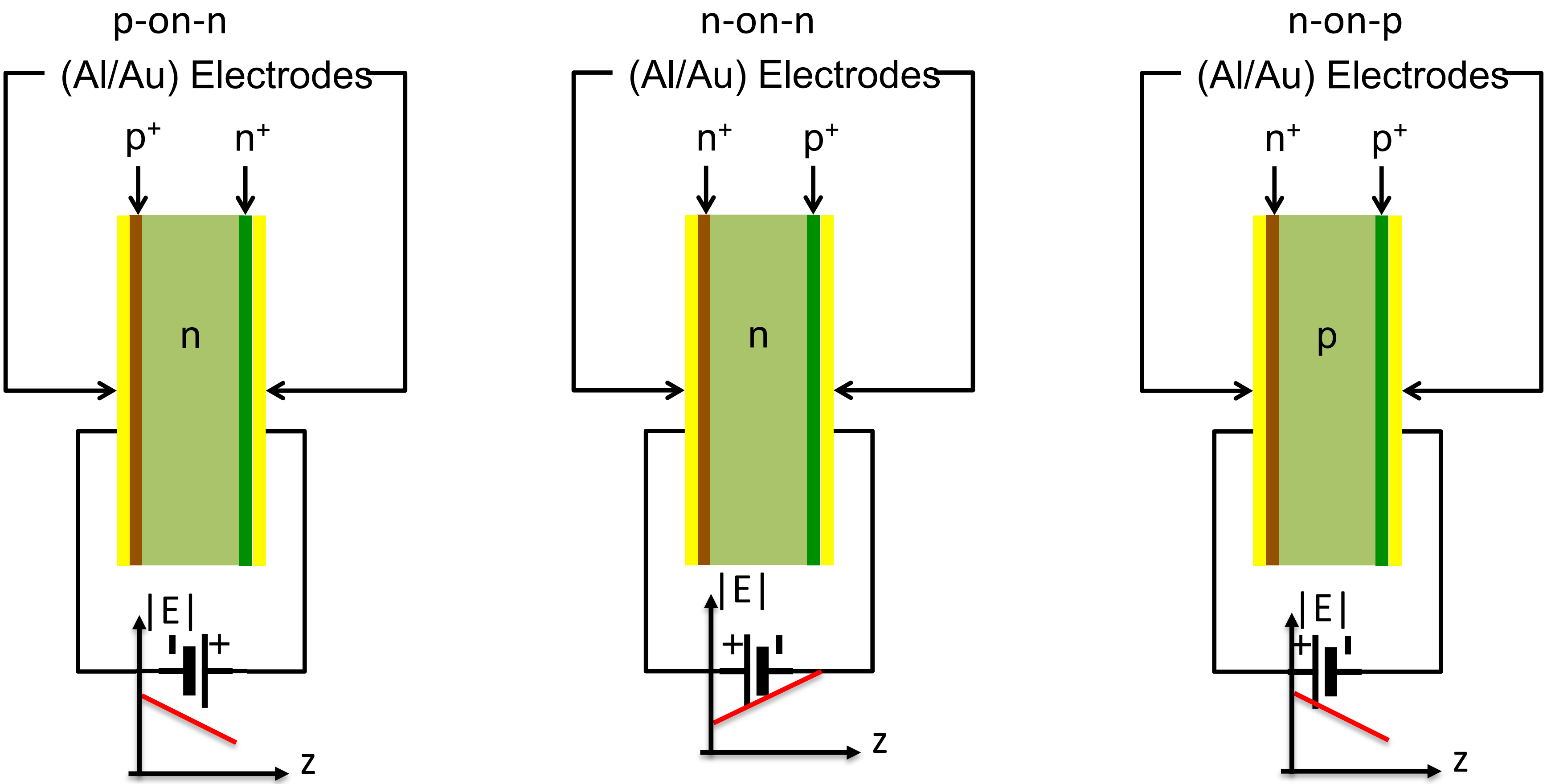

Electric field at depletion and beyond

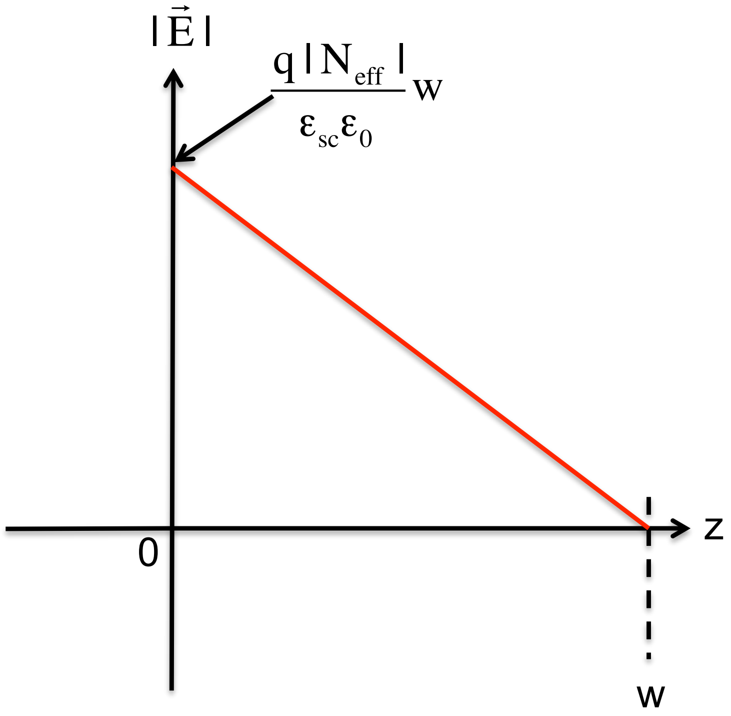

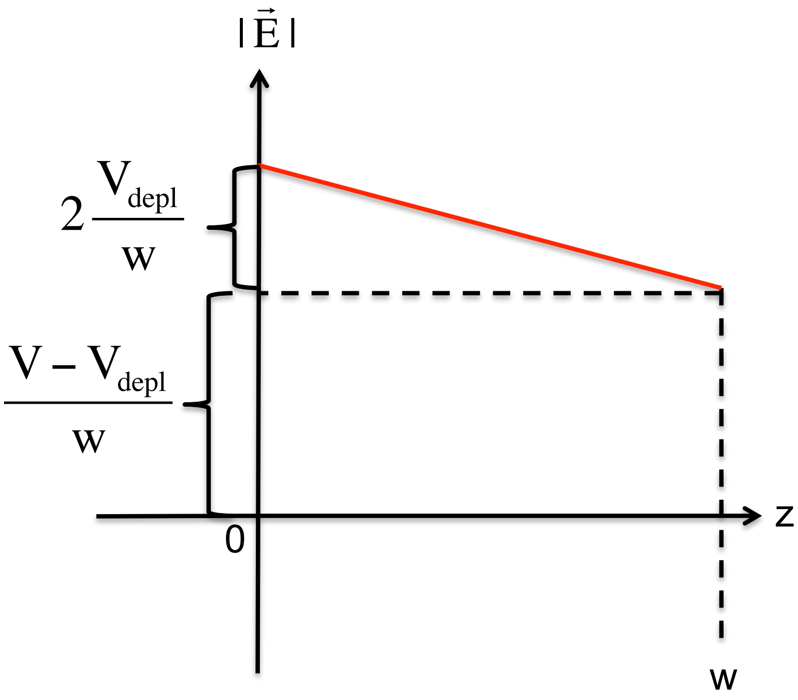

Quiz

(finite piece of) Metal

Everywhere: $V(\vec{r}) = 0$
$\varrho(\vec{r}) = 0$

Quiz

$V(\vec{r}) = ?$

$\varrho(\vec{r}) = ?$

Quiz

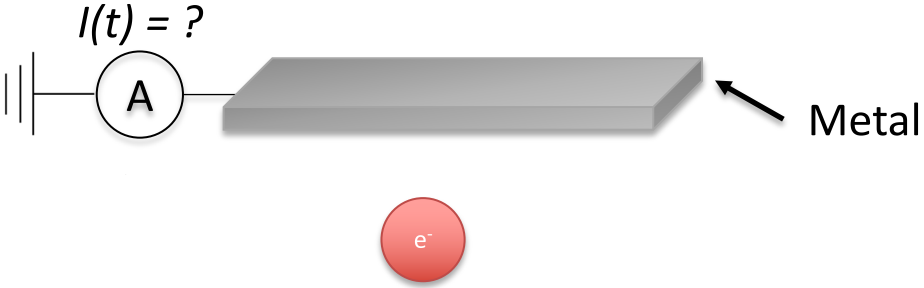

$V(\vec{r}) = ?$
$\varrho(\vec{r}) = ?$

Why does this matter?

Well, in your detector charges are moving towards electrodes at fixed voltage and you can measure currents…

Yes, you **ALWAYS MEASURE AN INDUCED SIGNAL DUE TO THE MOVEMENT OF CHARGE CARRIERS** **(electrons, holes – ions too)**

SIGNAL IS NEVER COLLECTED BY ELECTRODES BUT ALWAYS INDUCED ON THEM

More in slides from W. Riegler: https://indico.cern.ch/event/843083/

Signal formation in p-n junction

in principle like ionization chambers:
if E const: each drifting electron contributes to signal current while drifting

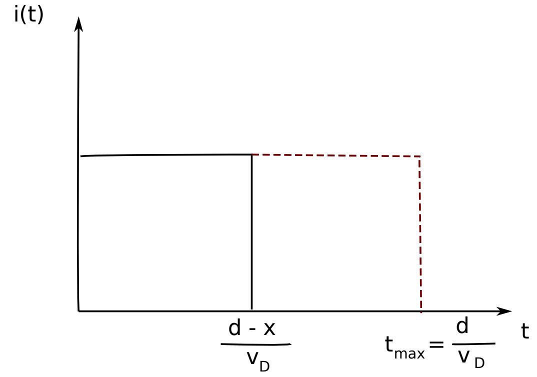

$$i = \frac{\mathrm{d}q}{\mathrm{d}t} = e\frac{\mathrm{d}x}{d}\frac{1}{\mathrm{d}x/v_D} = e\frac{v_D}{d}$$

d: width of depletion zone
x: location where electron was generated

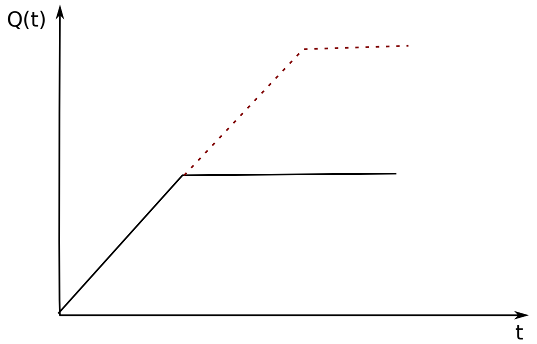

capacitor charges:

$$Q = e\frac{v_D}{d}\cdot t = e\frac{v_D}{d}\frac{d-x}{v_D}$$

Signal from uniform deposition

line charge of electrons across the depletion layer (constant ionization along track):

$$\begin{aligned} i &= N_0 e \frac{v_D}{d}\left(1-\frac{t v_D}{d}\right)\Theta\left(1-\frac{t v_D}{d}\right) \\ Q(t) &= N_0 e \frac{v_D}{d}\left(t-\frac{t^2 v_D}{d}\right)\Theta\left(1-\frac{t v_D}{d}\right) \end{aligned}$$

integrated:

$$Q\left(t=\frac{d}{v_D}\right) = \frac{N_0 e}{2}$$

same signal for positive carriers (holes), thus in total

$$\boxed{N_0 \cdot e = Q_{tot}}$$

Signal from point deposition

Conduction current density between 50 and 600 ps after the conversion at ~ mid plane

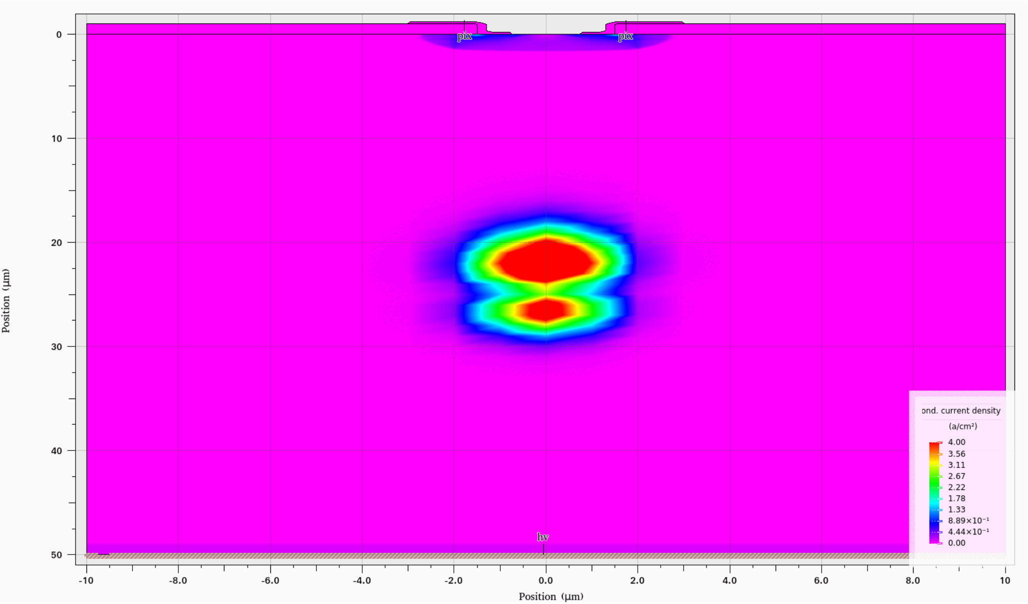

Photocurrent

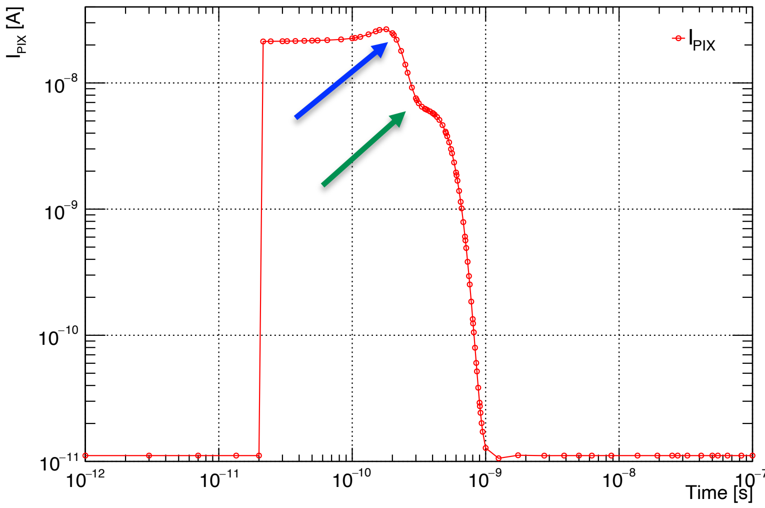

At 200 ps first e- arrive at PIX

By 300 ps they are gone

Want to know more? Ask me about TCAD ☺

Ionization yield and Fano factor

mean energy per electron-hole pair

	$E_0^{300\ \mathrm{K}}$	$E_0^{77\ \mathrm{K}}$	E_{gap}
Si	3.6 eV	3.8 eV	1.1 eV
Ge	-	2.9 eV	0.7 eV

$\sim \frac{2}{3}$ goes into excitation of crystal lattice

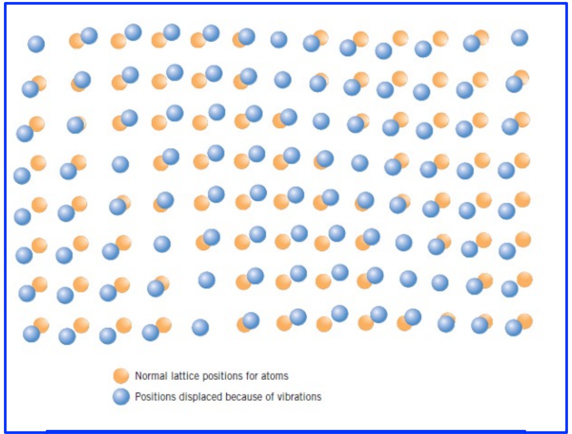

Schematic representation of the generation of lattice waves in a crystal by means of atomic vibrations. Source: Callister & Rethwisch (2010)

Energy loss $\Delta E \quad \Rightarrow \quad \begin{cases} \text{lattice vibrations: generation of phonons} \\ \qquad \text{typical quantum energy } E_x = 0.037 \text{ eV} \\ \text{ionization: characteristic energy } E_i = E_{\mathrm{gap}} = 1.1 \text{ eV in Si} \\ \text{total: } \Delta E = E_i N_i + E_x N_x \end{cases}$

assume Poisson distributions for both processes with $\sigma_i = \sqrt{N_i} \quad \sigma_x = \sqrt{N_x}$

for a fixed energy loss ΔE:
sharing between ionization and lattice excitation varies as $\quad E_x \Delta N_x + E_i \Delta N_i = 0$

on average: $\quad E_i \sigma_i = E_x \sigma_x$

$$\sigma_i = \frac{E_x}{E_i}\sigma_x = \frac{E_x}{E_i}\sqrt{N_x}$$

using $N_x = (\Delta E - E_i N_i)/E_x$

$$\sigma_i = \frac{E_x}{E_i}\sqrt{\frac{\Delta E}{E_x} - \frac{E_i}{E_x}N_i}$$

Ionization yield and Fano factor

$N_i = \frac{\Delta E}{E_0}$ in case of ideal charge collection without losses

$$\to \quad \sigma_i = \frac{E_x}{E_i}\sqrt{\frac{\Delta E}{E_x} - \frac{E_i}{E_x}\frac{\Delta E}{E_0}} = \underbrace{\sqrt{\frac{\Delta E}{E_0}}}_{\sqrt{N_i}} \underbrace{\sqrt{\frac{E_x}{E_i}\left(\frac{E_0}{E_i} - 1\right)}}_{\sqrt{F}}$$

F: Fano factor

Si: $E_0 \cong 3.6$ eV $F \cong 0.1$
Ge: $E_0 \cong 2.9$ eV $F \cong 0.1$

$\boxed{\sigma_i = \sqrt{N_i}\sqrt{F}}$ smaller than naive expectation

due to energy conservation, fluctuations are reduced for a given energy loss ΔE (the total absorbed energy does not fluctuate)

relative energy resolution

$$\boxed{\frac{\sigma_i}{N_i} = \frac{\sqrt{N_i\,F}}{N_i} = \frac{\sqrt{F}}{\sqrt{N_i}} = \frac{\sqrt{F\,E_0}}{\sqrt{\Delta E}} = \frac{\sigma_{\Delta E}}{\Delta E}}$$

Nature is so kind to offer > 60% discount on energy resolution ☺

example: photon of 5 keV, $E_\gamma = \Delta E$, $\sigma_{\Delta E} = 40$ eV $\cong 1\%$ instead of 2.7% w/o Fano factor

Intermezzo: Landau distribution

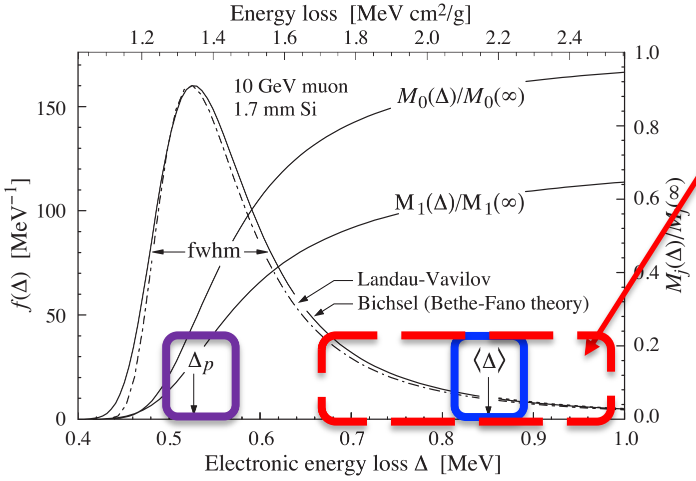

Very long tail

Average <Δ> and most probable value Δ_p (MPV) **are very different**

(If absorber is very thin Landau model fails)

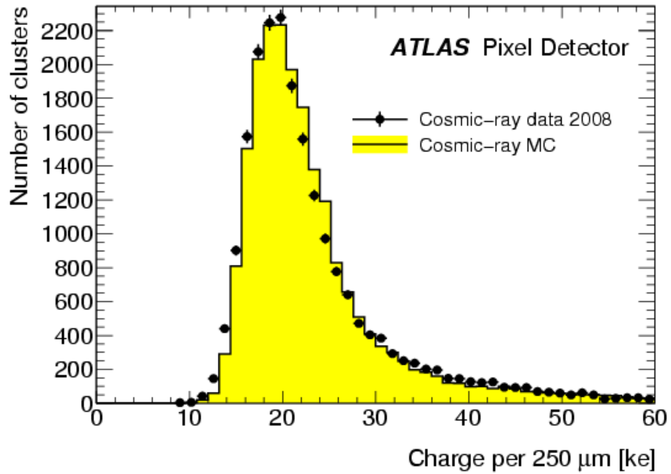

Energy resolution

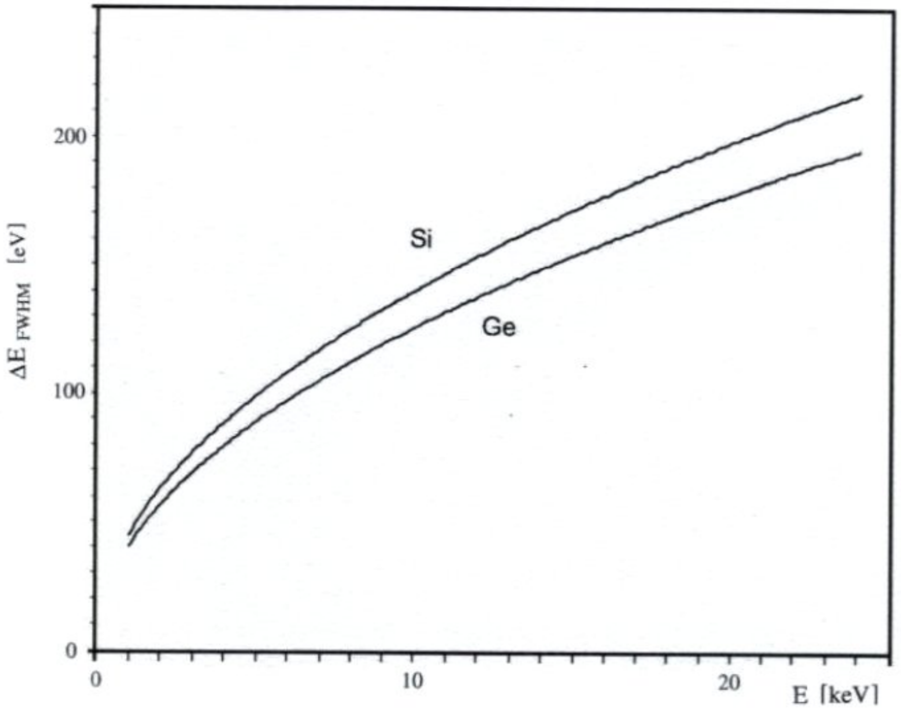

intrinsic resolution due to statistics of charge carriers generated, in addition noise and non-uniformities in charge-collection efficiency

Energy measurement – summary

Photons

Point-like interaction

- Infinitesimal interaction probability: *dP=μdx*

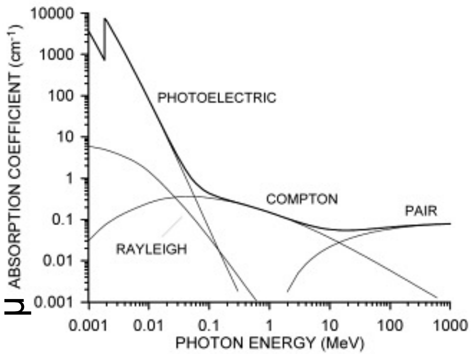

- Photo: 1 e-h pair per conversion
- e- from X-ray can trigger secondary emission

Charged particles in Silicon

Charges created along the track

- **3.6 eV (E_i) to create an e-h pair => 80 e-h / μm (most probable)**
- **Most probable charge (300 μm) ≈ 24000 e ≈ 4 fC**
- <-dE/dx> (MIP) ~ 3.87 MeV/cm

Energy *E* intrinsic resolution of a semiconductor detector:

$$\boxed{\Delta E_{FWHM} = 2.35 \cdot \sqrt{FEE_i}}$$

F the Fano factor; F ~ 0.1 for Si.

E.g. for photons of few keV a 100 eV resolution can be achieved

Intermezzo: noise

$$ENC \propto C_d$$

$$ENC \propto \sqrt{I}$$

$$ENC \propto \sqrt{k_B T / R}$$

- Landau distribution has a low energy tail
  - becomes even lower by noise broadening
  - Noise sources: (ENC = Equivalent Noise Charge)
    - Capacitance
    - Leakage Current
    - Thermal Noise (bias resistor)
  - Figure of Merit: Signal-to-Noise Ratio S/N
  - Typical values >10-15, people get nervous if < 10.
    Radiation damage severely degrades the S/N.
  - If threshold is too high ➔ inefficiency
  - If threshold is too low ➔ noise occupancy

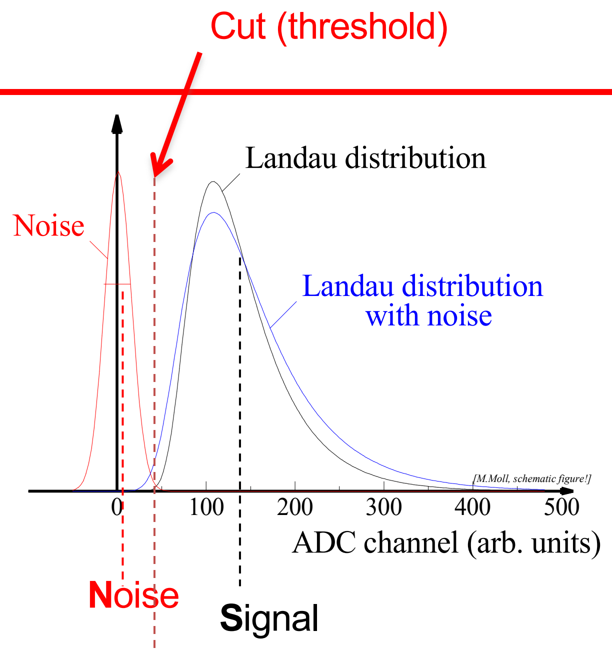

The complete detecting chain

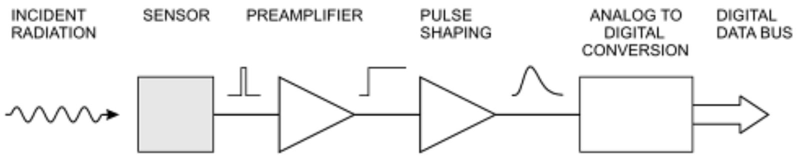

Preamplifier: signals in silicon (0.05-4 fC) must be amplified. Minimize noise amplification!

Pulse shaping: its primary function is to improve the signal-to-noise ratio. This is done by applying filters that tailor the frequency response
Typically bandwidth reduction which translates into an increase of the pulse duration (*"shaping time"*)

Absorption coefficient

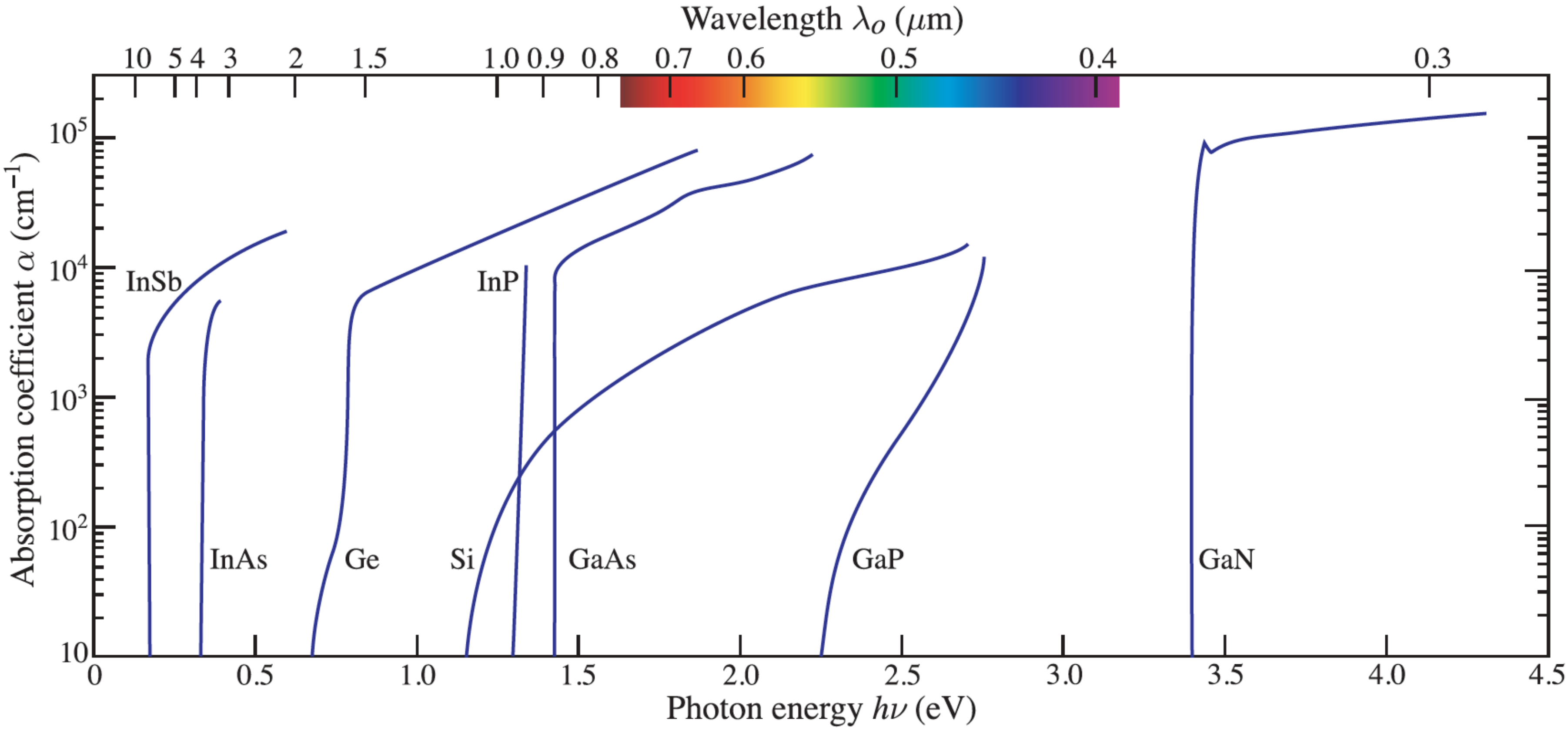

Absorption coefficient

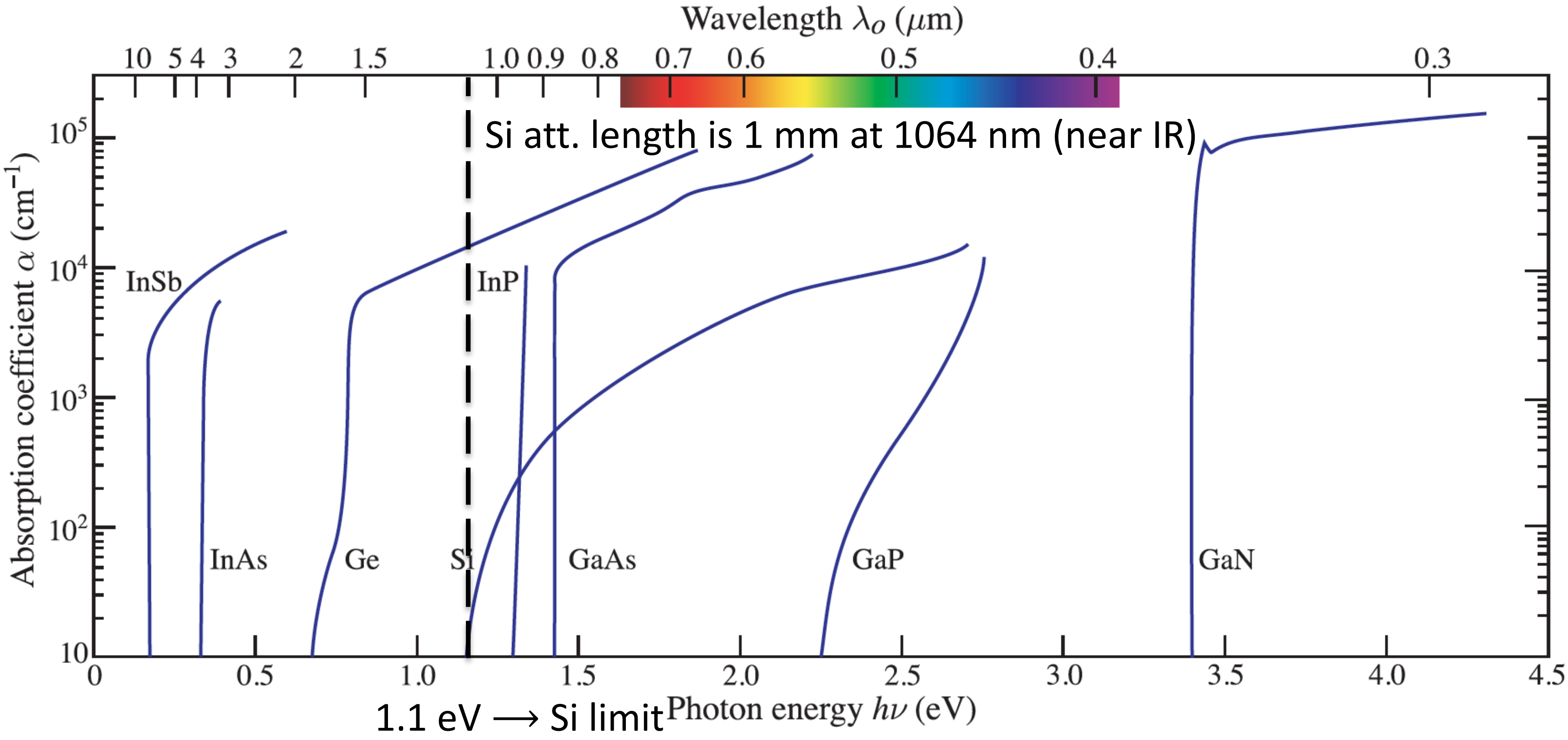

Absorption coefficient

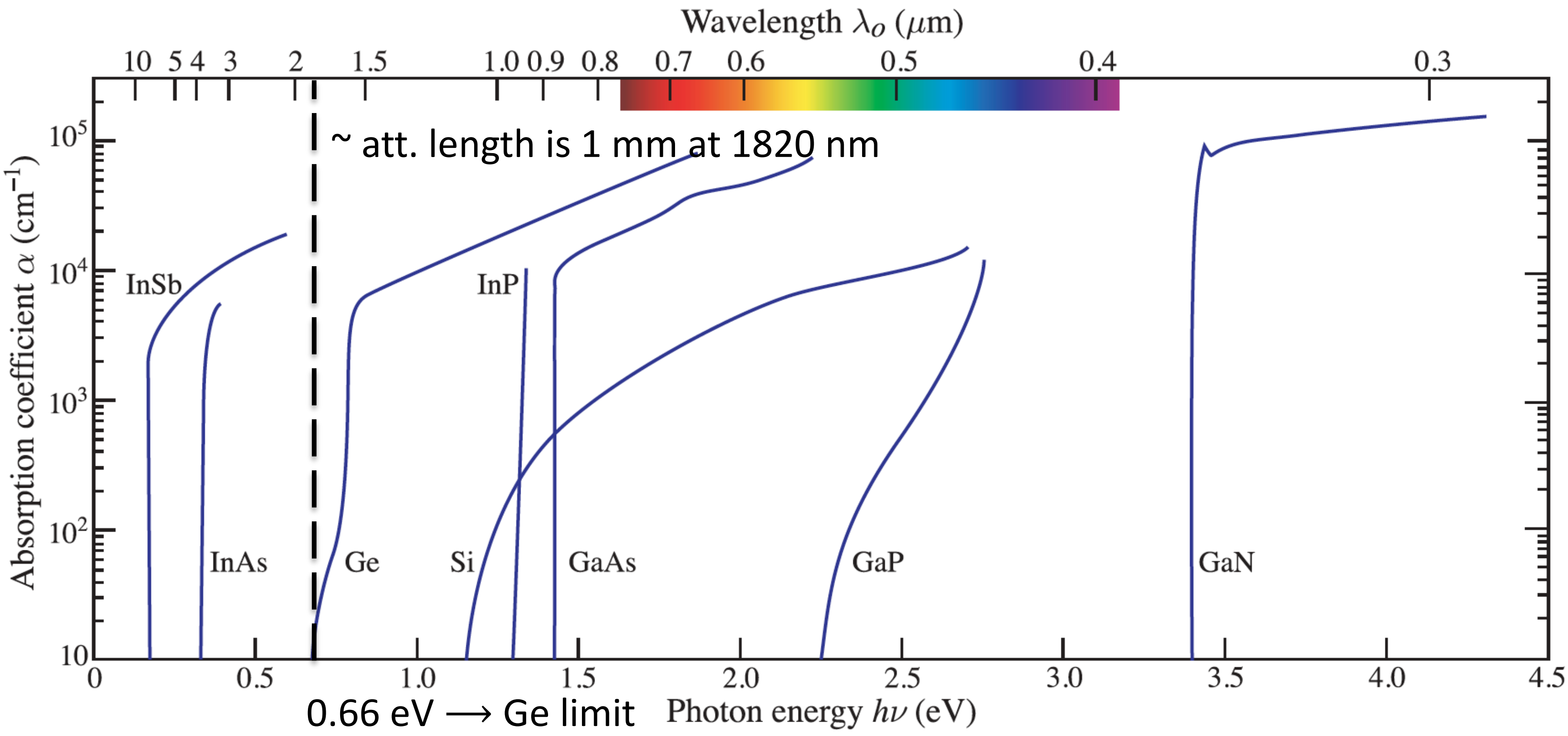

Photon attenuation coeff. – keV to 100 MeV

[https://www.nist.gov/pml/x-ray-mass-attenuation-coefficients]

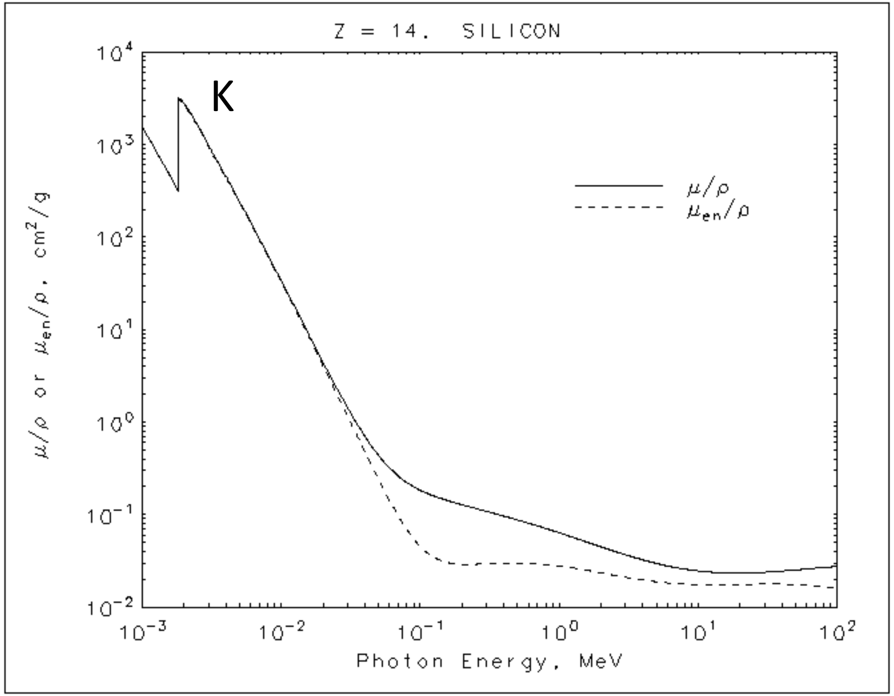

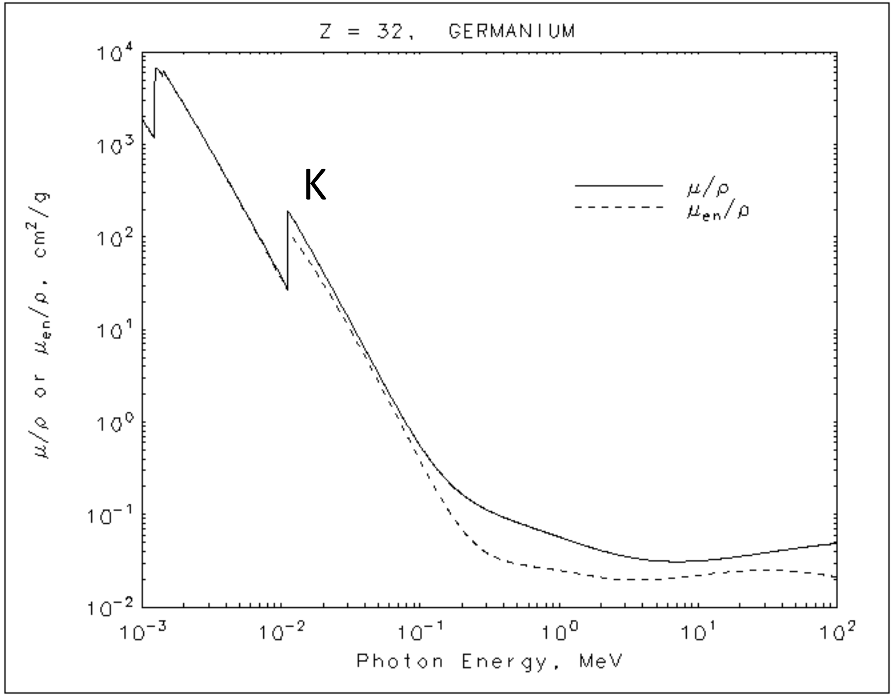

ρ_{Si} ~ 2.3 g/cm^3

ρ_{Ge} ~ 5.3 g/cm^3

Photon attenuation coeff. – keV to 100 MeV

[https://www.nist.gov/pml/x-ray-mass-attenuation-coefficients]

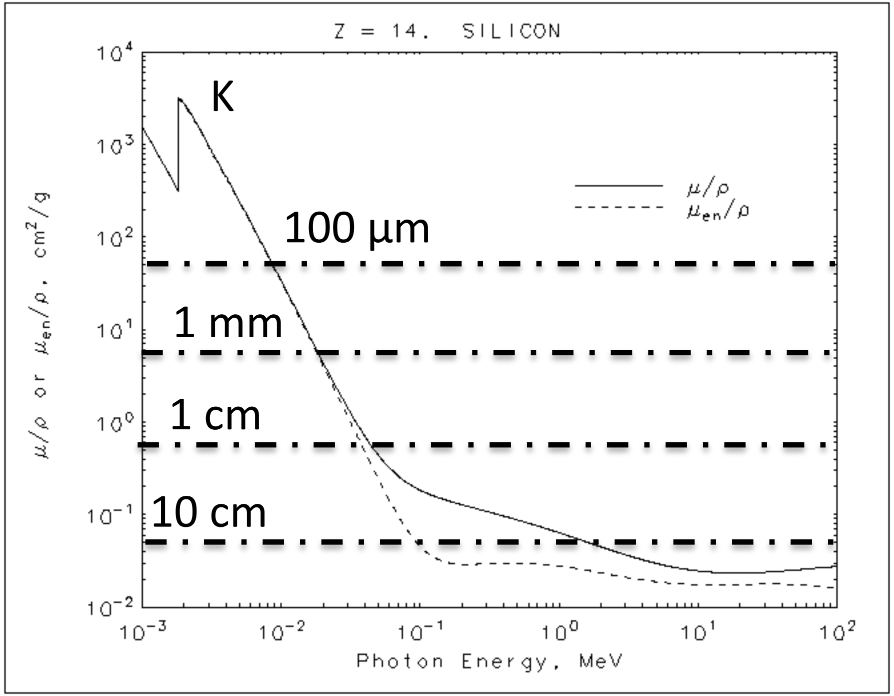

ρ_{Si} ~ 2.3 g/cm^3

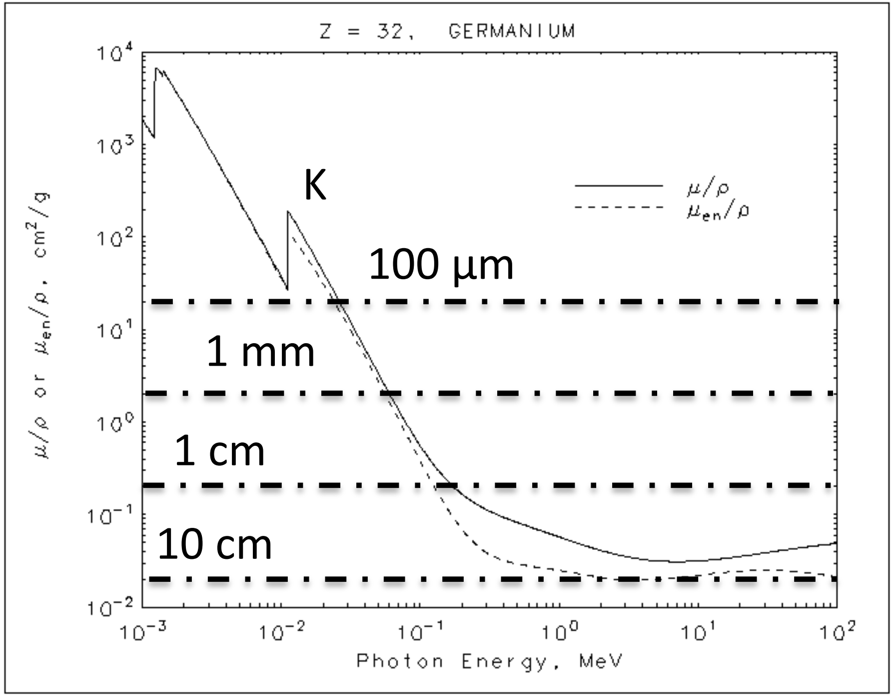

ρ_{Ge} ~ 5.3 g/cm^3

Position measurement

The position resolution depends on physical processes and on external parameters

Physical processes:

- statistical fluctuations in the energy loss
- diffusion: $\sigma_D = \sqrt{2Dt}$ →

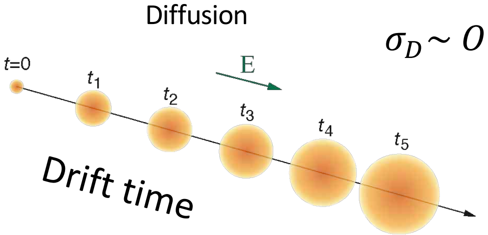

$\sigma_D \sim O(3-4\ \mu m)$ for 200 μm thick sensor

External parameters:

- analogue/binary signal readout
- detector segmentation (“pitch” *p*)
- signal-to-noise-ratio *SNR*

Single channel, binary r.o.

x = strip position

$\sigma = p/\sqrt{12}$

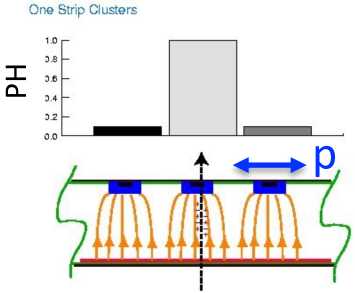

Analogue r.o.

$x = (x_1h_1+x_2h_2)/(h_1+h_2)$

x_i = *i-th* strip pos.

h_i = *i-th* strip PH

$\sigma \approx p/SNR$

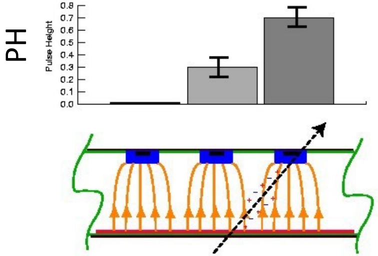

[Turchetta, 1993]

Position measurement in magnetic field

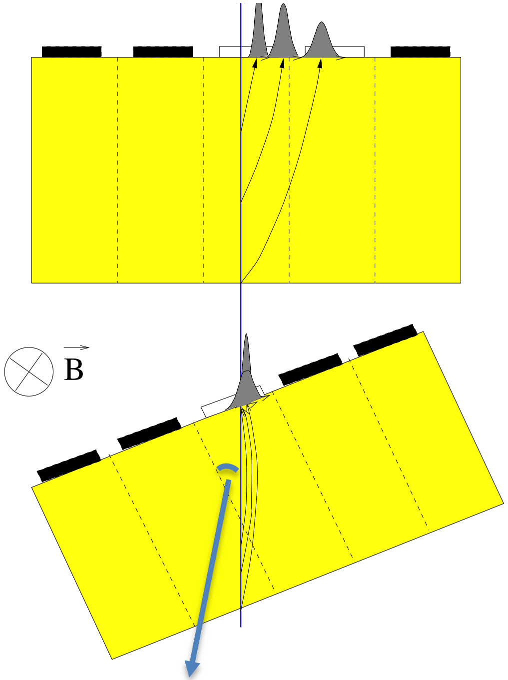

Lorentz angle

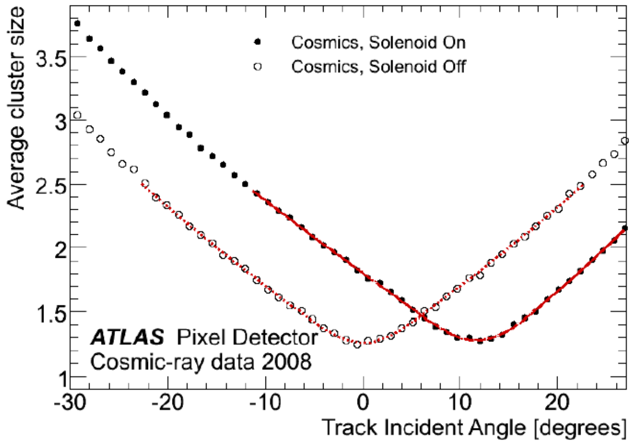

(a) Pixel Detector mean cluster width

Eur. Phys. J. C (2010) 70: 787–821
10.1140/epjc/s10052-010-1366-7

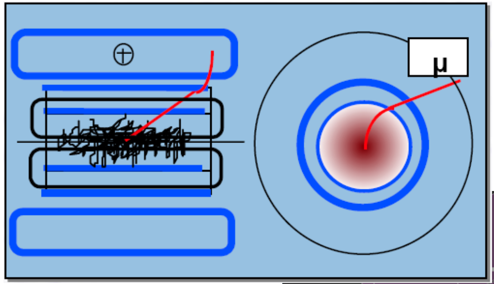

ATLAS: (air-core) toroid magnet + inner solenoid

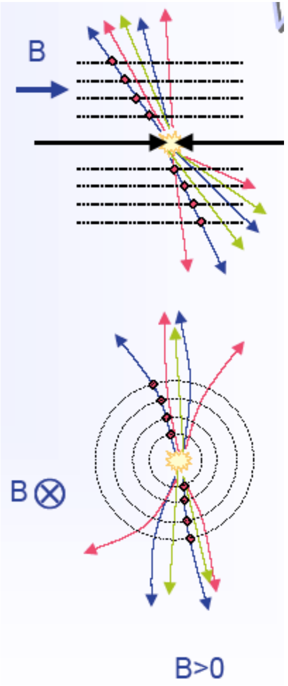

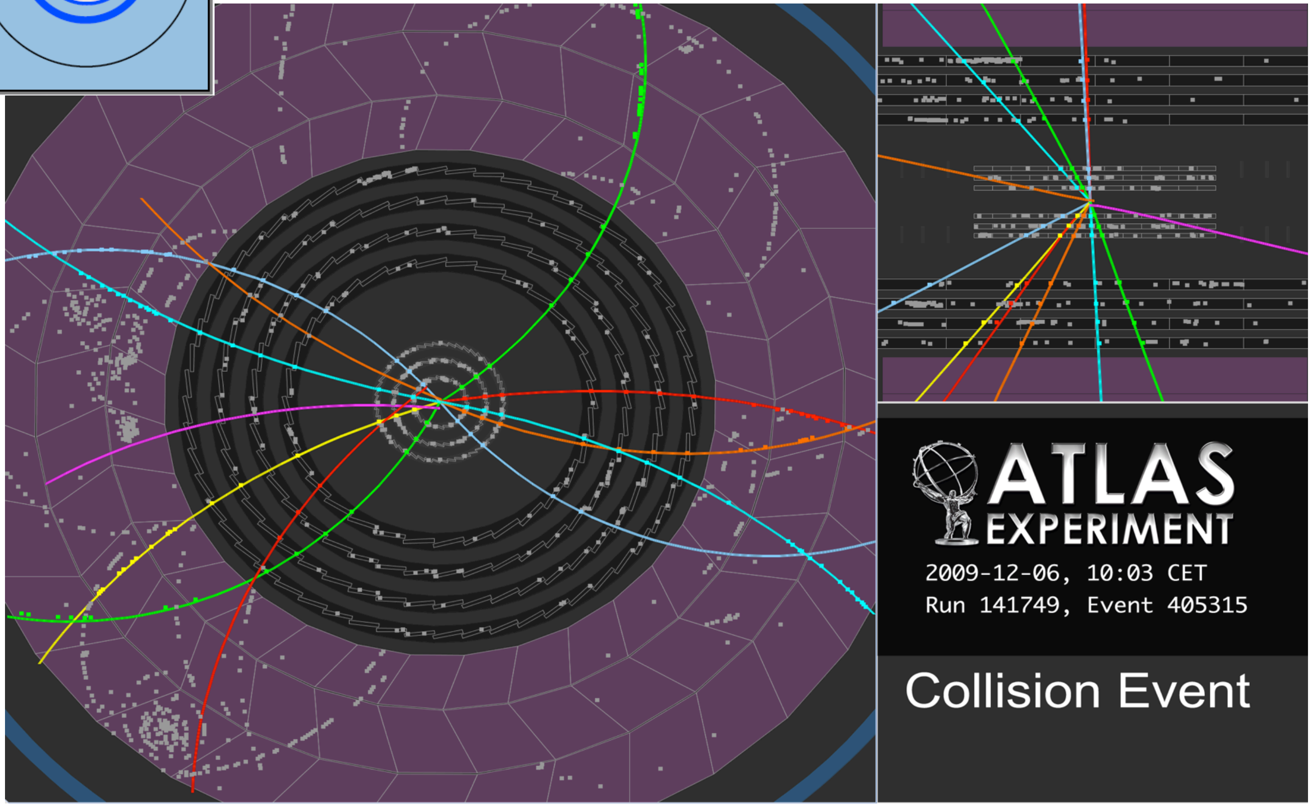

http://atlas.web.cern.ch/Atlas/public/EVTDISPLAY/events.html

Tracking detectors

Momentum determination
in a cylindrical drift chamber ...

$$\frac{mv^2}{R} = evB \quad \rightarrow \quad p = eB \cdot R$$

$$\boxed{p\left[\frac{GeV}{c}\right] = 0.3\ \mathrm{B[T]\ R[m]}}$$

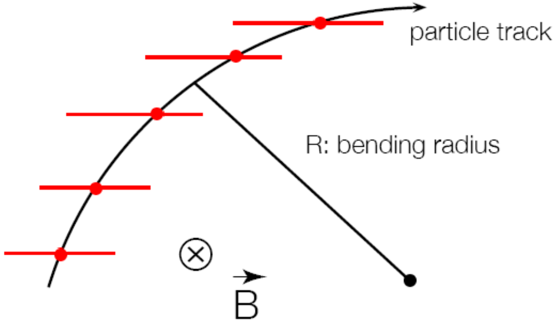

[Garutti]

momentum component perpendicular to the B-field
transverse momentum p_t

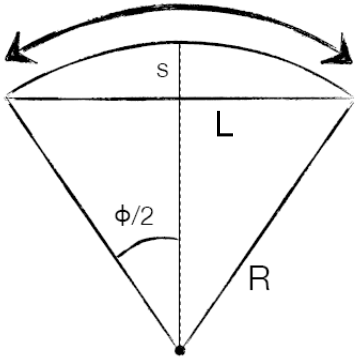

For Sagitta s:

$$s = R - R\cos\frac{\phi}{2} \approx R\frac{\phi^2}{8} \qquad \text{with } \phi = \frac{L}{R}$$

$$s = R\frac{L^2}{8R^2} = \frac{L^2}{8R} \quad \text{and} \quad R = \frac{L^2}{8s}$$

$$\rightarrow \quad \frac{\Delta p}{p} = \frac{\Delta R}{R} = \frac{L^2}{8Rs} \cdot \frac{\Delta s}{s}$$

➔ radius is obtained by a circle fit through measurement points along the track with point resolution $\sigma_{r\phi}$

1T = 1kg/C/s^2
1eV/c = 0.535 10^{-27} kg m/s
1eV = 1.6 10^{-19} C

18

Numerical example

ATLAS

$$p\left[\frac{GeV}{c}\right] = 0.3\ B[T]\ R[m] \qquad s = \frac{L^2}{8R}$$

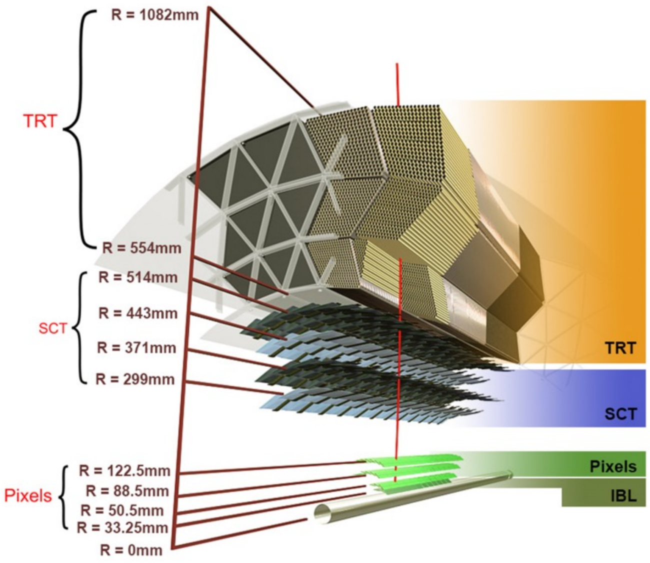

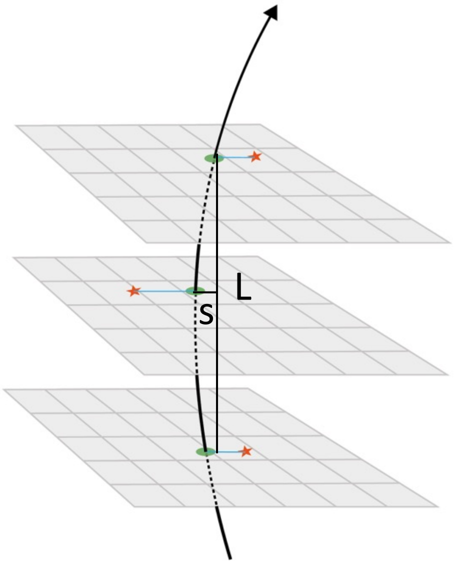

If we assume L = 1 m and B = 2 T and p = 1 TeV/c then:

R = p/(0.3 * B) = 1000 / 0.6 ~ 1670 m

s = 1/(8*1670) m ~ 0.075 mm

If we want to measure the momentum with a relative precision of 20% at p = 1 TeV/c, then:

$\Delta p/p \sim \Delta s/s = 20\% \Rightarrow \Delta s \sim 15\ \mu m$

Momentum resolution

from PDG

Multiple scattering contribution:

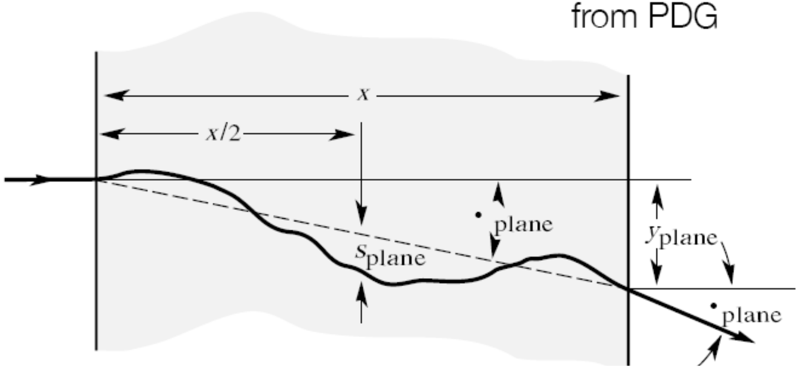

$$\sigma_\phi \approx \frac{14\ \mathrm{MeV}/c}{p}\sqrt{\frac{L}{X_0}}$$

$$\frac{\sigma_p}{p} = \frac{\sigma_R}{R} = \frac{\sigma_\phi}{\phi}$$

as $R = \frac{L}{\phi}$

At small momenta this limits resolution of momentum measurement ...

momentum independent

$$\frac{\sigma_p}{p} = \frac{\sigma_\phi}{\phi} = \frac{14\ \mathrm{MeV}/c}{p}\sqrt{\frac{L}{X_0}} \cdot \frac{R}{L} = \frac{14\ \mathrm{MeV}/c}{p}\sqrt{\frac{1}{LX_0}} \cdot \frac{p}{eB} \sim \frac{1}{\sqrt{LX_0}B}$$

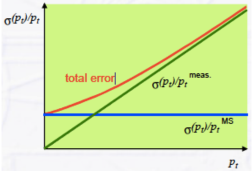

$$\left(\frac{\sigma_{p_t}}{p_t}\right)^2 = \boxed{\mathrm{const}\cdot\left(\frac{p_t}{BL^2}\right)^2} + \boxed{\mathrm{const}\cdot\left(\frac{1}{B\sqrt{LX_0}}\right)^2}$$

21

Take home message on momentum resolution

- At low momentum the resolution is dominated by multiple scattering
- ➢ Important to reduce the material budget x/X_0

Si: X_0 ~ 9.4 cm

- At high momentum the sagitta determination is the dominant factor
- ➢ Finer and finer segmentation is necessary
- ➢ Longer and longer lever arm
- ➢ Stronger and stronger magnetic field

$$\frac{\sigma_{p_T}}{p_T} = \frac{8p_T}{0.3BL^2}\sigma_s$$

- ➢ **Very important: the larger the p_T the worse the resolution**

Vertexing resolution

Looking for significant impact parameter IP, d_0, and maybe form a reconstructed secondary vertex.

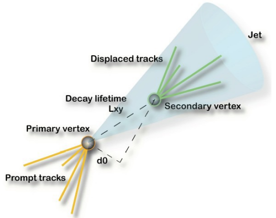

The IP resolutions depends on geometry, material and track momentum

Simplified model
w/ 2 layers only

$$\sigma_{d_0} \approx \sqrt{\frac{r_2^2\sigma_1^2 + r_1^2\sigma_2^2}{(r_2 - r_1)^2}} \oplus \frac{r}{p\sin^{3/2}\theta} 13.6\mathrm{MeV}\sqrt{\frac{x}{X_0}}$$

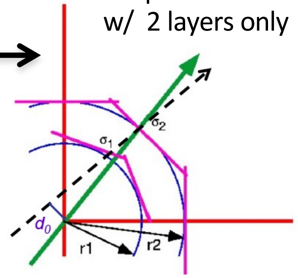

Geometry: use small r_1, large r_2, and small intrinsic spatial resolution σ_1 , σ_2

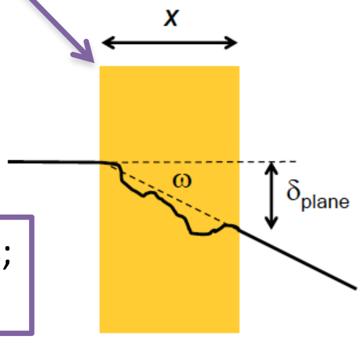

Multiple Scattering: important for low momentum tracks; best precision with small radius *r* and minimum thickness *x*

Semiconductor detectors for vertexing

'70s-'80s: ~ps lifetime particles discovered

Lifetimes of tau leptons, charm and beauty hadrons: from 0.2 to 1.5 ps

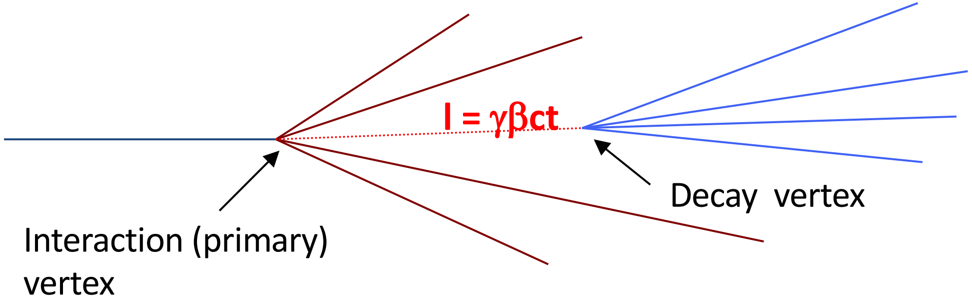

decay length $l = \gamma\beta ct$, so typically the decay vertex is at a distance **of single millimeters** from the interaction vertex

History – MESD by Pisa group (1980)

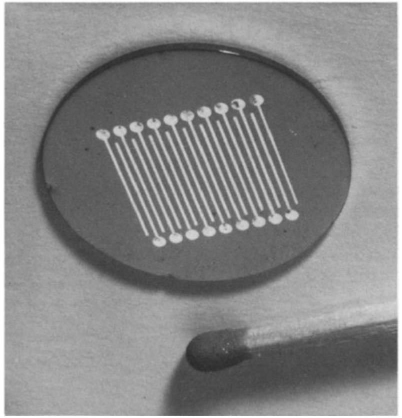

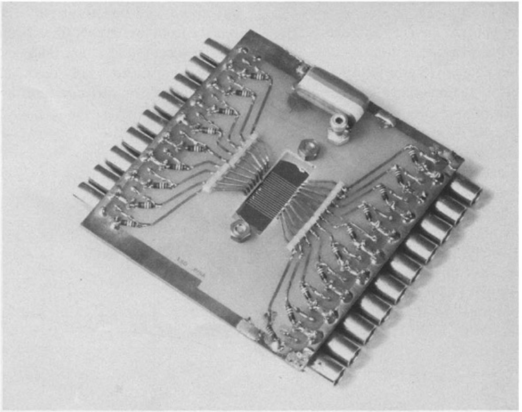

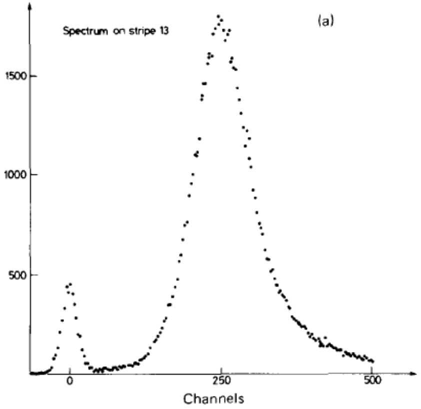

MESD featured 12 mm long 300 μm wide aluminium strips on a high resistivity Silicon wafer.
The signal was proportional to the energy released by the impinging particle.
It assured good spatial resolution with low noise at room temperature.

All the desirable features of silicon detectors were already exploited by the first high energy physics detectors

S. R. Amendolia et al., A Multi-Electrode Silicon Detector for High Energy Experiments, Nucl. Instr. Meth. 176 (1980)

Want to know more?

Silicon as detector material: summary

Reverse biased p-n junction as radiation detector: the depletion region is virtually free of mobile carriers ➔ in absence of radiation only the (small) diode reverse current flows in the junction

Energy deposition: creation of a e-h pair for E ~ 3.6 eV (gas: 15-30 eV)➔Large signals!

High electric field in the depleted bulk
➔ elec's and holes drift very fast across the depletion zone: t_{coll} ~ 10-30 ns

Low doping concentration (high resistivity) of the bulk ➔ V_{depl} at low bias voltages (safely below V_{BD})

$$N_{eff} \sim 10^{12}\ /cm^3 \Leftrightarrow \rho \sim 5\text{-}10\ k\Omega$$

Excellent spatial resolution thanks to fine segmentation (due to progress in µ-electronics)

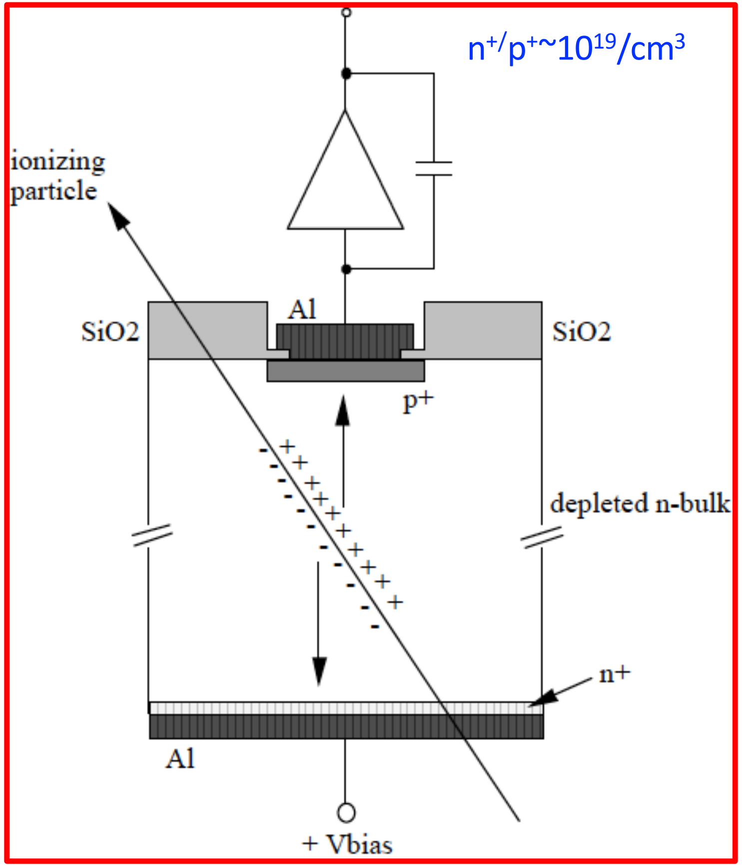

Outline

- Main applications, motivations and history
- Semiconductors physics
- Silicon radiation detectors
- Timing with silicon detectors
- Perspectives

Float Zone Silicon

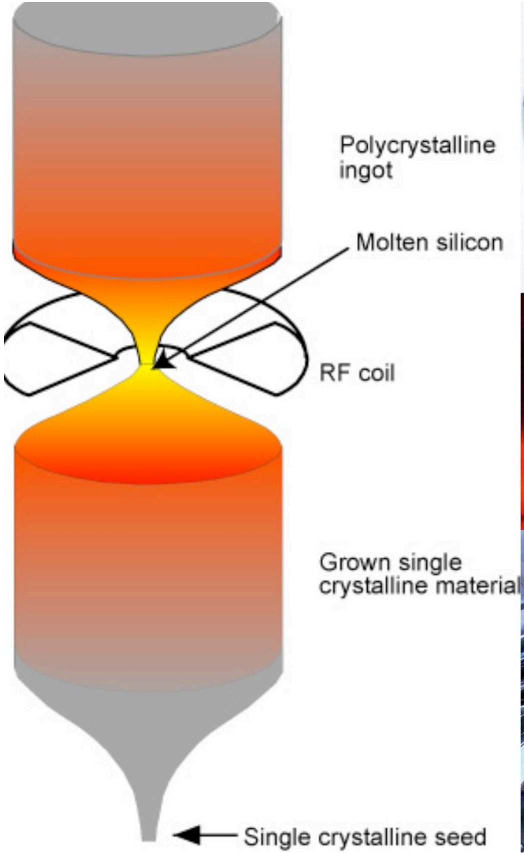

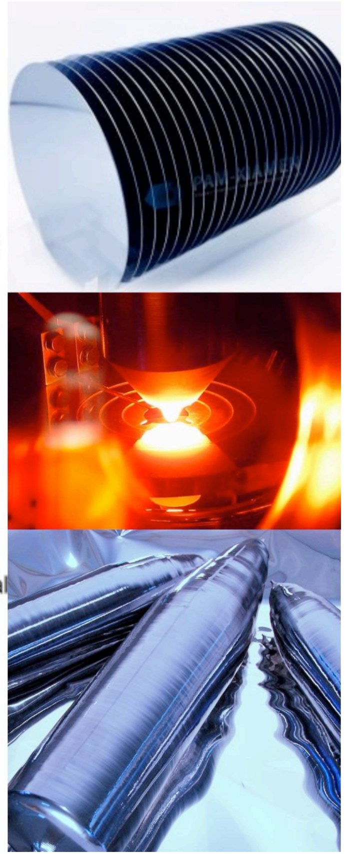

Very pure Silicon is obtained

A polycrystalline rod of ultrapure electronic-grade silicon is passed through an RF heating coil

A seed crystal is used at one end to start the growth. The whole process is carried out in an evacuated chamber or in an inert gas purge

History – Planar process, Munich group (‘80s)

NUCLEAR INSTRUMENTS AND METHODS 169 (1980) 499-502, © NORTH HOLLAND PUBLISHING CO

FABRICATION OF LOW NOISE SILICON RADIATION DETECTORS BY THE PLANAR PROCESS

J KEMMER

Fachbereich Physik der Technischen Universitat Munchen, 8046 Garching, Germany

“Combining the techniques of oxide passivation, photo engraving and ion implantation, it’s possible to get a large number of detector chips with only small tolerances in their geometrical and electrical properties”

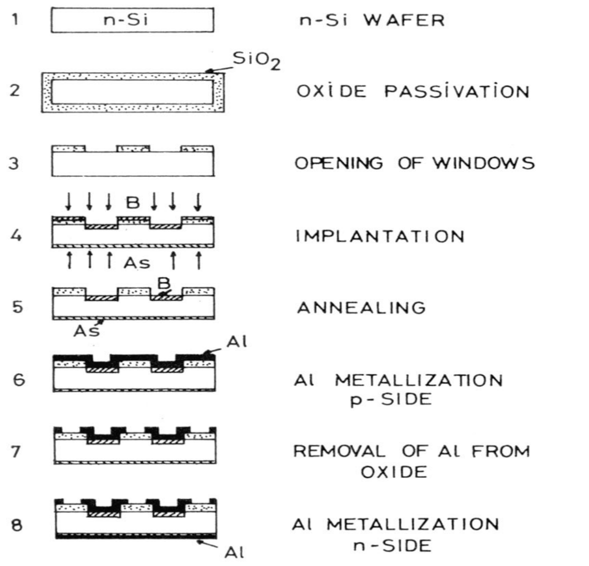

Fig. 1 : Successive steps of the manufacturing process of passivated ion-implanted silicon detectors

Performance:
- ✓ leakage current < 1 nA / cm^2/100 µm
- ✓ energy resolution of 100 keV for 5486 keV alphas of ^{241}Am

Silicon pad diode

N-on-p production

A single p-n diode in reverse bias is the simplest silicon radiation detector
Often it is called pad diode

The size varies between few mm^2 to few cm^2

Guard Rings (GRs) assure a smooth transition between the High Voltage (HV) and the Ground (GND) potential

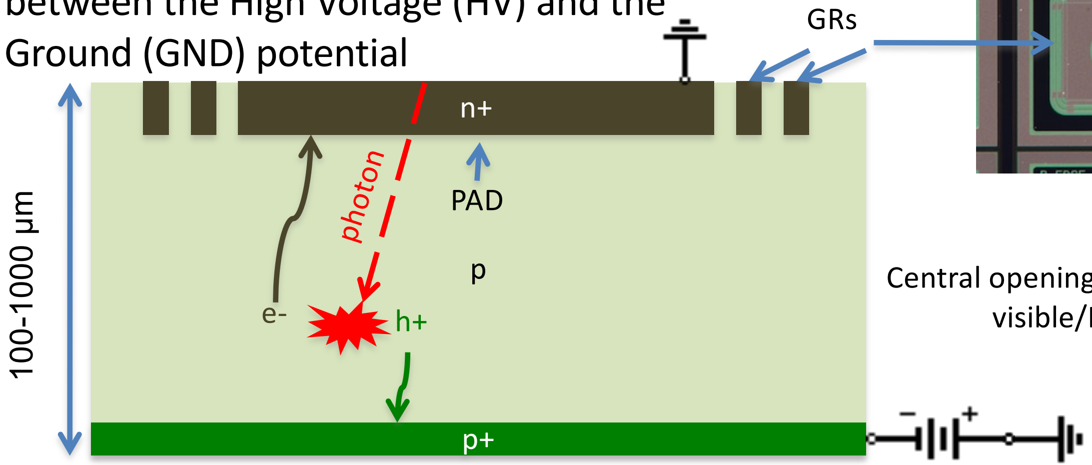

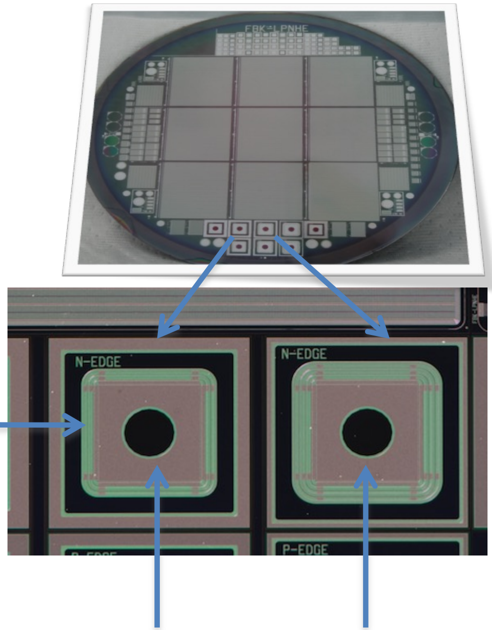

Central openings in the aluminium layer for visible/IR photon detection

Silicon PIN diodes

- Sixties evolution: the p-i-n (PIN) photodiode
- Wavelength range of some 150 to 1100 nm, covering:
  - the emission wavelength of almost all organic and inorganic scintillators
  - Cherenkov radiators used in particle physics
- Very successful device
- Still used in
  - high energy physics (PMTs replacemet)
  - radiation detection
  - and medical imaging

Hamamatsu S2744-08

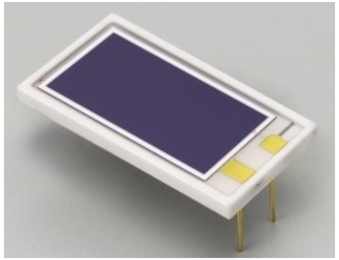

PIN diode: electrical properties

needs to be cooled permanently (liq. N_2) to avoid separation of Li from impurities by diffusion!

application: γ-spectroscopy

larger cross section for photo effect in Ge as compared to Si
$\rightarrow$ Ge(Li) preferred

however: full energy peak contains only order of 10 % of the signal in a 50 cm^3 crystal (30 % in a 170 cm^3 crystal))

- resolution much better than NaI
- efficiency significantly lower

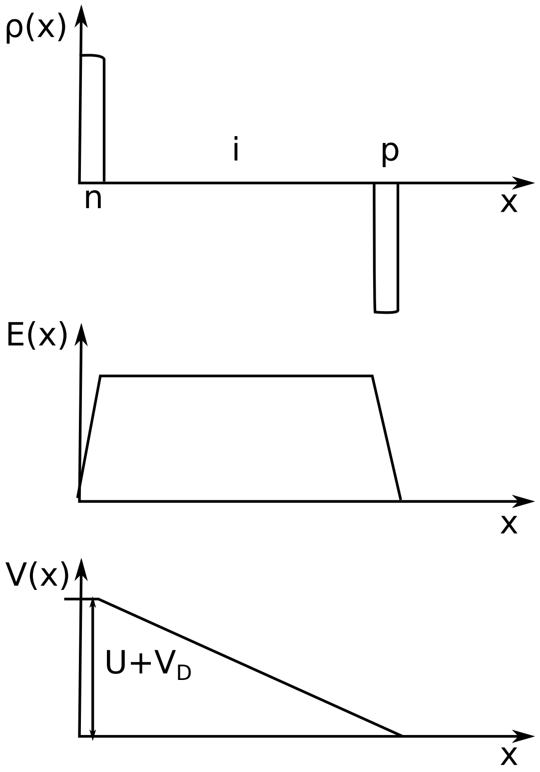

external voltage U and diffusion voltage V_D

PIN diode: energy resolution

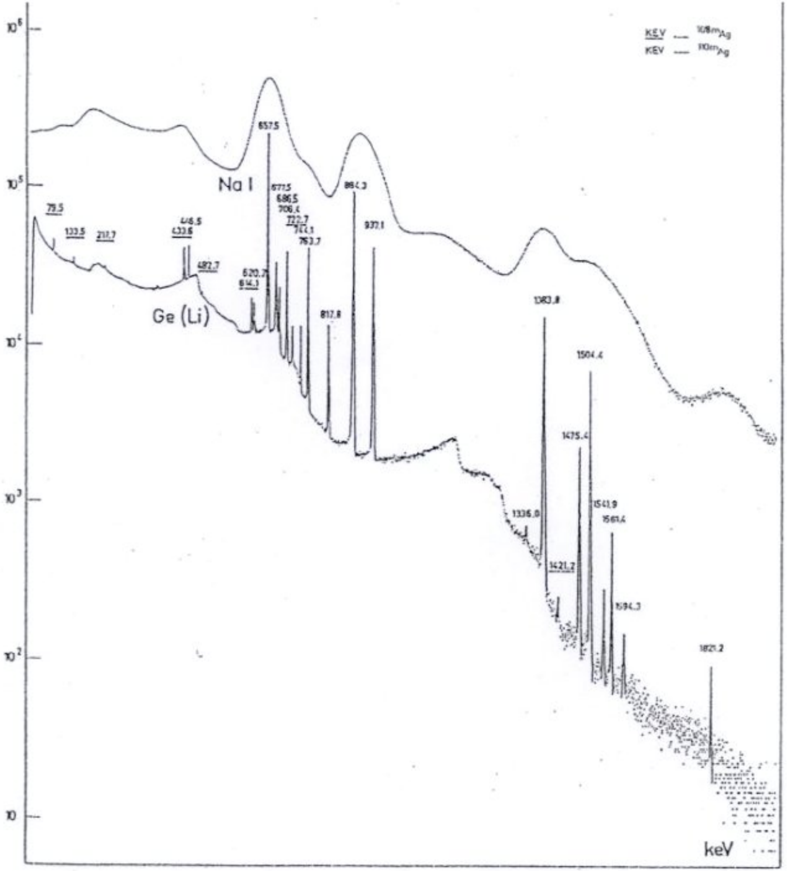

Ge(Li) detectors - a revolution in γ spectroscopy in the mid 1960ies:
comparison of spectra obtained with NaI (state of the art technique until then) and Ge(Li)

comparative pulse height spectra recorded using a sodium iodide scintillator and a Ge(Li) detector
source of γ radiation: decay of ^{108m}Ag and ^{110m}Ag, energies of peaks are labeled in keV

Si PIN diodes for a CsI(Tl) calorimeter (*BaBar*)

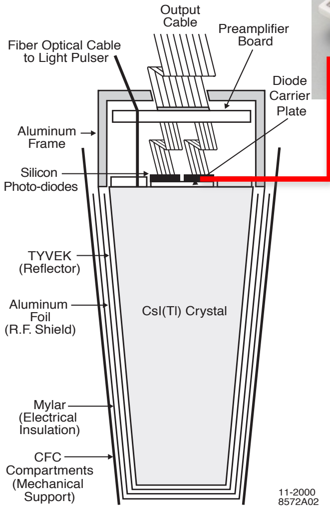

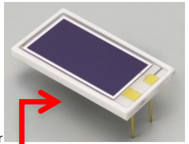

Table 2.6: Properties of CsI(Tl) .

Parameter	Values
Radiation Length	1.85 cm
Molière Radius	3.8 cm
Density	4.53 g/cm^3
Light Yield	50,000 γ/ MeV
Light Yield Temp. Coeff.	0.28%/°C
Peak Emission λ_{max}	565 nm
Refractive Index (λ_{max})	1.80
Signal Decay Time	680 ns (64%)
	3.34 μs (36%)

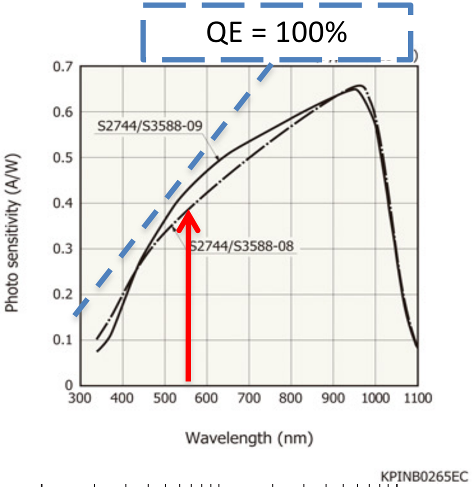

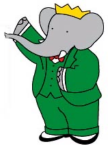

PIN diode: Vdepl ~ 70 V, I ~ 4nA, S~2cm^2

QE for peak emission close to 80%

PMTs only 10-15%

Photon energy resolution ~ 2-3% @ 1GeV

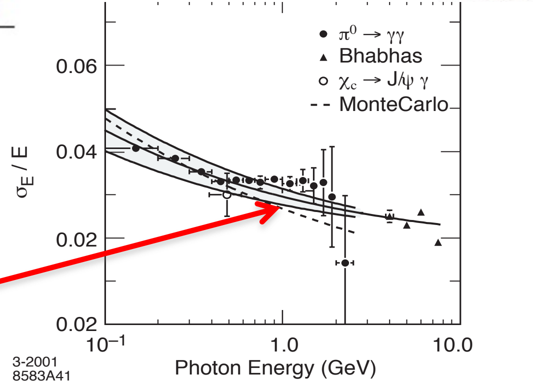

Si PIN diodes: pros and cons

✓ Simple and reliable

✓ Can operate in B

✓ Low voltage wrt PMTs

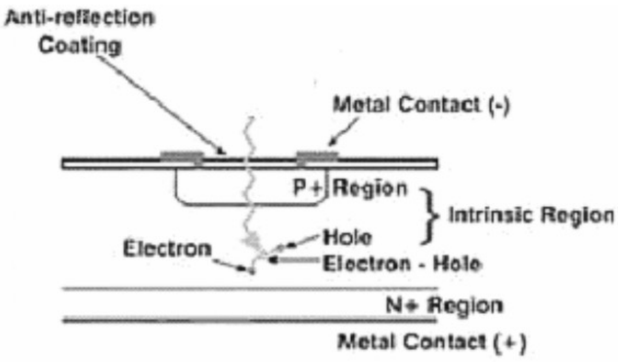

No internal gain:

✓ Output very stable

X Charge sensitive preamplifier is needed

X Low bandwidth filter is needed

- To cope with noise (leakage current + capacitance)

X Preamp & filter makes signal slow

- E.g.: minimal detectable signal: O(100)/cm^2 photons with a filter time constant of few μs

Position measurement: Silicon microstrip detector

Segmentation of the collecting electrode, independent readout of them
➔position sensitive detector

Typical strip pitch 20-50 μm

Single sided strip detector

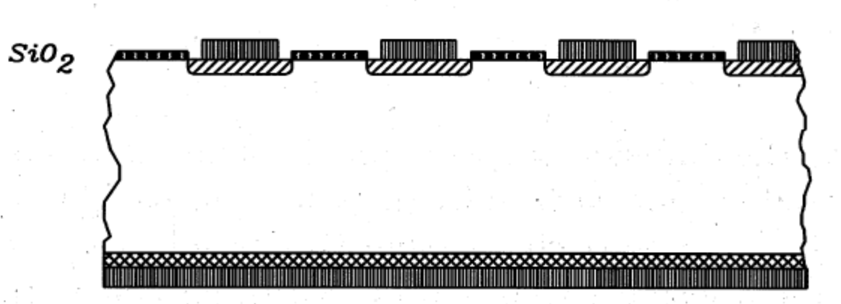

The connection between the strips and the readout chips is done via micro-bonding techniques (wires ~20 μm diameter)

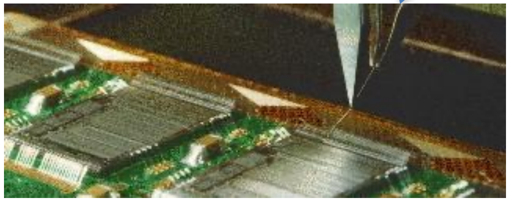

Single sided microstrip detector
➔ Excellent position resolution in one dimension
Reminder:

Binary r.o., single strip: $\sigma = p/\sqrt{12}$

Analogue r.o., 2 strips cluster: x (C.O.G.) = $(x_1h_1+x_2h_2)/(h_1+h_2)$, $\sigma \sim p/(SNR)$ (h_i=sign. amp.)

Double-sided microstrip detectors (DSSD)

Single sided detector measures only one coordinate. To measure second coordinate requires second detector layer

Double sided strip detector measures two coordinates in one detector layer (minimizes material)

In n-type detector the n^+ backside becomes segmented, e.g. strips orthogonal to p^+ strips

Drawback: expensive as production, handling, and tests are more complicated

Reminder

Single channel, binary r.o.

x = strip position

$\sigma = p/\sqrt{12}$

Analogue r.o.

$x = (x_1 h_1 + x_2 h_2)/(h_1 + h_2)$

$\sigma \approx p/SNR$

Scheme of a double sided strip detector (biasing structures not shown):

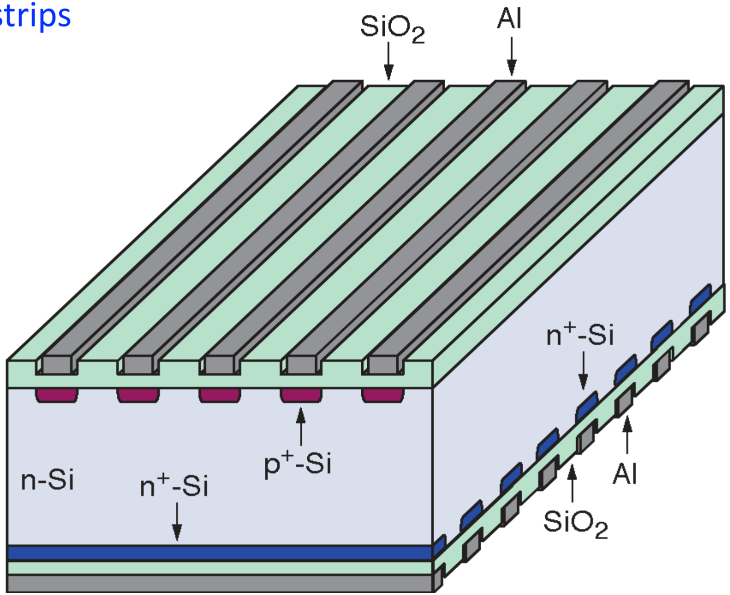

DSSD limitations

DSSD measure the 2 dimensional position of a particle track.
However, if more than one particle hits the strip detector the measured position is no longer unambiguous. “Ghost”-hits appear!

True hits and ghost hits in a double sided strip detector in case of two particles traversing the detector:

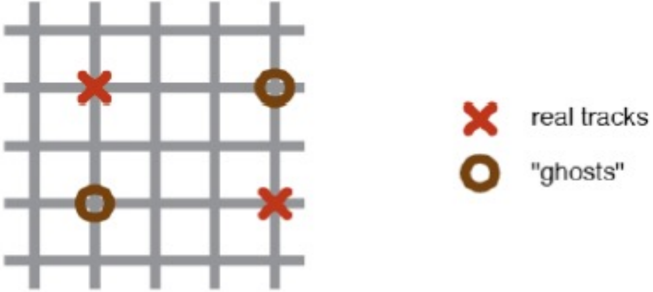

Pixel detectors produce unambiguous hits!

Measured hits in a pixel detector in case of two particles traversing the detector:

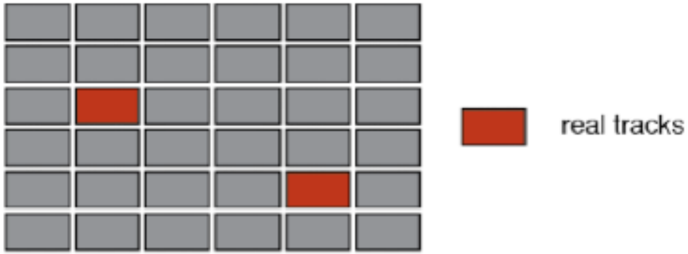

Hybrid Pixel Detectors

HPD: Typical size is (50-400) μm x 50 μm

If signal pulse height is not recorded, resolution is the digital resolution: $\sigma = p/\sqrt{12}$

e.g. σ = 14 μm for p = 50 μm

Reminder: better resolution is achieved with analogue readout

Small pixel area ➔ low detector capacitance (~ few fF/pixel) ➔ large SNR (>> 10)

Small pixel volume ➔ low leakage current (~ few pA/pixel)

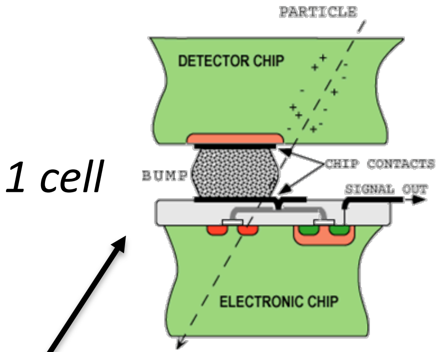

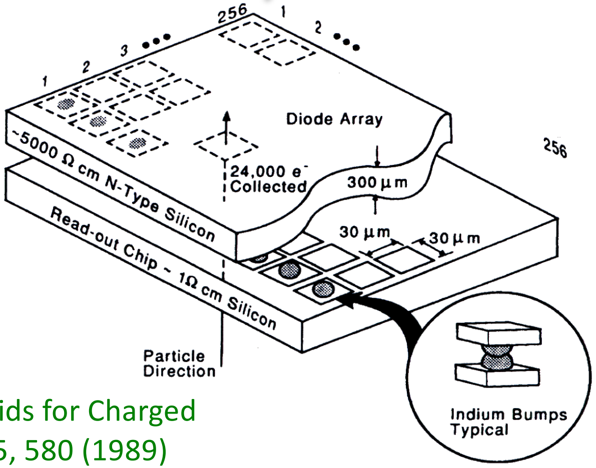

Drawbacks of HPD: large number of readout channels

DSSD ~ 2n

HPD ~ n^2

Large number of electrical connections in case of HPD

Large power consumptions of electronics

S.L. Shapiro et al., Si PIN Diode Array Hybrids for Charged Particle Detection, Nucl. Instr. Meth. A 275, 580 (1989)

HPD – bump bonding process

Electron microscope picture of pixel detector with long strip.
Left: Detector chip, right: readout chip with bump bonds applied.

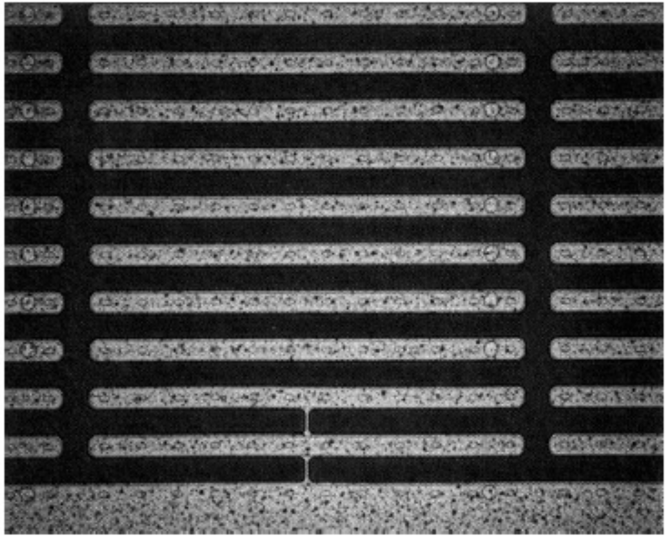

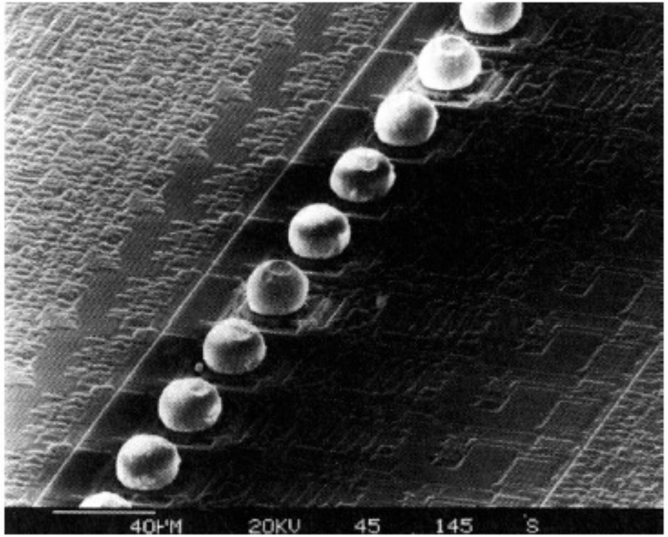

G. Lutz, *Semiconductor Radiation Detectors*, Springer-Verlag, 1999

Example: ATLAS IBL & Pixel Detector

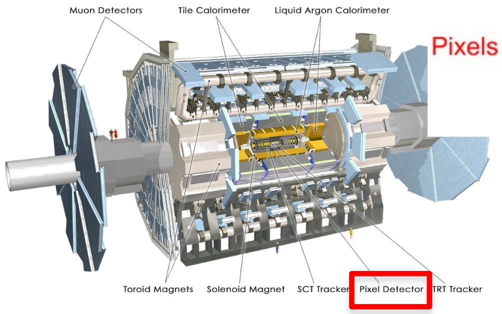

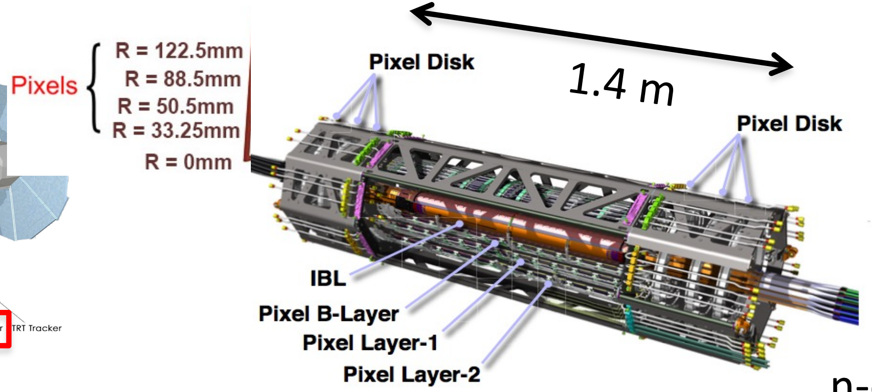

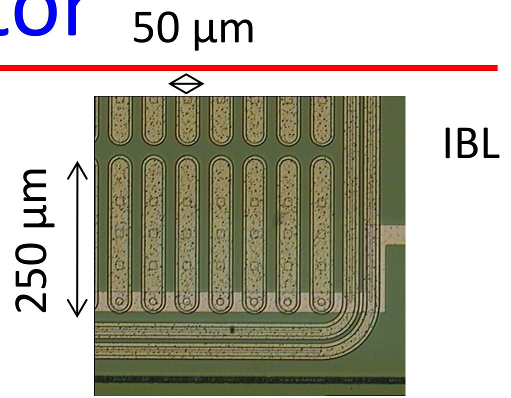

n-on-n. IBL/PX: w = 200-250 µm

80M readout channels

Average number of pixel hits per module per event for each layer vs number of pp collisions per bunch crossing

- IBL/PX: 26880/46080 pixels per module

A very “quiet” detector”!

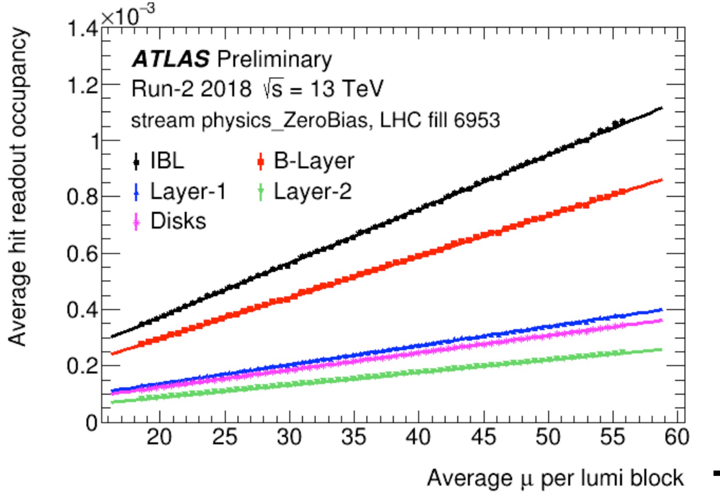

Example: ATLAS IBL & Pixel Detector

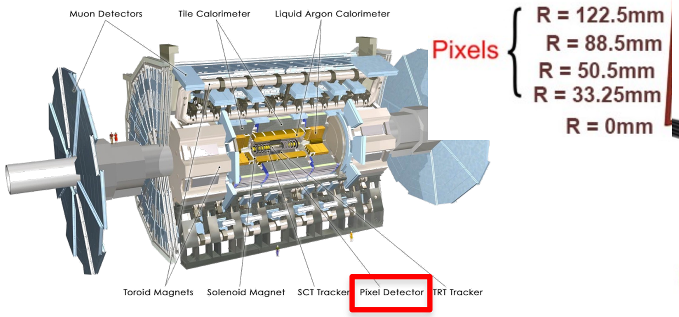

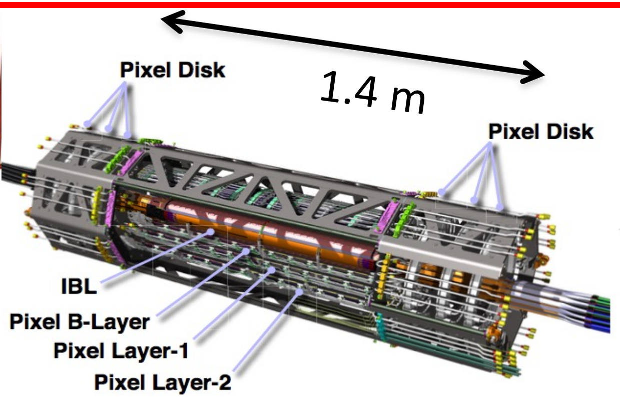

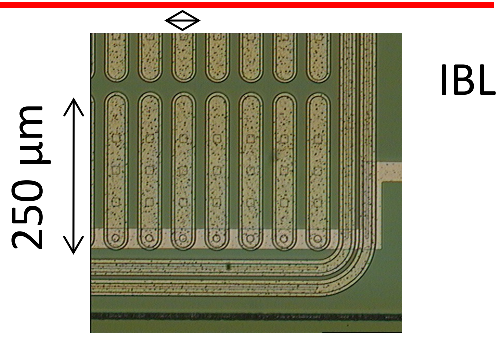

n-on-n, 200-250 µm

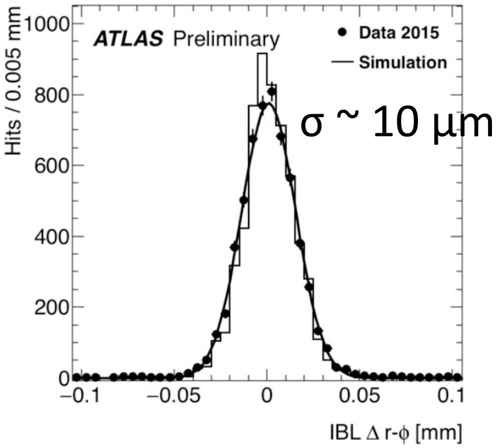

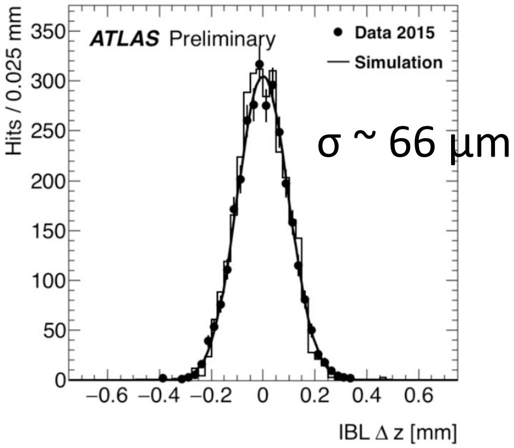

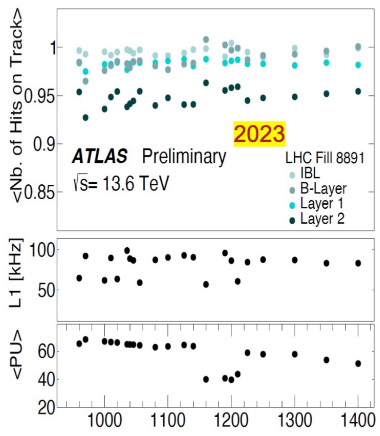

Efficiency high despite the radiation damage to sensors and electronics

Segmented silicon detectors

various design concepts

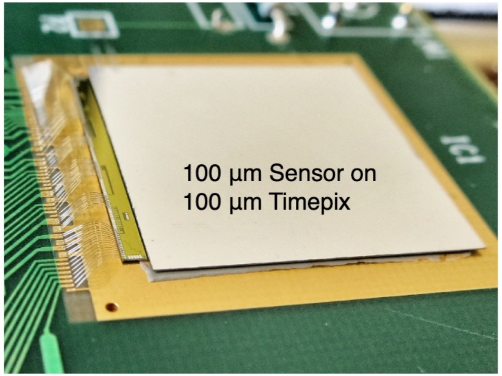

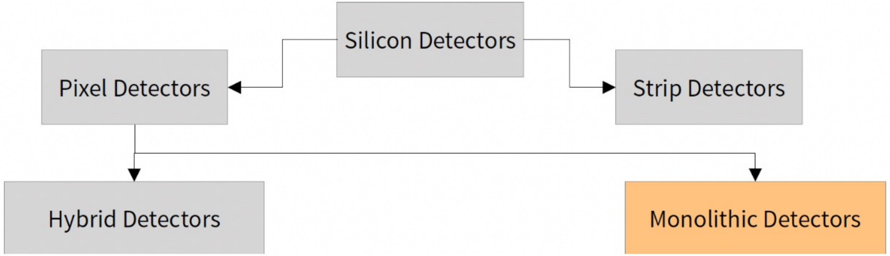

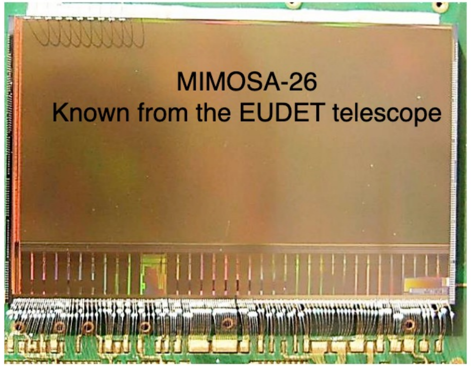

Sensor and readout chip separately optimised and tested before hybridisation

All-in-one approach: sensing volume with intelligence

at LHC beginning

	Hybrid pixels (2000)	MAPS (2000)
Single point resolution	~ 30 µm	~2 µm
Material budget	~ 500 µm Si	~ 50 µm Si
Time resolution	25 ns	~10 ms
Radiation hardness	$\sim 10^{15}\ n_{eq}/cm^2$	$10^{12}\ n_{eq}/cm^2$

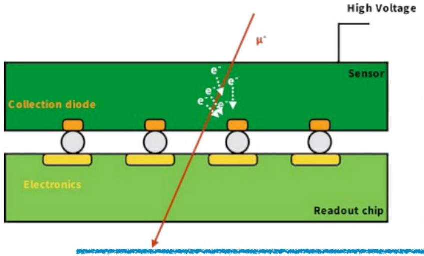

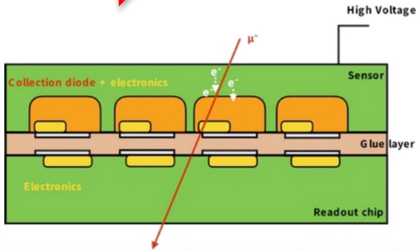

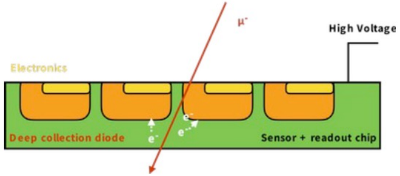

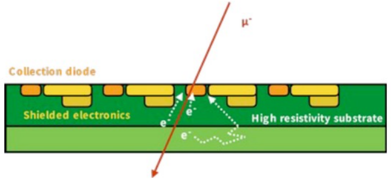

Displacement Damage

particle → *Si_S* → $E_K>25$ eV → 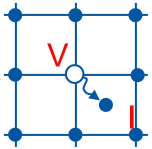

Vacancy + Interstitial → ..... *a wide range of **point defects***

$E_K>5$ keV → *point defects and clusters of defects*

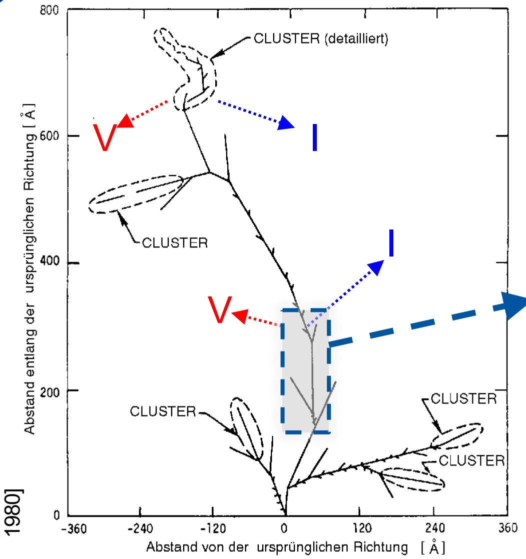

[van Lint 1980]

Can we see the defects?

HRTEM on Si: n-irradiated 10^{19} n_{eq}/cm^2

High Resolution Transmission Electron Microscopy

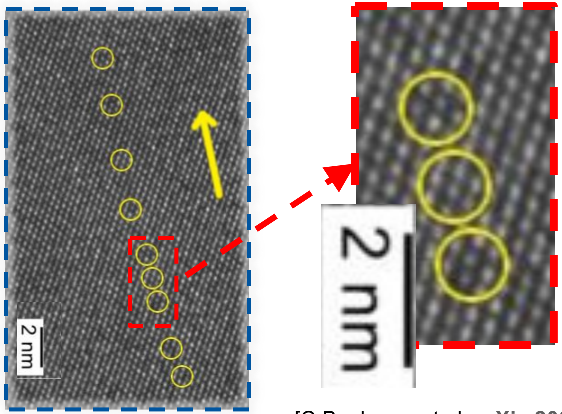

[C.Besleaga et al. arXiv 2021]

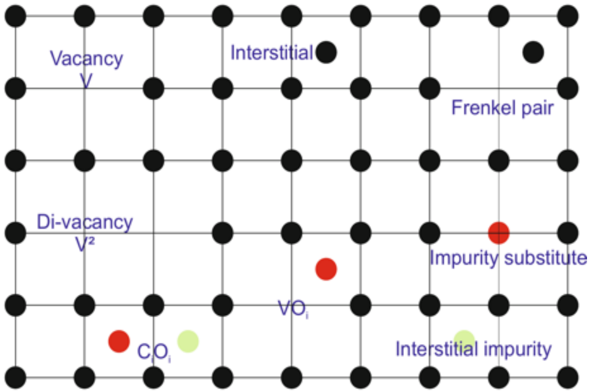

- example of point defect reactions:

V: $V+O \rightarrow VO;\quad V+P \rightarrow VP$ ← "dopant removal"

I: $I+C_S \rightarrow C_i \rightarrow C_i + O \rightarrow C_iO_i$

$I+B_S \rightarrow B_i \rightarrow B_i + O \rightarrow B_iO_i$

... many more reactions!

Radiation damage in Silicon

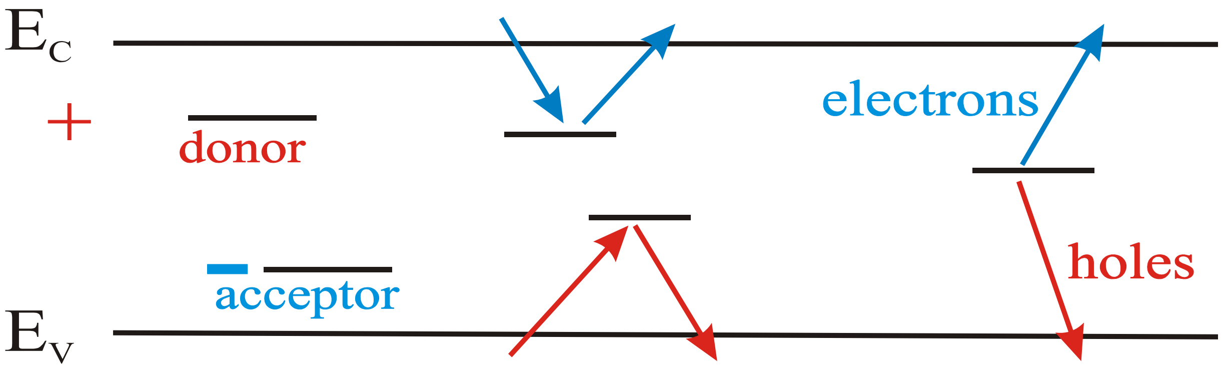

charged defects
⇒ N_{eff} , V_{dep}
e.g. donors in upper and acceptors in lower half of band gap

Trapping (e and h)
⇒ CCE
shallow defects do not contribute at room temperature due to fast detrapping

generation
⇒ leakage current
Levels close to midgap most effective

Radiation damage: macroscopic effects

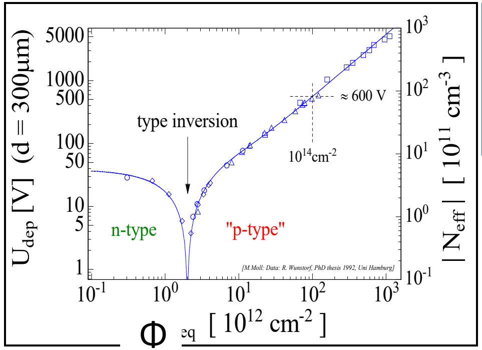

Depletion voltage increase

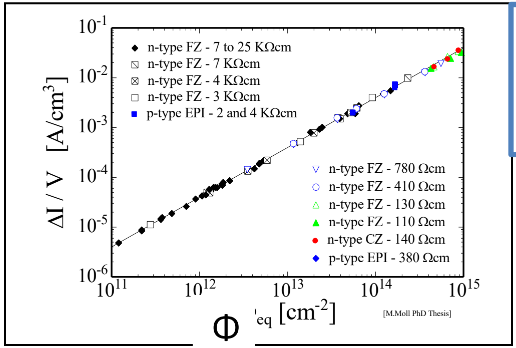

Leakage current increase

From LHC to HL-LHC upgrade

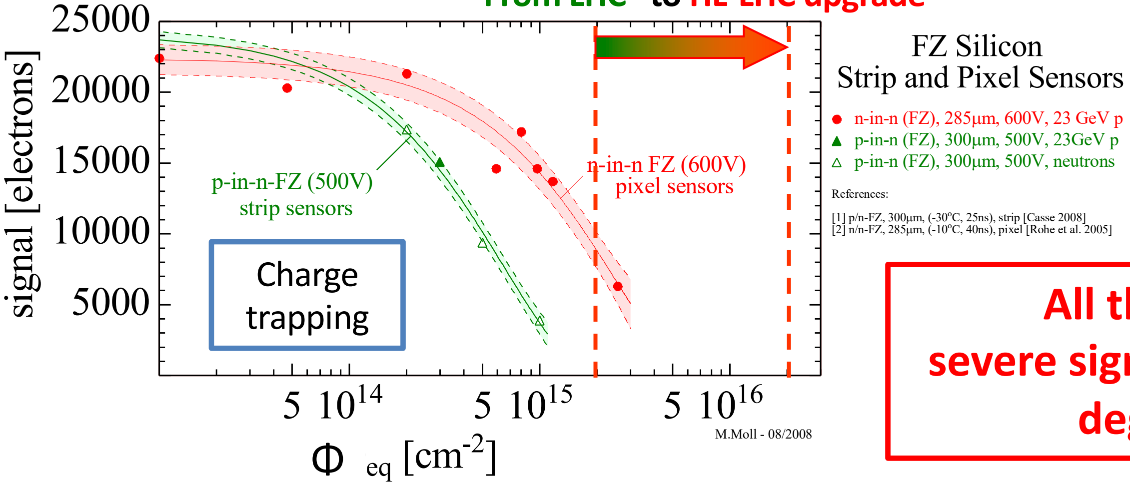

Charge trapping

All these mean: severe signal-to-noise-ratio degradation

3D sensor technology

S. Parker et. al. NIMA 395 (1997) 328

- “3D” electrodes:
  - narrow columns along detector thickness,
  - diameter: 10mm, distance: 50 - 100mm
- Lateral depletion:
  - lower depletion voltage needed
  - thicker detectors possible
  - fast signal
  - radiation hard: smaller collection path!

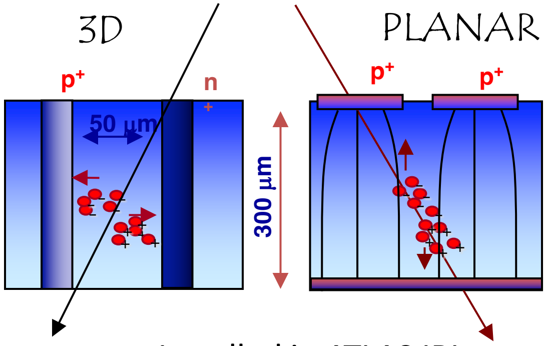

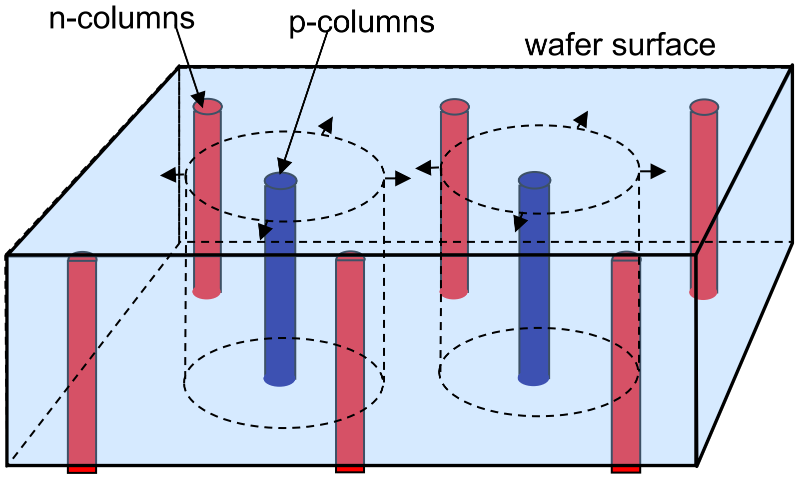

n-type substrate

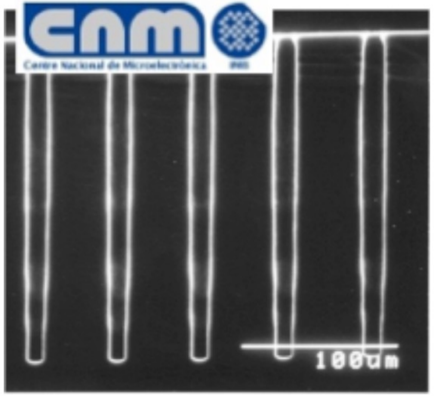

Installed in ATLAS IBL

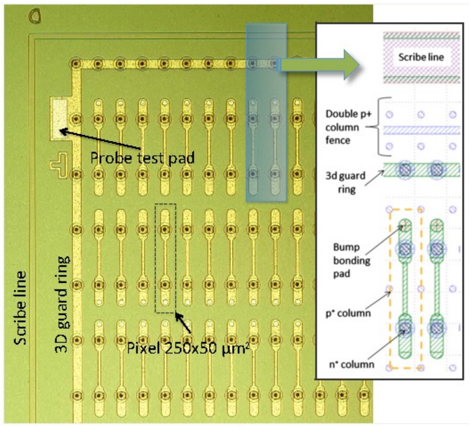

3D sensors in ATLAS IBL

ATLAS, 2024 JINST 19 P10008

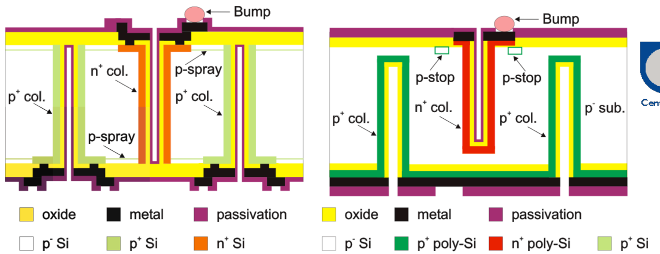

Figure 2. Pixel layout and schematic cross-sections of IBL 3D sensors from FBK (left) with columns passing fully through the substrate and CNM (right), where both column types stop about 20 μm from the surface. In both cases the substrate thickness is 230 μm and the inter-electrode spacing is 67.3 μm. Reproduced from [10]. Published under licence by IOP Publishing Ltd. All rights reserved.

First time in HEP experiment

Two vendors

Two designs

Superior radiation tolerance

Testbench for high luminosity phase

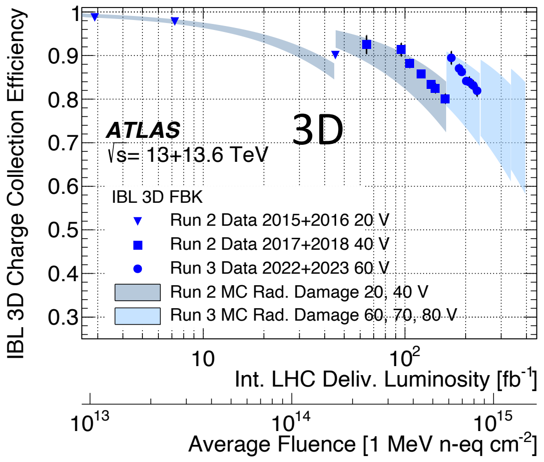

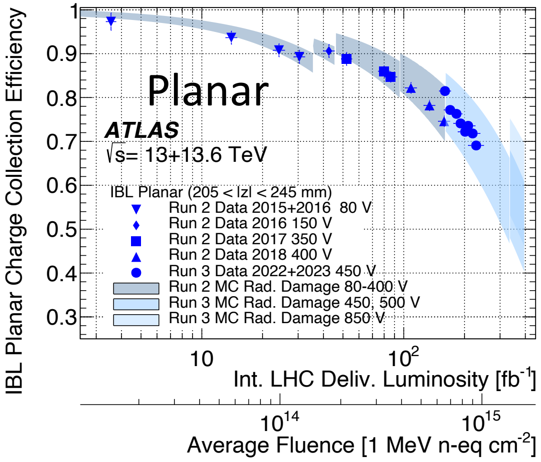

Other Si Detector Structures

Silicon (PIN) diodes, Silicon Single and Double Sided Strip detectors and Hybrid Pixels detectors are mature technologies employed in almost every experiment in High Energy Physics

Let's now look at other interesting Silicon Detector Structures

- Charged Coupled Devices (CCD)
- ~~Silicon Drift Detectors (SDD)~~ *not enough time*
- Avalanche Photo Diode (APD)
- Silicon Photo Multipliers (SiPM – or Pixelized Photon Detector (PPD) or Multi-Pixel Photo Counters (MPPC))

Intermezzo: the MOS structure

MOS: Metal Oxide Semiconductor
Gate: Metal (or Polysilicon)
Oxide: SiO_2, grown on substrate

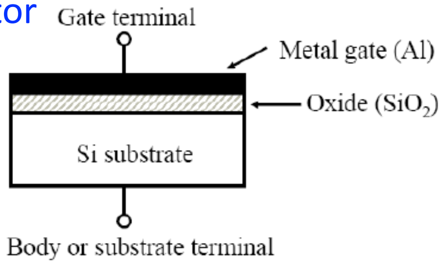

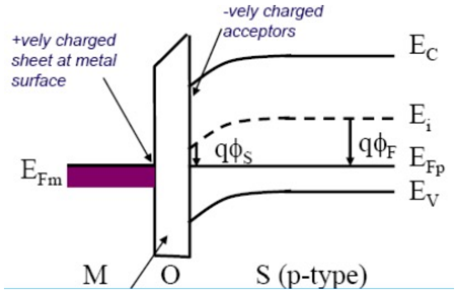

No applied voltage:
a charged MOS capacitor

3 states

Accumulation

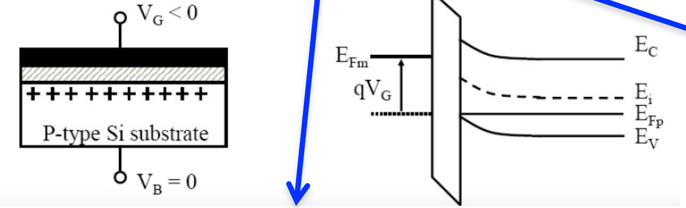

Depletion

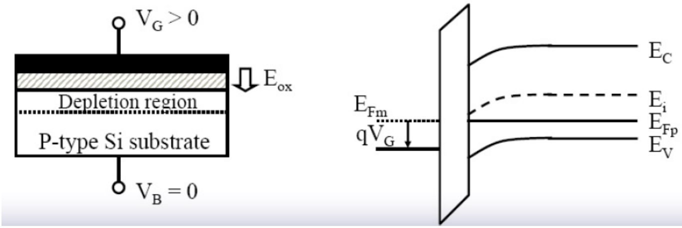

Inversion

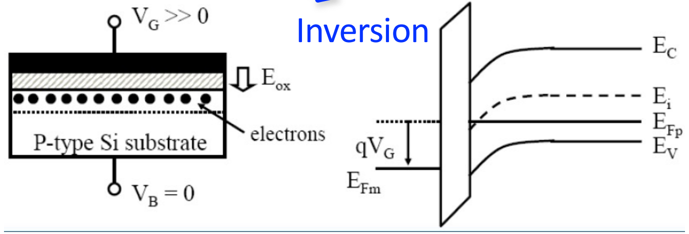

MOS CCDs detectors

Invented in 1969, CCDs have been used for a long time as memories (storing and transfer of charge) and as optical sensors (image devices in video cameras)

Most important field of application as detectors: imaging in Astrophysics, from near infrared to X-rays.

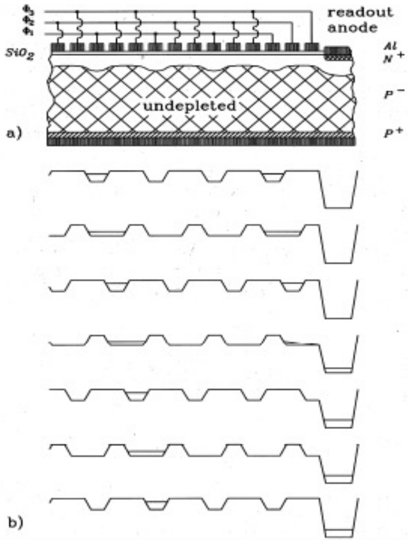

Conceptually: an array of MOS capacitors operated in overdepletion mode.

Electrons are created by ionization in the thin depleted region close to the silicon- oxide interface.

Charges are stored in the local energy minima at the Si-SiO_2 interface. The charge can be moved towards the collecting electrode by periodically switching the voltages ϕ1, ϕ2 and ϕ3.

Slow device, hence not suitable for fast detectors

Problem: charge losses during transport are high because of the large density of trapping defects at the Si-SiO2 interface.

CCDs for astronomy and astrophysics today

Scientific CCDs typically use the same 3-phase clocking as in the original Boyle and Smith concept with overlapping polysilicon gate electrodes (triple poly)

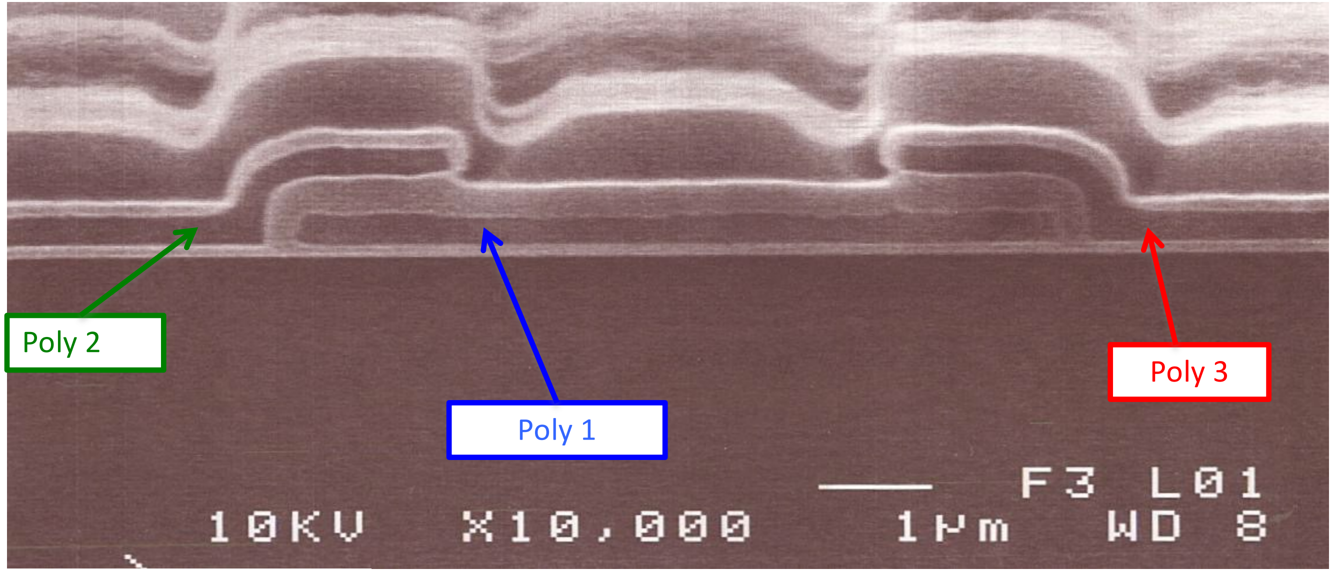

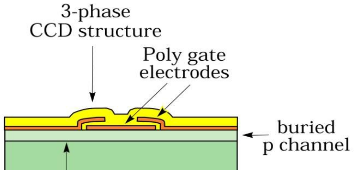

Scientific CCDs: front vs back illumination

Front illumination: Quantum efficiency loss from absorption in polysilicon gates

Reflections from complicated thin film stack

To overcome the problem of charge losses, the "buried channel" CCD (BCCD) has been developed.

An n-doping region shifts the electrons energy minimum from to the surface into the bulk

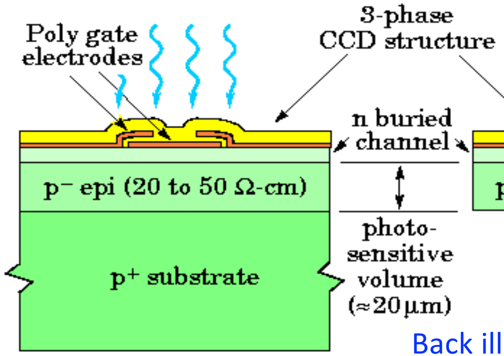

Back illumination of thinned CCDs

Remove p^+ substrate

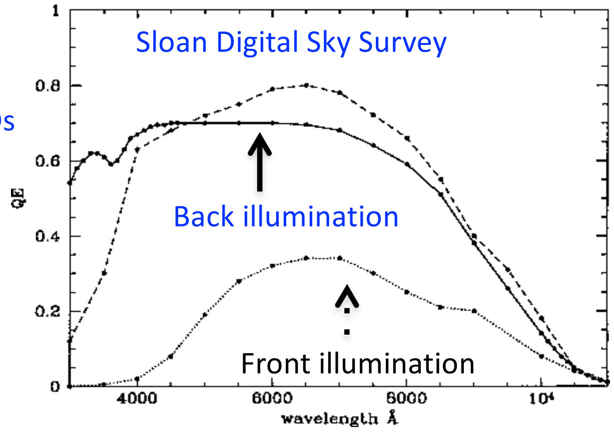

http://www.astro.princeton.edu/PBOOK/camera/camera.htm

Scientific CCDs for Astronomy

Scientific charge-coupled devices are the detector of choice for astronomy

Wavelength range: $\lambda \sim 350$ nm to 1100 nm (from atmospheric cutoff to Silicon bandagap)
➔UV, visible and near-infrared wavelengths

Back illuminated: for high QE ➔ up to 90% at peak

Slow readout for low noise: less than 5 e- at 100 kpixels/s readout

Cryogenically cooled for low dark current: for -100 ° C < t < -140 ° C few e-/pixel/hour

Quite expensive (10MPixel ~ 100k€)

In the following some examples of astronomy cameras

LSST: Large Synoptic Survey Telescope

The Large Synoptic Survey Telescope (LSST) is a ~~planned~~ wide-field "survey" telescope
It photographs the entire available sky every few nights
The telescope is located in northern Chile
Science first light in 2025 (this year!)

Some of the LSST Physics Goals:

Measure gravitational lensing for DE/DM detection
Map small objects in Solar System
(Super)Novæ detection
Milky Way mapping

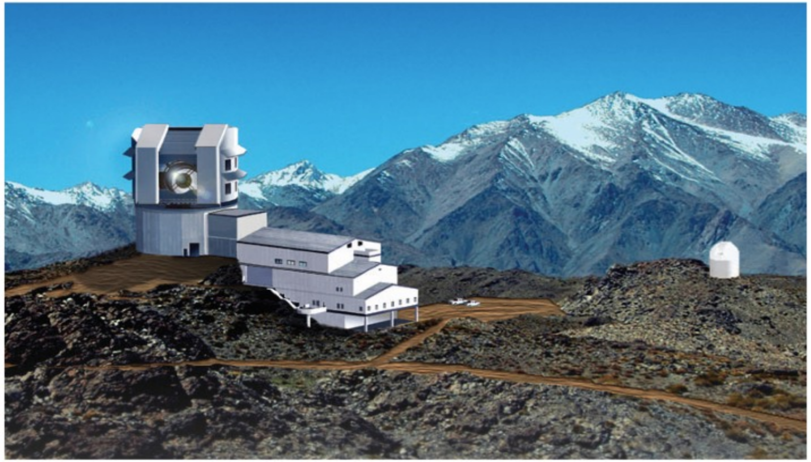

LSST Science Book
http://arxiv.org/pdf/0912.0201v1.pdf

LSST camera and CCDs

CCD sensors: deep depletion, back-illuminated devices
16 channels, r.o. in 2 seconds
t = -100 ° C

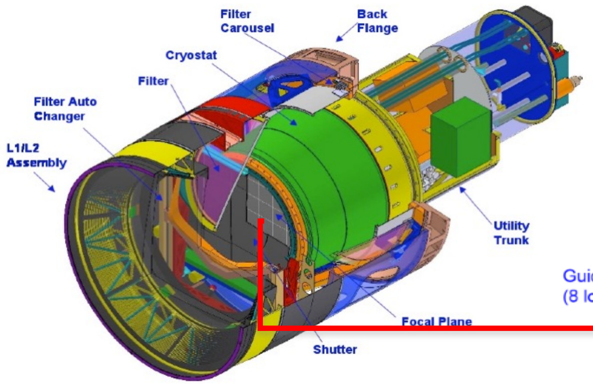

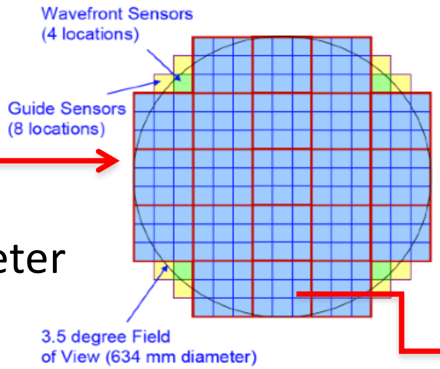

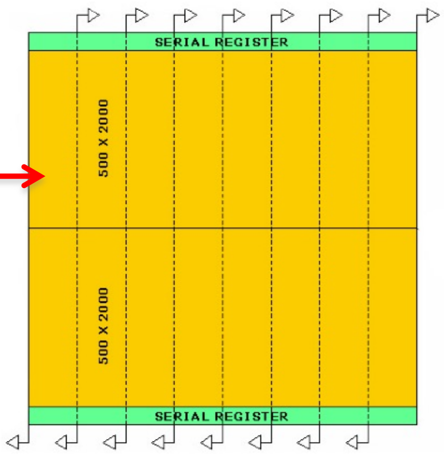

Focal plane: 0.64 m in diameter
9.6 deg^2 filed-of-view

3.2 Gpixels comprised of
189 4k x 4k 10µm pixels
➔ plate scale of 0.2”/pixel

LS

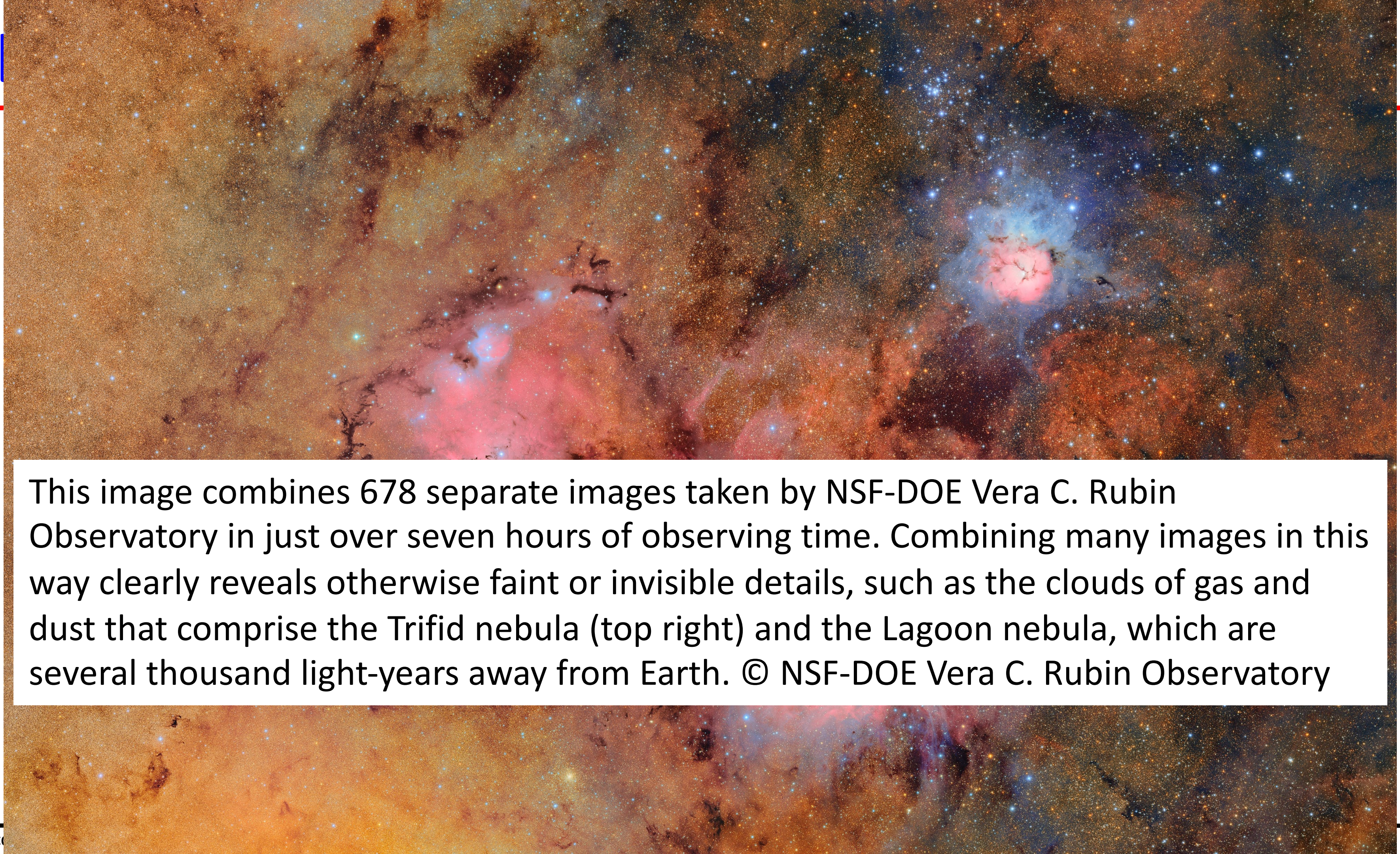

This image combines 678 separate images taken by NSF-DOE Vera C. Rubin Observatory in just over seven hours of observing time. Combining many images in this way clearly reveals otherwise faint or invisible details, such as the clouds of gas and dust that comprise the Trifid nebula (top right) and the Lagoon nebula, which are several thousand light-years away from Earth. © NSF-DOE Vera C. Rubin Observatory

Avalanche Photo Diodes (APDs)

The avalanche photodiode (APD): p-n device with internal gain due to the high internal field at the junction of positive and negative doped silicon

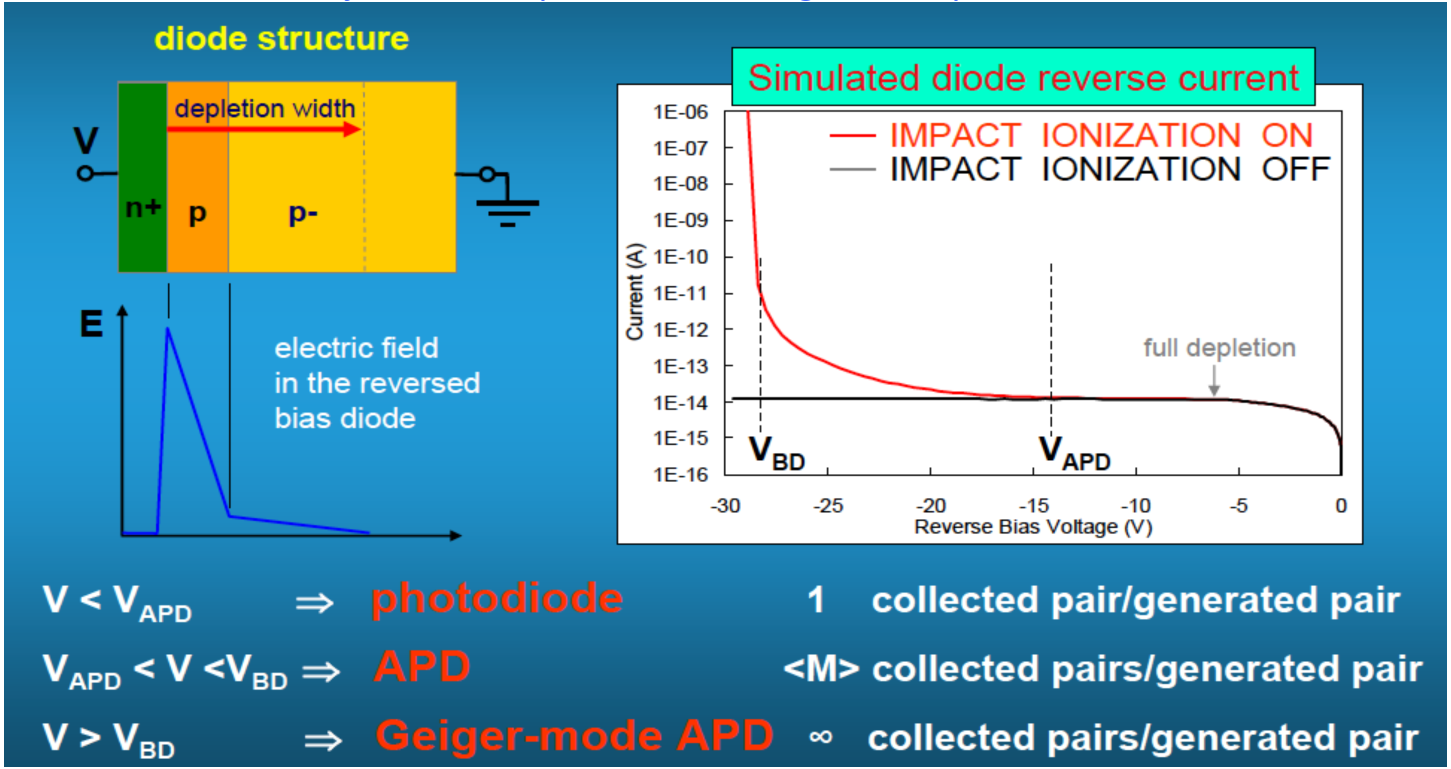

Silicon Photo Multiplier (SiPM)

A Silicon Photo Multiplier is a matrix of n pixels connected in parallel (e.g. few hundreds /mm^2) on a common Si substrate

Each pixels is a GM-APD in series with R_{quench}

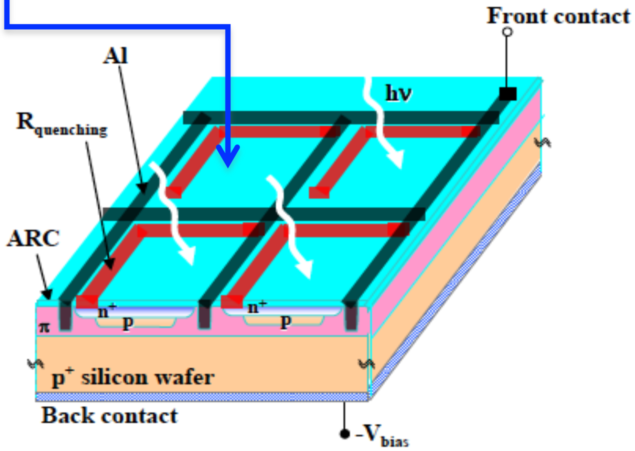

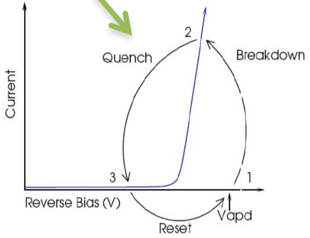

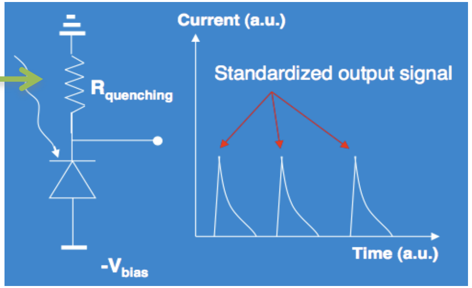

V.M. Golovin and A. Sadygov
(Russian patents 1996-2002)

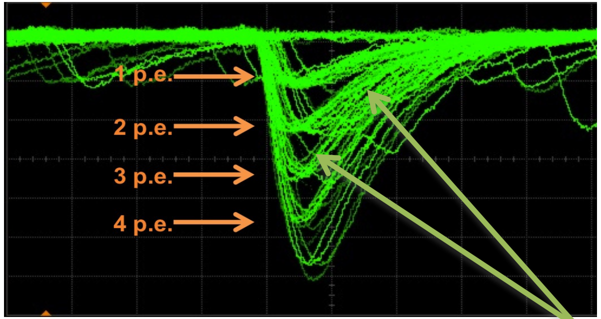

A single GM-APD gives no information about light intensity ➔ in a SiPM the output charge is proportional to the number of triggered cells, that is (for PDE = 1) the number of photons

SiPM features

The characteristics of a SiPM are:

- possibility to detect single photons and give a signal proportional to the number of photons for low fluxes;
- extremely fast response (determined by avalanche spreading): in the order of few hundreds of ps.

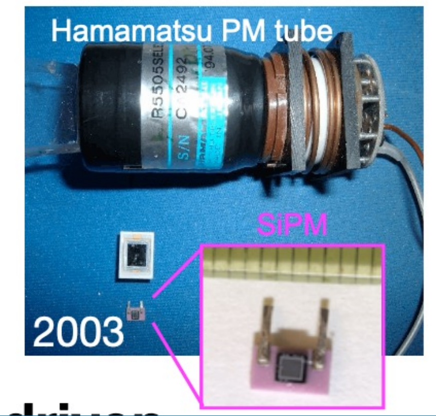

Other features are:

- Low bias voltage (20-60V)
- Low power consumption
- Insensitive to magnetic fields
- Compact and rugged

Possible applications are: scintillator read-out, PET, photon correlation studies, calorimetry…)

Example: T2K ND280

T2K: Measure ν_μ disappearance and ν_e appearance

N. Dinu, T. Gys, C. Joram, S. Korpar, Y. Musienko, V. Puill, D. Renker EDIT 2011

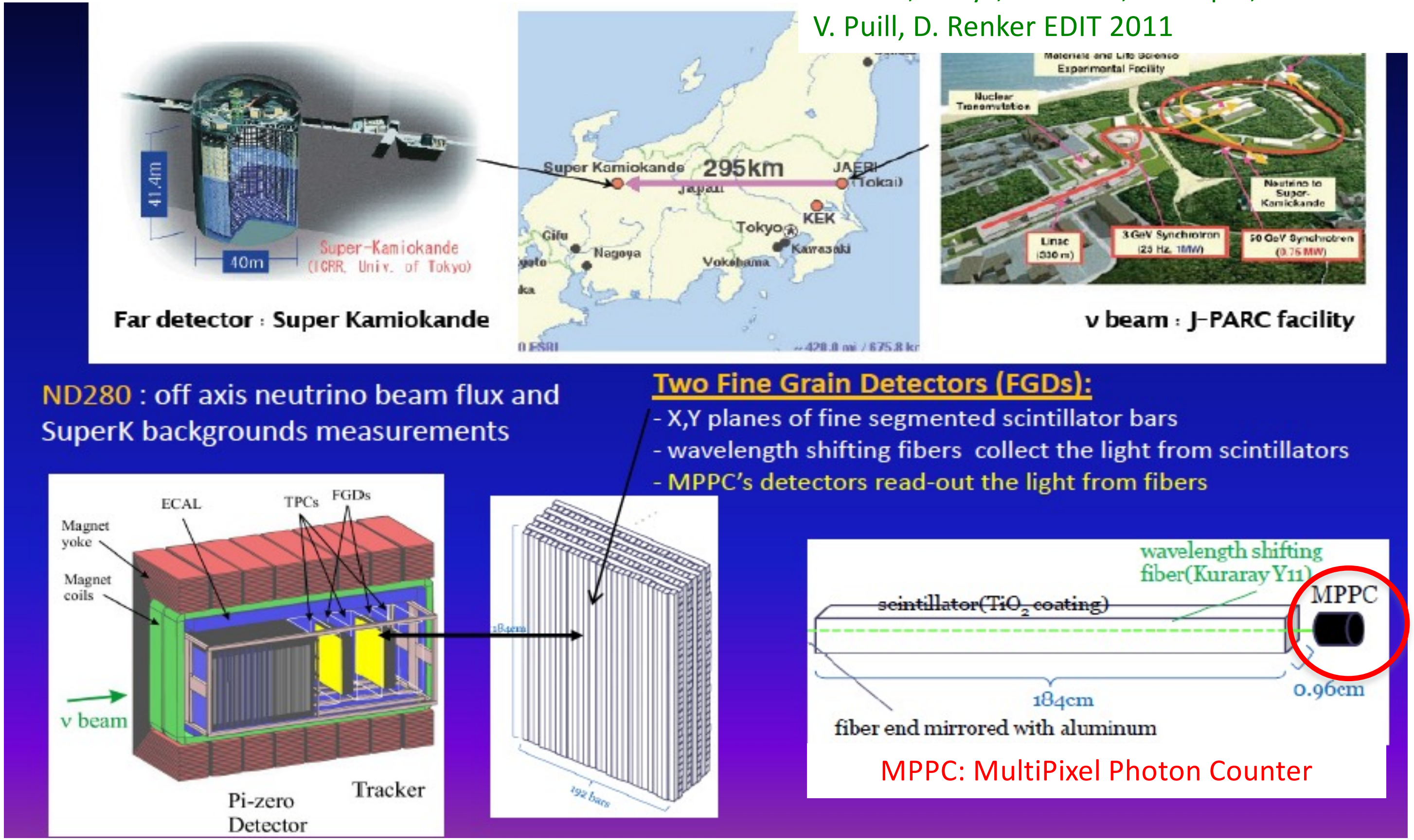

MPPC: MultiPixel Photon Counter

Example: T2K ND280

UPGRADED NEAR DETECTOR ND280: CONFIGURATION

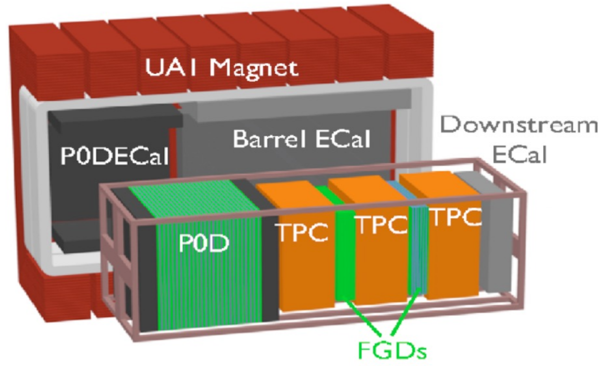

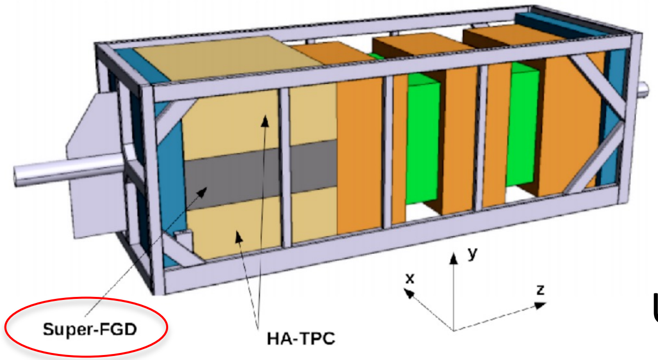

Upgraded

- 2 new High Angle TPC (HA-TPC)
- New Time Of Flight detector (TOF)
- 1 Super-fine-grained-detector (super-FGD) => the core of the detector where the LLR is involved

NGUYEN Quoc Viet

7

Example: T2K ND280

SUPER FGD DETECTOR

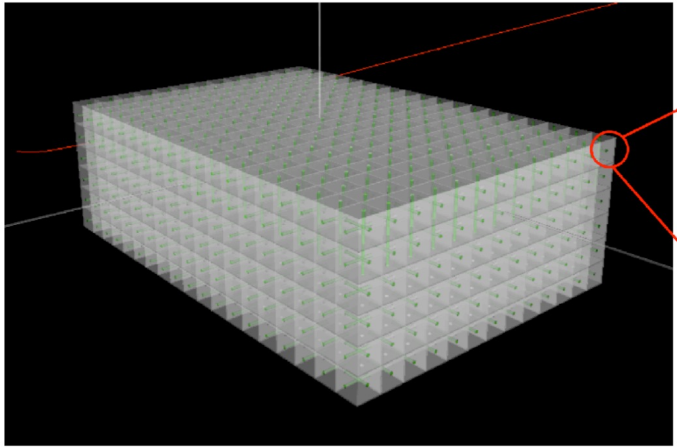

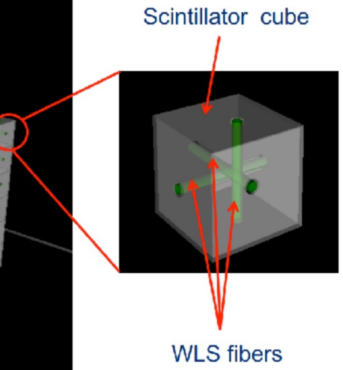

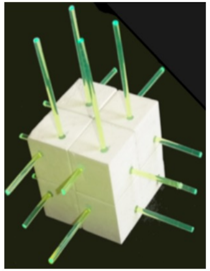

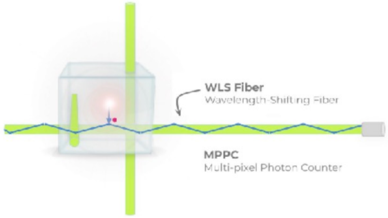

- Super-FGD: 192 × 192 × 56 scintillator cubes (2 million) with 3D readout => 2 tons of fully active target

- Wavelength shifting (WLS) fibers are used to collect light from scintillator cubes. (70 km of WLS fiber in total)
- One end of the fibers is connected to a Multi-Pixel Photon Counter (MPPC) the other end is mirrored. => around 60.000 channels.

Outline

- Main applications, motivations and history
- Semiconductors physics
- Silicon radiation detectors
- Timing with silicon detectors
- Perspectives

Time resolution of silicon sensors

Werner Riegler, CERN, werner.riegler@cern.ch

October 15, 2021

W. Riegler, CERN seminar

Abstract

Precision timing with solid state detectors is being employed in many areas of particle physics instrumentation. Applications for pileup rejection and time of flight measurements at the LHC are just two of many notable examples.

During the past years the principal contributions to the time resolution for various types of silicon sensors have been studied. The principal contributors to the time resolution are Landau fluctuations, electronics noise, signal shape fluctuations due to a varying pad response function as well as gain fluctuations.

We discuss silicon pad and silicon pixel sensors, LGAD sensors as well as SPADs and SiPMs. These sensors have been simulated using the Garfield++ toolkit. The analytic statistical analysis of the contributions to the time resolution has been performed, resulting in elementary expressions for the timing performance of these sensors. These expressions show the basic directions for optimization of these sensors as well as the fundamental limits to the time resolution.

Time resolution of silicon sensors W. Riegler, CERN seminar

Intrinsic time resolution of a 'large' silicon pad detector

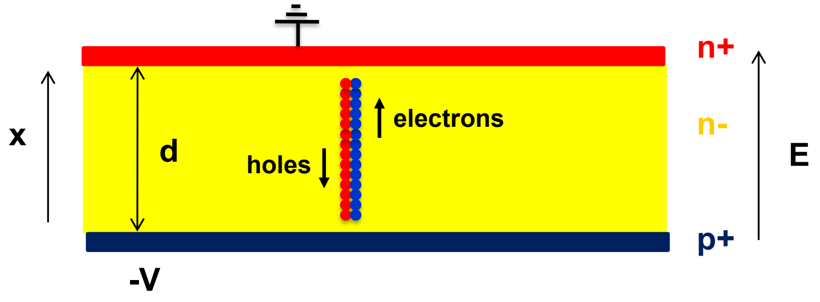

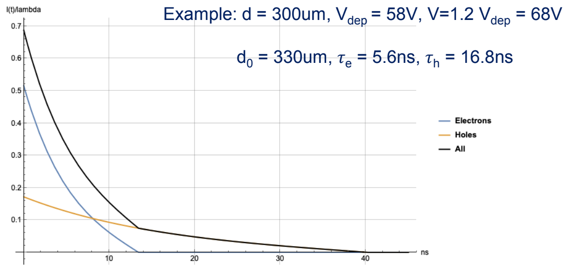

In silicon sensors the signal edge is instantaneous (i.e. sub ps level)

- acceleration of electrons to 10^7cm/s in vacuum is 0.14ps
- passage of the particle through a 50um sensor takes 0.16ps

In Wire Chambers the electrons first have to move to the wires before an avalanche at the wire leads to an appreciable signal
→ intrinsic resolution limit.

In RPCs the avalanche starts instantly, but it still takes some time until the signal reaches the threshold
→ intrinsic resolution limit.

→ The intrinsic time resolution of a silicon sensor is infinite (sub ps).

→ The time resolution in a planar silicon sensor without gain is a question of signal/noise/electronics and specifically the Landau fluctuations within the electronics integration time.

Electronics processing of a detector signal

Signal duration of T i.e. f(t) = 0 for t>T

Electronics peaking time t_p >> T

We are interested in times t>T

$$
\begin{aligned}
v(t) &= \int_0^t h(t-t')f(t')dt' \\
&\approx \int_0^T \left[h(t) - h'(t)t'\right] f(t')dt' \\
&= h(t)\int_0^T f(t')dt' - h'(t)\int_0^T t' f(t')dt' \\
&= \int_0^T f(t')dt' \left[h(t) - h'(t)\frac{\int_0^T t' f(t')dt'}{\int_0^T f(t')dt'}\right] \\
&= q\left[h(t) - h'(t)t_{cog}\right] \\
&= q\,h(t-t_{cog})
\end{aligned}
$$

In case the electronics peaking time t_p is longer than the signal duration T, the electronics output signal has

- the same shape as the delta response
- a pulse-height equal to the total charge of the signal
- a 'time displacement' of this delta response by the center of gravity time t_{cog} of the signal.

→ An amplifier that is 'slower' than the signal measures the center of gravity time of the signal

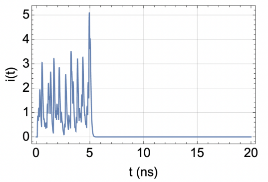

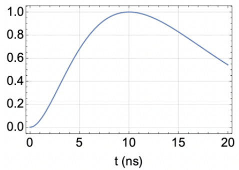

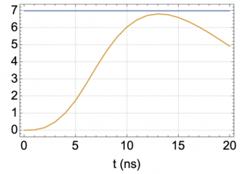

$$
q = \int_0^T f(t')dt' \qquad t_{cog} = \frac{\int_0^T t' f(t')dt'}{\int_0^T f(t')dt'} = \frac{1}{q}\int_0^T t' f(t')dt'
$$

W. Riegler, CERN seminar

Electronics 'slower' than the detector signal, time slewing

Delta response shifted by t_{cog} and scaled by Q

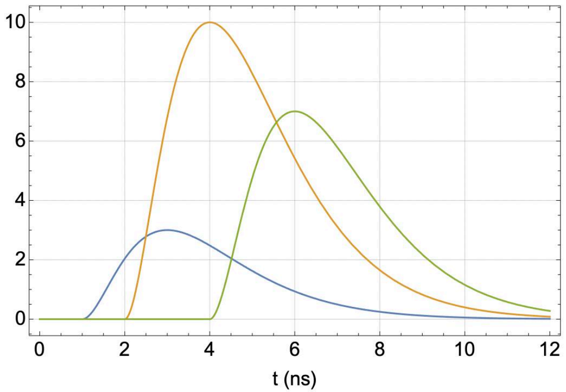

'time slewing'

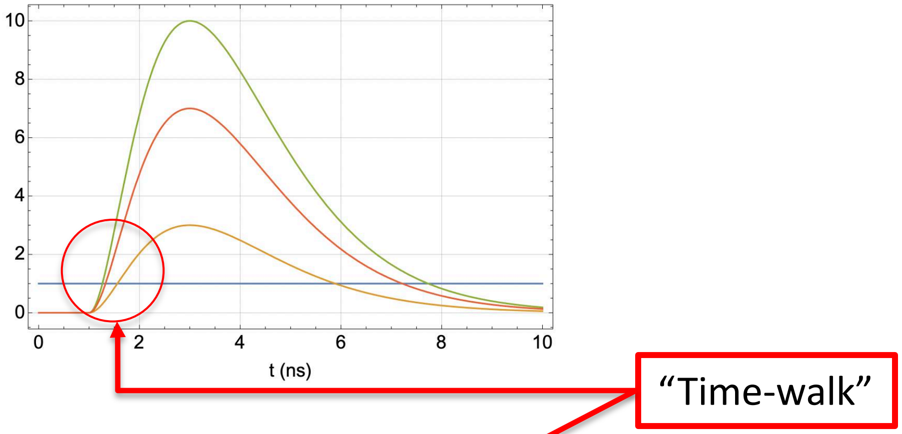

Signal normalized to same amplitude → time

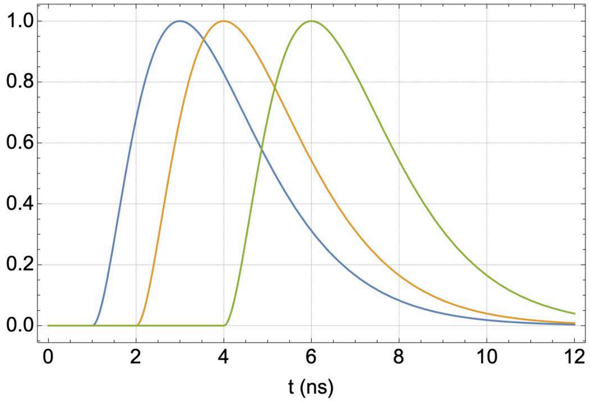

There are many different ways to correct for this slewing effect

- Constant Fraction discrimination
- Standard discrimination using time over threshold to correct for pulse-height
- Standard discrimination + pulseheight to correct for pulse-height
- Standard discrimination + total charge to correct for pulse-height
- Multiple sampling and 'fitting' the know signal shape
- ….

→ What is the c.o.g. time resolution of a silicon sensor ?

W. Riegler, CERN seminar

Center of gravity time of a silicon detector signal

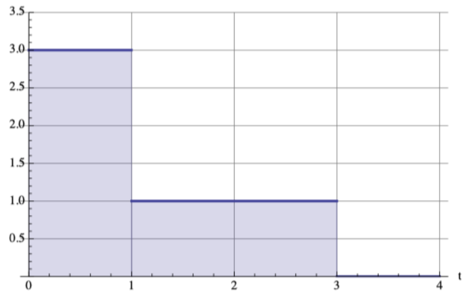

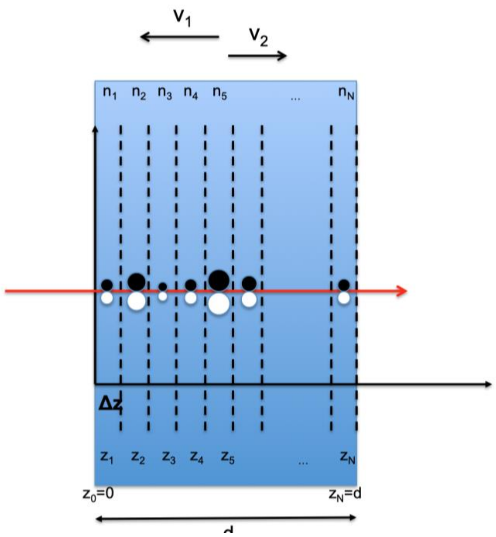

Single e-h pair

$$i(t) = -\frac{qv_1}{d}\Theta(z/v_1 - t) - \frac{qv_2}{d}\Theta((d-z)/v_2 - t) \tag{4.1}$$

with $\Theta(t)$ being the Heaviside step function. An example is shown in figure 3b. We have $\int i(t)dt = -q$ and according to eq. (3.1) the centroid time of this signal is then

$$\tau = \frac{1}{2d}\left[\frac{z^2}{v_1} + \frac{(d-z)^2}{v_2}\right] \tag{4.2}$$

If $n_1, n_2, \ldots, n_N$ charges are produced at positions $z_1, z_2, \ldots, z_N$ and are moving to the electrodes with v_1 and v_2, the resulting centroid time of the signal is

$$\tau(n_1, n_2, \ldots, n_N) = \frac{1}{2d\left(\sum_{k=1}^N n_k\right)}\sum_{k=1}^N n_k\left[\frac{z_k^2}{v_1} + \frac{(d-z_k)^2}{v_2}\right] \tag{4.3}$$

We now divide the sensor of thickness d into N slices of $\Delta z = d/N$ as shown in figure 1. The probability to have n_k e/h pairs in slice k is given by the Landau distribution $p(n_k, \Delta z)$ and if we

After some lengthy evaluation:

$$\Delta_\tau^2 = \overline{\tau^2} - \overline{\tau}^2 \tag{4.4}$$

with $\overline{\tau}$ and $\overline{\tau^2}$ being the average and the second moment of τ. The evaluation is given in B and we find

$$\Delta_\tau = w(d)\sqrt{\frac{4}{180}\frac{d^2}{v_1^2} - \frac{7}{180}\frac{d^2}{v_1 v_2} + \frac{4}{180}\frac{d^2}{v_2^2}} \tag{4.5}$$

with

$$w(d)^2 = \frac{d}{\lambda}\int_0^\infty\left[\int_0^\infty \frac{n_1^2\, p_{\mathrm{clu}}(n_1)}{(n_1+n)^2}dn_1\right]p(n,d)dn \tag{4.6}$$

W. Riegler, CERN seminar

Center of gravity time resolution for silicon sensors

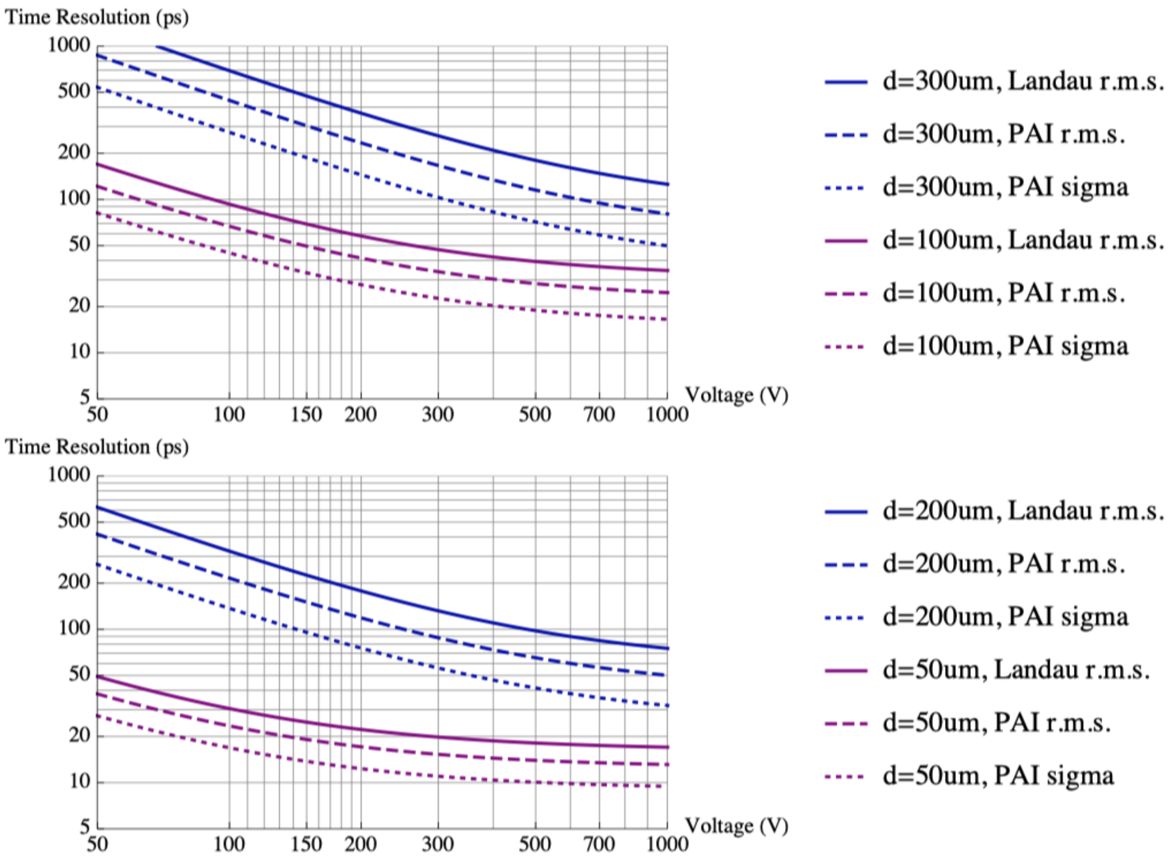

50um sensor, 10ps

[W. Riegler, CERN seminar]

Noise and Optimum filters

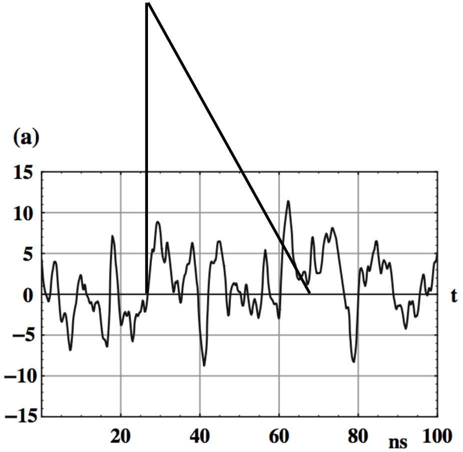

$$\sigma_{time} = \frac{\sigma_{noise}}{k} \qquad k = \frac{\Delta v}{\Delta t}$$

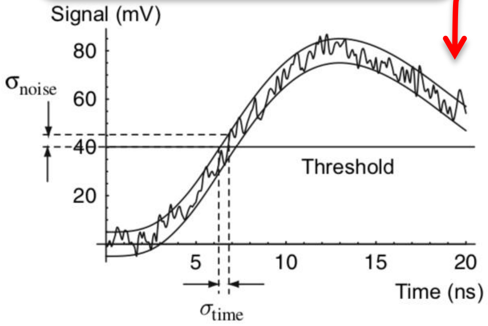

Let us assume we have a signal f(t) with superimposed noise of a given noise power spectrum and we want to find the amplifier transfer function that maximizes

- the signal to noise ratio for the best amplitude measurement, or
- the slope to noise ratio for the best time measurement

→ Theory of optimum filters

W. Riegler, Detector Signals 18

[W. Riegler, CERN seminar]

Optimum filter for best slope to noise ratio

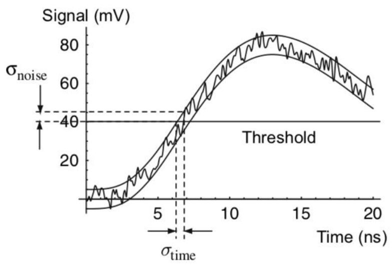

$$\sigma_{time} = \frac{\sigma_{noise}}{k} \qquad k = \frac{\Delta v}{\Delta t}$$

We want to minimise the time resolution i.e. maximise the slope to noise

$$\left(\frac{k}{\sigma}\right)^2 = \left(\frac{g'(t_m)}{\sigma}\right)^2 = \frac{1}{\pi}\frac{\left(\int_{-\infty}^{\infty} i\omega F(i\omega)H(i\omega)e^{i\omega t_m}d\omega\right)^2}{\int_{-\infty}^{\infty} w(\omega)|H(i\omega)|^2 d\omega}.$$

Following the steps from before we find an upper bound for the slope to noise ratio of

$$\left(\frac{k}{\sigma}\right)^2 \leq \frac{2}{\pi}\int_0^{\infty}\frac{|\omega F(i\omega)|^2}{w(\omega)}d\omega$$

And the optimum transfer function as well as the output signal are

$$H(i\omega) = i\omega\frac{F^*(i\omega)}{w(\omega)}e^{-i\omega t_m} \qquad G(i\omega) = i\omega\frac{|F(i\omega)|^2}{w(\omega)}e^{-it_m\omega}.$$

Since multiplication with iω refers to the derivative in the time domain we have the following relation:

The filter maximising the slope to noise ratio, i.e. the filter giving the best time resolution, is equal to the time derivative of the filter that maximises the signal to noise ratio !

W. Riegler, CERN seminar

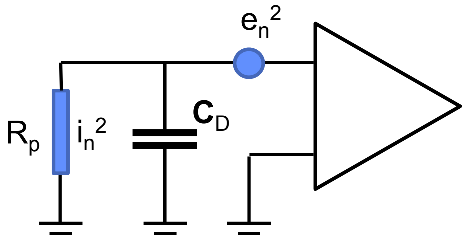

Realistic preamp transfer function

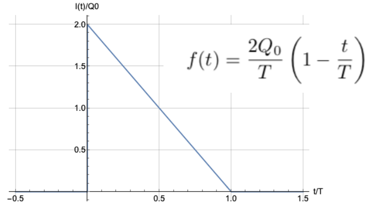

Preamp delta response

$$h(t) = e^n n^{-n} \left(\frac{n\,t}{t_p}\right)^n e^{-nt/t_p} \qquad H(i\omega) = \frac{t_p e^n n!}{(n + i\omega t_p)^{n+1}}$$

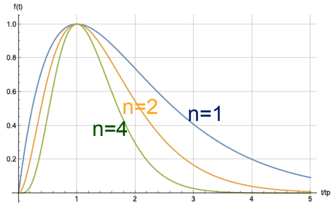

For the noise we assume series noise and parallel noise together with a detector capacitance C_D

$$\sigma^2(t_p) = \frac{1}{2\pi}\int_0^\infty w(\omega)|H(i\omega)|^2 d\omega = a^2 K_p t_p + b^2 \frac{K_s}{t_p}$$

$$K_p = \frac{1}{2}\left(\frac{e}{2n}\right)^{2n}(2n-1)!$$

$$K_s = \frac{1}{2}\left(\frac{e}{2n}\right)^{2n} n^2 (2n-2)!$$

The output signal is

$$g(t) = \int_0^t h(t-t')g(t')dt'$$

And the maximum slope evaluates to

$$k(t_p) = \frac{2Q_0}{T^2}\frac{e^n}{n^{n+1}}\left(e^{-nt/t_p} nT(nt/t_p)^n - t_p n! + t_p \Gamma(n+1, nt/t_p)\right)$$

$$\lim_{t_p \to 0} k(t_p) = \frac{2Q_0}{T}$$

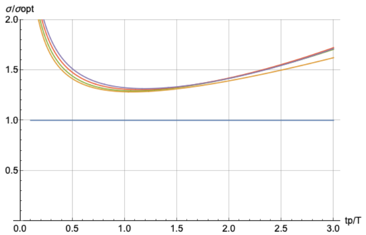

To find the optimum peaking time and best time resolution we therefore have to minimise the function

$$\frac{\sigma(t_p)^2}{k(tp)^2} \quad \rightarrow \quad min.$$

W. Riegler, CERN seminar

Realistic preamp transfer function

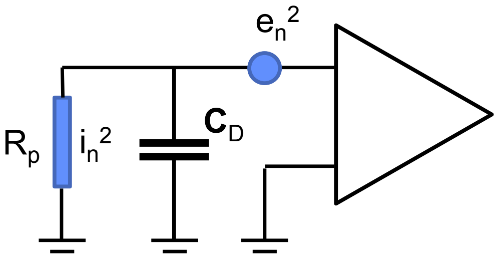

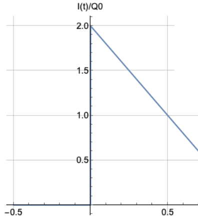

$$f(t) = \frac{2Q_0}{T}\left(1 - \frac{t}{T}\right)$$

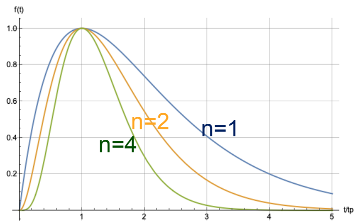

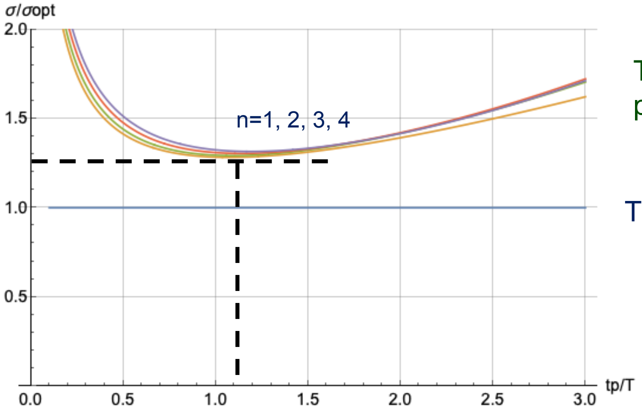

Time resolution for ‘standard’ preamp delta response.

Time resolution with optimum filter

Neglecting parallel noise (which is a good approximation in most practical applications) the optimum electronics peaking time t_p is between T and 1.5T.

The achieved time resolution is only about 30% worse than the best achievable one with the optimum filter !

This will give the smallest noise contribution to the time resolution.

W. Riegler, CERN seminar

Combined effect of Landau fluctuations and noise

If the noise dominates, the optimum peaking time is about t_p ~ 1-1.5T

If the noise is at a similar level to the contribution from Landau fluctuations, the optimum peaking time is still around the same level t_p ~ 1-1.5T and the time resolution is equal to the the c.o.g. time resolution of the silicon sensor.

If the noise is subdominant, shorter peaking times can be improve the time resolution, but with the divergence of the noise contribution at low t_p this will not reach far below the c.o.g. time resolution.

In short: t_p ~ T and $\sigma = \sigma_{c.o.g.} \oplus \sigma_{noise}$ give a good order of magnitude for the achievable time resolution

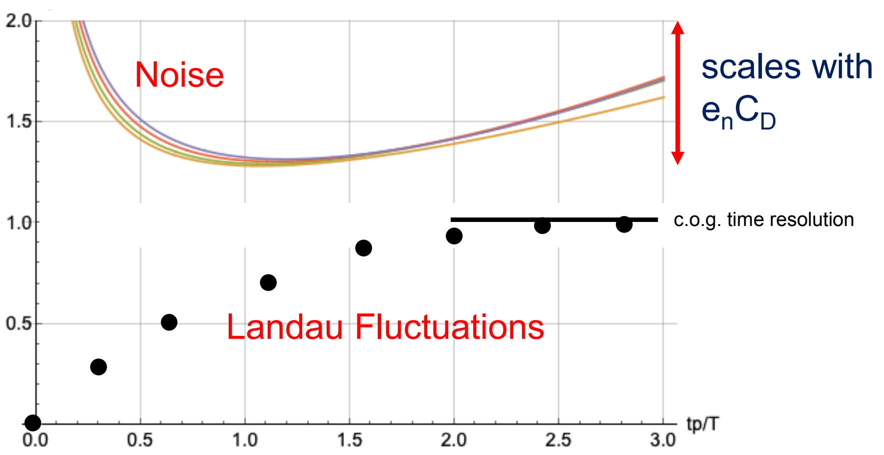

Landau Fluctuations ⊕ Noise

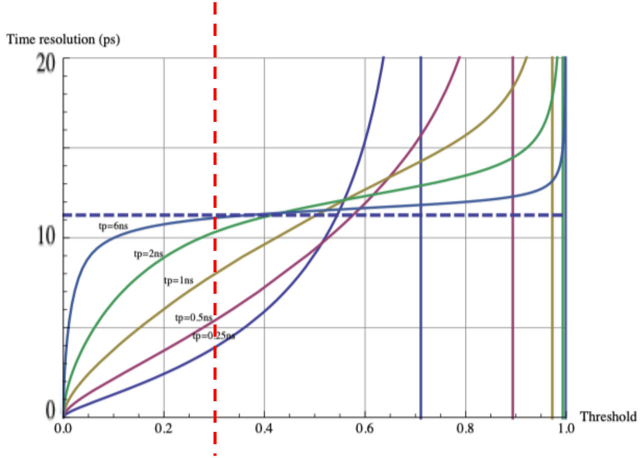

W. Riegler, CERN seminar

Time resolution of 'standard' silicon sensors

In case noise is not dominant, the time resolution of a silicon sensor is somewhere between zero and the c.o.g. time resolution.

For a silicon detector signal with total duration T, the series noise contribution is minimised for amplifiers of $t_p \sim T$.

For very low noise a time resolution better than the c.o.g. time resolution can be achieved, but the divergence of the noise contribution for $t_p \rightarrow 0$ will limit this improvement.

$$\Delta_\tau = w(d)\sqrt{\frac{4}{180}\frac{d^2}{v_1^2} - \frac{7}{180}\frac{d^2}{v_1 v_2} + \frac{4}{180}\frac{d^2}{v_2^2}}$$

$$w(d)^2 = \frac{d}{\lambda}\int_0^\infty \left[\int_0^\infty \frac{n_1^2\, p_{\mathrm{clu}}(n_1)}{(n_1+n)^2}\, dn_1\right] p(n,d)\, dn$$

W. Riegler, CERN seminar

Time resolution of ‘standard’ silicon sensors

No time di discuss segmented sensors…

Good time resolution demands thin sensors.

Thin sensors give small charge and large capacitance i.e. unfavorable S/N and k/N.

Capacitance can be reduced by making the pixels small.

If the pixel size is in the same order as the sensor thickness, the weighting field fluctuations start to dominate … and there will be many channels …

… between a rock and a hard place …

→ Sensors with internal gain to overcome the noise limit (like gas detectors !)

→ Turn the by sensor 90 degrees and realise a parallel plate geometry in 3D !
(see slide 62, 63)

[W. Riegler, CERN seminar]

Avalanche Photo Diode, Low Gain Avalanche Diode

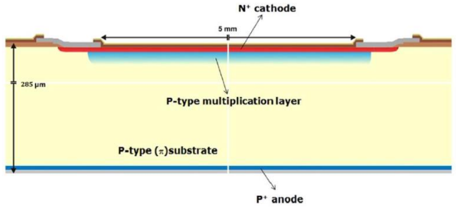

ure 2.2. Cross-section of the core layout of LGAD. A p-type layer is diffused below t

Idea goes back to the 1960ies.

A high field region is implemented in a silicon sensor by doping.

Electrons will produce an avalanche in this high field region.

The high field region is implemented by doping and related 'space-charge' in the volume.

The sensor is operated in a region where there is electron multiplication but not yet hole multiplication.

This allows to have thin sensors (high field, short signal) but still have enough signal charge to overcome the limitation from noise.

For higher fields → electron+hole multiplication → avalanche divergence → quench resistor → SiPM

W. Riegler, CERN seminar

Avalanche Photodiode

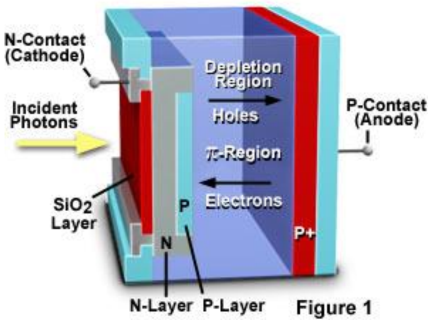

Figure 1

IEEE TRANSACTIONS ON ELECTRON DEVICES, JUNE 1972

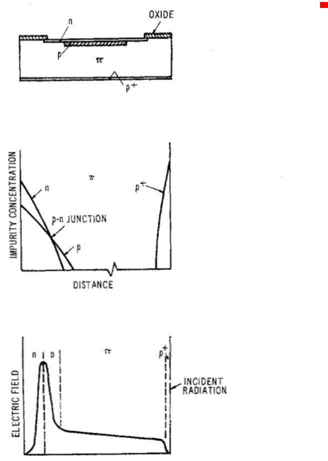

Fig. 1. Sketeches of reach-through avalanche-diode structure impurity-concentration profile, and electric-field distribution.

Electron (alpha) and hole (beta) multiplication coefficient in silicon

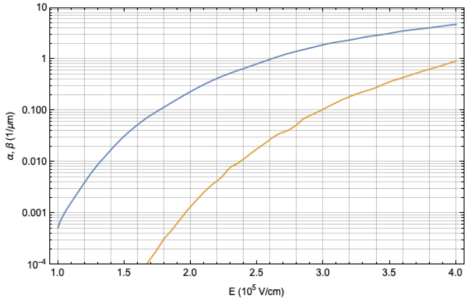

AvalanchePhotoDiode

Nuclear Instruments and Methods in Physics Research A 796 (2015) 141–148

Design optimization of ultra-fast silicon detectors

N. Cartiglia [a,*], R. Arcidiacono [c], M. Baselga [e], R. Bellan [b], M. Boscardin [f], F. Cenna [a], G.F. Dalla Betta [g], P. Fernndez-Martnez [e], M. Ferrero [a,b], D. Flores [e], Z. Galloway [d], V. Greco [e], S. Hidalgo [e], F. Marchetto [a], V. Monaco [b], M. Obertino [c], L. Pancheri [g], G. Paternoster [f], A. Picerno [b], G. Pellegrini [e], D. Quirion [e], F. Ravera [b], R. Sacchi [b], H.F.-W. Sadrozinski [d], A. Seiden [d], A. Solano [b], N. Spencer [d]

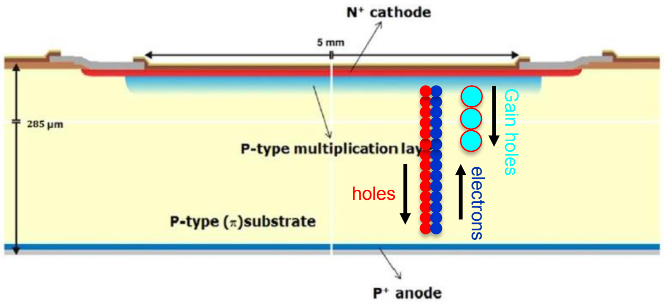

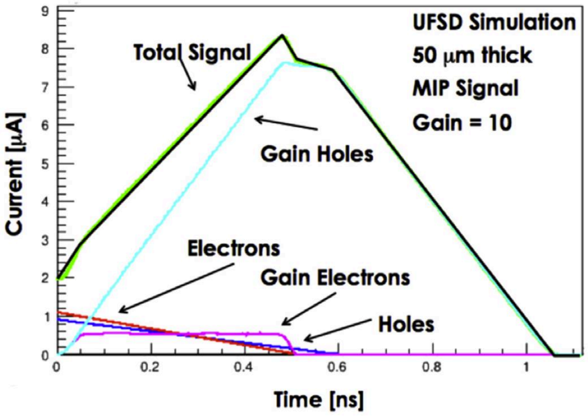

Total drift time for a given sensor thickness

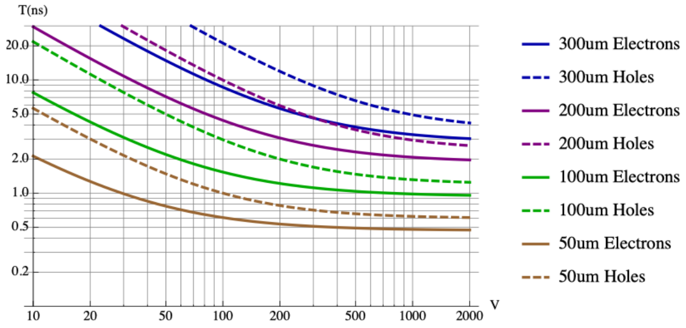

A high field region is implemented in a silicon sensor by doping.

Electrons will produce an avalanche in this high field region.

W. Riegler, CERN seminar

LGAD

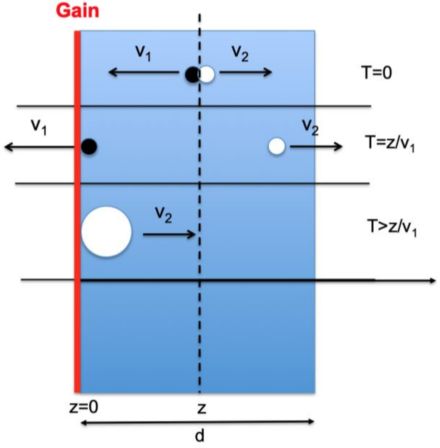

$$w(d)^2 = \frac{d}{\lambda}\int_0^\infty \left[\int_0^\infty \frac{n_1^2\, p_{\mathrm{clu}}(n_1)}{(n_1+n)^2}\, dn_1\right] p(n,d)\, dn$$

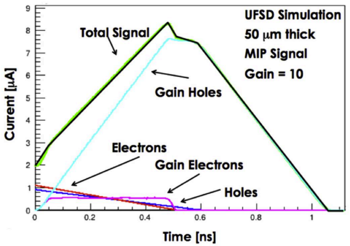

An e-h pair is produced at position z.

The electron arrives at z=0 at time $T=z/v_1$.

The electron multiplies in the high field in the layer at z=0 (infinitely thin).

The holes move back to z=d inducing the dominant part of the signal (all in this approximation).

Centroid time resolution for standard silicon sensor:

$$\Delta_\tau = w(d)\sqrt{\frac{4}{180}\frac{d^2}{v_1^2} - \frac{7}{180}\frac{d^2}{v_1 v_2} + \frac{4}{180}\frac{d^2}{v_2^2}}$$

Centroid time resolution for LGAD

$$\Delta_\tau = w(d)\frac{d}{\sqrt{12}v_1}$$

The signal is now defined by the arrival time distribution of the electrons at the gain layer.

W. Riegler, CERN seminar

W. Riegler, CERN seminar

LGAD

LGAD centroid time resolution

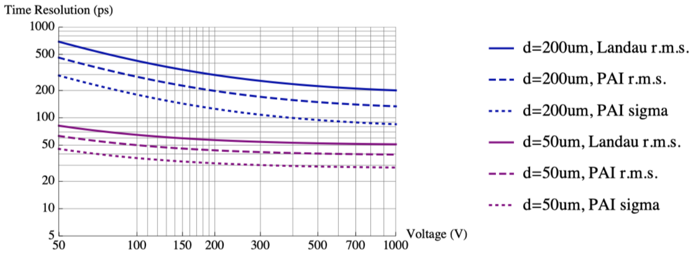

Figure 22. Time resolution for the centroid time from eq. (5.4) for 50, 100, 200, 300μm silicon sensors with internal gain of electrons, assuming a signal only from gain holes. The three curves for each sensor thickness correspond to the Landau theory, the PAI model and a Gaussian fit to the PAI model.

50um sensor at 200V: 30ps

200um sensor at 200V: 140ps

Standard silicon sensor centroid time resolution

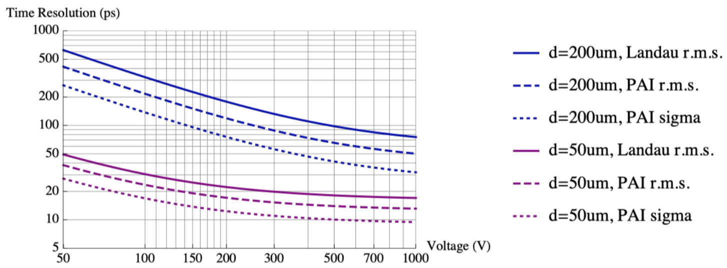

Figure 6. Time resolution from eq. (4.5) for different values of silicon sensor thickness as a function of applied voltage V for the Landau model, the PAI model and a Gaussian fit to the PAI model results.

50um sensor at 200V: 13ps

200um sensor at 200V: 70ps

The c.o.g. time resolution of LGADs is worse than the one for standard silicon sensors due to the very different signal characteristics – essentially an electron arrival time distribution.

Of course – the fact that the signal is larger by a factor 10-15 allows much more relaxed noise requirements, larger pixels etc. …

Single Photon Avalanche Diodes

For very large electric fields, also the holes start to contribute to the avalanche.

α dx = probability for an electron to produce an additional e-h pair along a distance dx

β dx = probability for a hole to produce an additional e-h pair along a distance dx

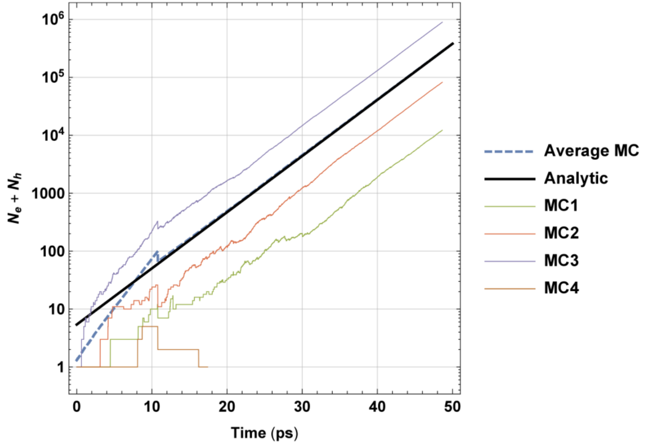

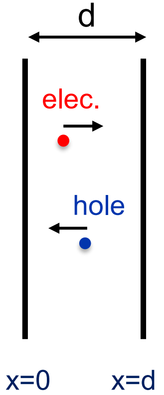

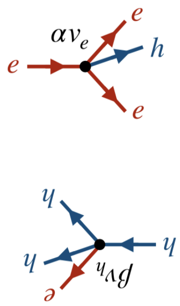

W. Riegler, CERN seminar

2014 International Conference on Optical MEMS and Nanophotonics

SIMULATION OF ELECTRIC FIELD DISTRIBUTION IN CMOS SINGLE PHOTON AVALANCHE DIODES AT BREAKDOWN VOLTAGE

Jau-Yang Wu and Sheng-Di Lin
Department of Electronics Engineering, National Chiao Tung University, Hsinchu, Taiwan
E-mail: judewu.ee95g@nctu.edu.tw

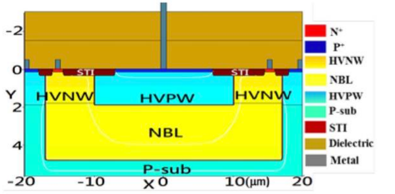

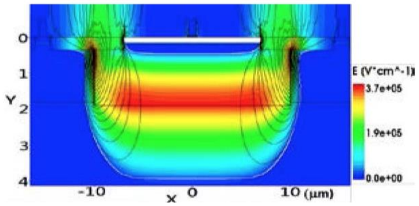

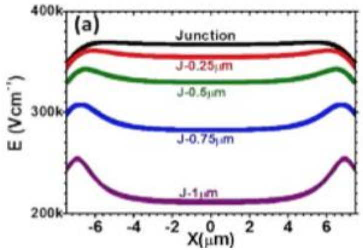

Time resolution aSPAD

Approximate r.m.s. SPAD time resolution $1/\gamma v^*$

<10ps is in the cards …

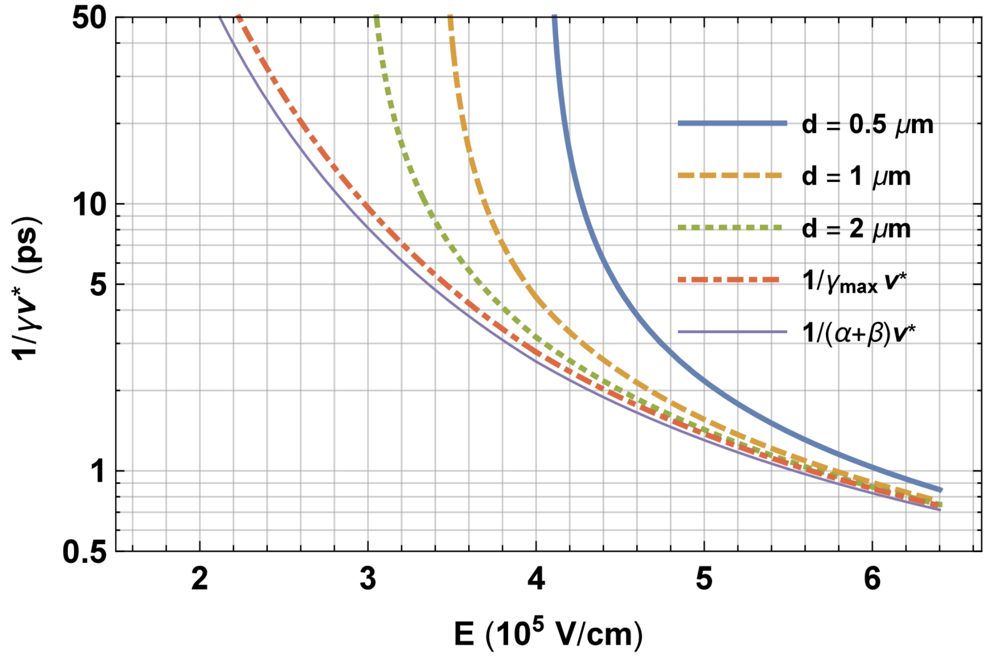

W. Riegler, CERN seminar

3D sensor realising a parallel plate geometry, TimeSPOT

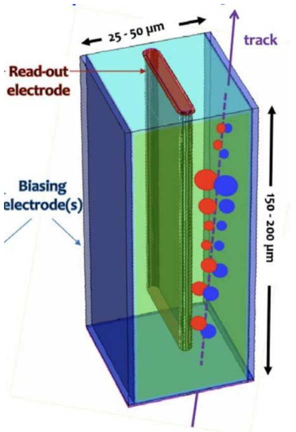

trenches

Total charge from the 200um sensor but timing characteristics from a 25um sensor !

L. Anderlini et al., *Intrinsic time resolution of 3D-trench silicon pixels for charged particle detection*. JINST 15, P09029, 2020.

D. Brundu et al., *Accurate modelling of 3D-trench silicon sensor with enhanced timing performance and comparison with test beam measurements*. JINST 16, P09028, 2021.

For a perfectly perpendicular track: 'box' signals from electrons and holes.

Landau fluctuations affect just the total pulse-height, which can be corrected.

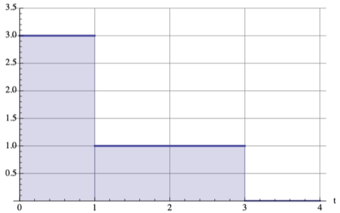

$$i(t) = -\frac{qv_1}{d}\Theta(z/v_1 - t) - \frac{qv_2}{d}\Theta((d-z)/v_2 - t)$$

c.o.g. time of the signal

$$\tau(z) = \frac{1}{2d}\left(\frac{z^2}{v_e} + \frac{(d-z)^2}{v_h}\right)$$

Variance of the c.o.g. Time for uniform distribution of tracks

$$\overline{\tau} = \frac{1}{d}\int_0^d \tau(z)dz \qquad \overline{\tau^2} = \frac{1}{d}\int_0^d \tau(z)^2 dz$$

$$\sigma_\tau = \sqrt{\overline{\tau^2} - \overline{\tau}^2} = \sqrt{\frac{4}{180}\frac{d^2}{v_e^2} - \frac{7}{180}\frac{d^2}{v_e v_h} + \frac{4}{180}\frac{d^2}{v_h^2}}$$

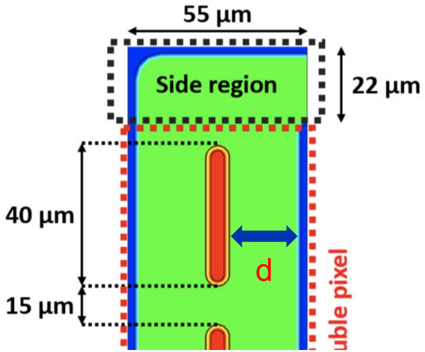

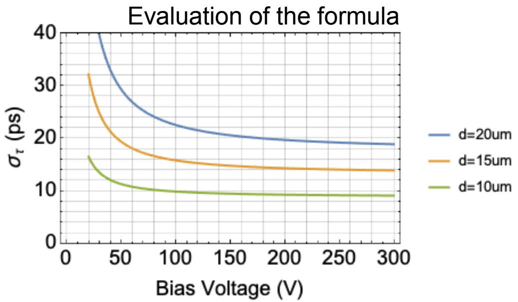

→ 10-20ps achievable and indeed achieved !

10/21/2021

62

W. Riegler, CERN seminar

Outline

- Main applications, motivations and history
- Semiconductors physics
- Silicon radiation detectors
- Timing with silicon detectors
- Perspectives

Perspectives … but already here

New detector development

application driven

European Strategy Update

hadron colliders experiments

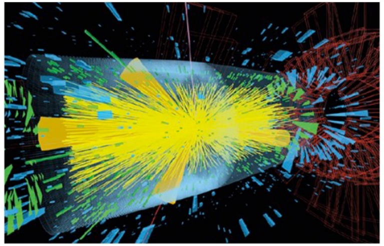

dominated by ***running conditions***

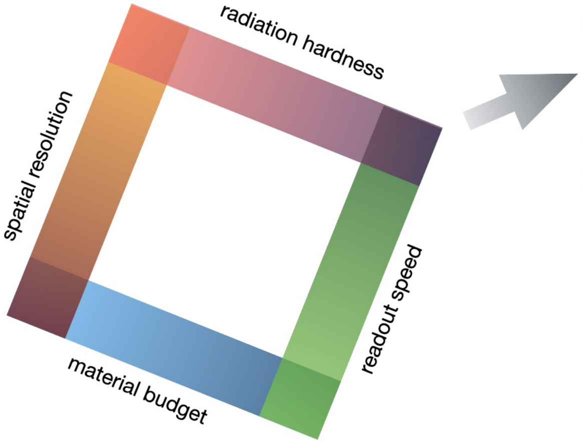

e+e- colliders, non-collider experiments

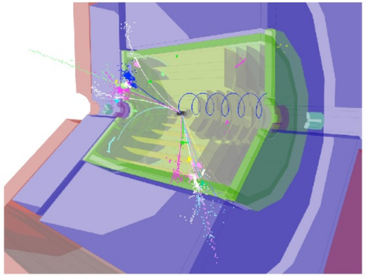

dominated by ***physics performance***

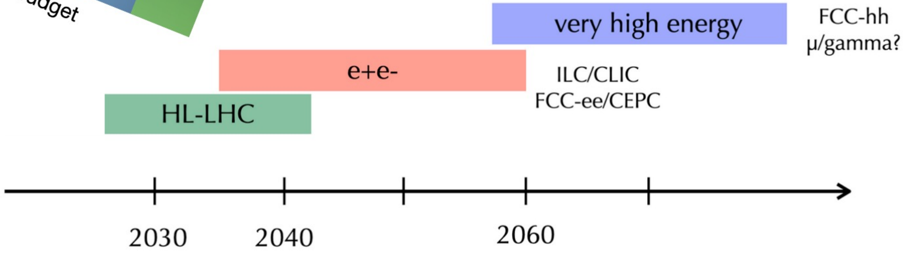

Challenges

the challenges

e⁺e⁻ colliders, non-collider

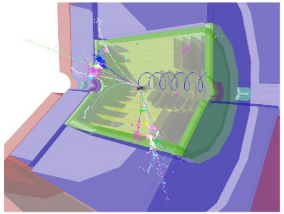

dominated by
physics performance

hadron colliders

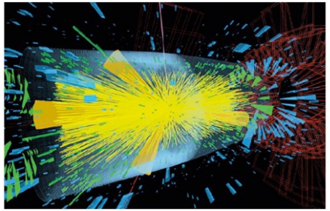

dominated by
running conditions

	Lepton Colliders	(HL-) LHC (ATLAS/CMS)
Material budget	$< 1\%\ X_0$	$10\%\ X_0$ * 2% for ALICE
Single-point resolution	≤ 3 µm	~ 15µm
Time resolution	~ ps – ns	25ns
Granularity	≤ 25 µm x 25 µm	50µm x 50µm
Radiation tolerance	$< 10^{11}\ n_{eq} / cm^2$	$O(10^{16}\ n_{eq} / cm^2)$
Max. hit rate	20 MHz / cm²	2-4 GHz / cm² *)

Performance optimisation

Survival optimisation

*) max. output rate for LHCb

CMOS Monolithic Active Pixel Sensors

sensor and readout elements all-in-one

Monolithic Detectors

CMOS MAPS for ALICE ITS3 (Run 4):
(LOI: CERN-LHCC-2019-018, M. Mager)

- Three fully cylindrical, wafer-sized layers based on curved ultra-thin sensors (20-40 µm), air flow cooling
- Very low mass, < 0.02-0.04% per layer

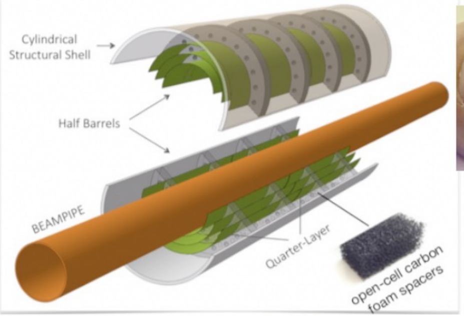

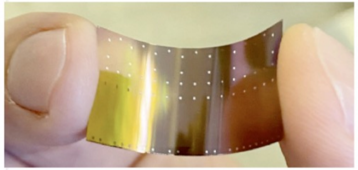

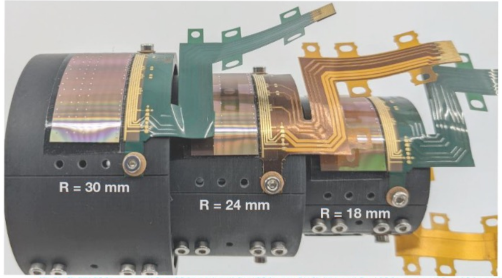

Radiation hardness of MAPS: From ALPIDE to MALTA/Monopix with modified Tower Jazz 180 nm process

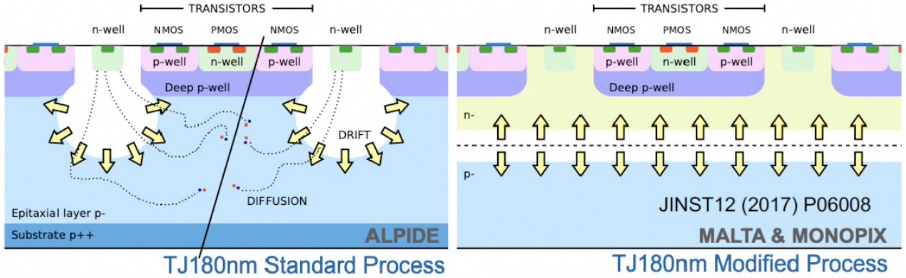

→ Up to 97% efficiency after fluence of $1\times10^{15}\ n_{eq}/cm^2$ H. Pernegger

New CMOS TPSCo 65 nm technology
Validated on Digital and Analog Pixel Test Structures up to 10^{15} cm^{-2} and 100 kGy
Currently testing **stitching** for wafer scale sensors (now 26 x 1.4 cm^2)

A. Kotliarov

→ Efficiency > 99.9% independent on bending radius

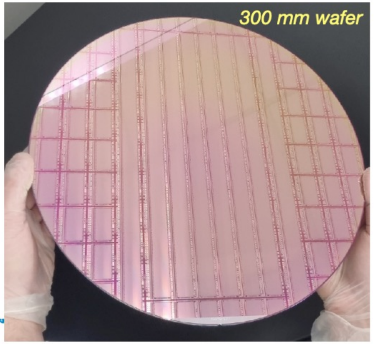

ALICE ITS3

https://ep-news.web.cern.ch/content/ultralight-air-cooled-mechanics-alice-its3

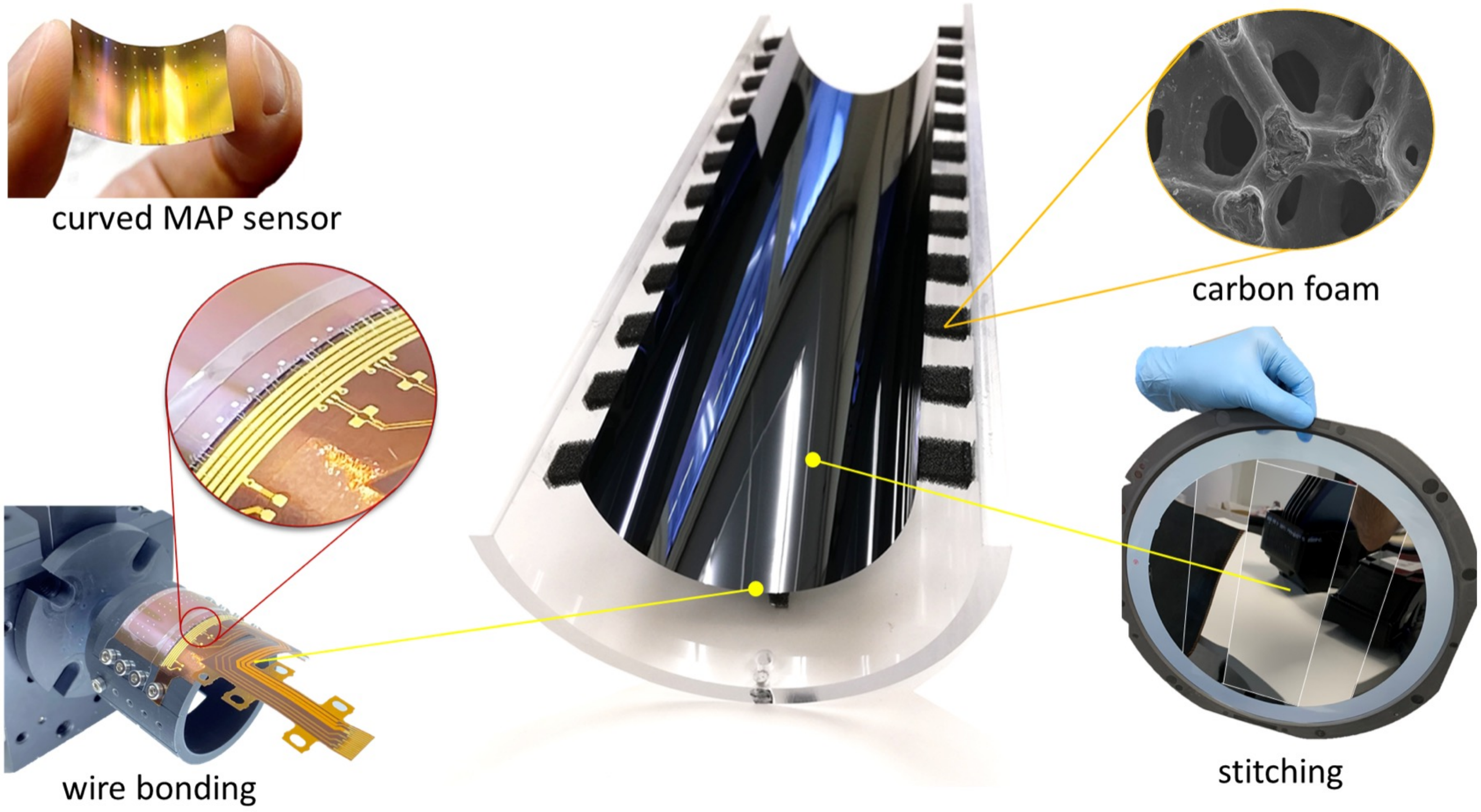

Low Gain Avalange Detectors

fast timing

Sensors for 4D-Tracking:

- Position resolution: ~ 10 µm
  ~ 5% of electrodes distance
- Time resolution: ~ 25 ps
  for 50 µm sensors
- Radiation Hardness up to
  ~ 2 x 10^{15} cm^{-2}

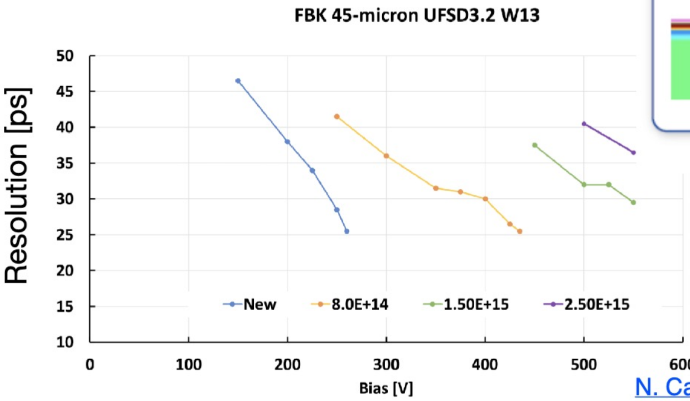

N. Cartiglia

LGAD: Fill factor & performance improvements

RD50

- Two opposing requirements:
  - Good timing reconstruction needs homogeneous signal (i.e. no dead areas and homogeneous weighting field)
  - A pixel-border termination is necessary to host all structures controlling the electric field
- Several new approaches to optimize/mitigate followed:

Trench Isolation LGAD | AC-LGAD | Invers LGAD | Deep Junction LGAD

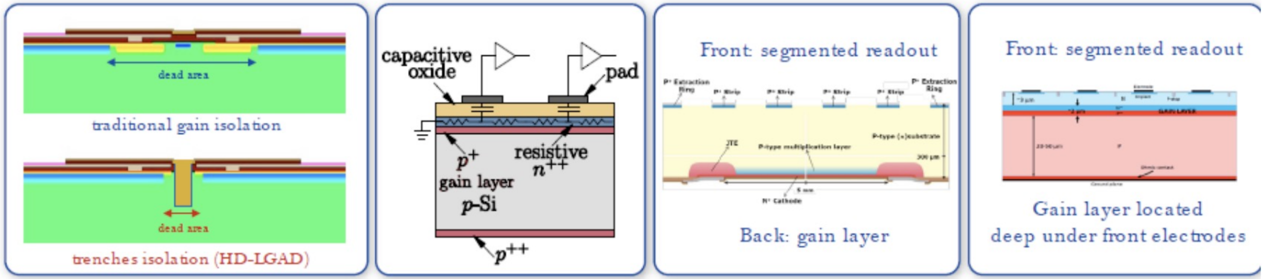

Concepts simulated, designed, produced and tested in 2018/19

..new concept 2020

Use Carbon enriched substrates (C helps to diminish the effect of gain reduction with irradiation)

Ongoing:

- Improve fill factor and signal homogeneity

Next employed in ATLAS / CMS fast timing layers

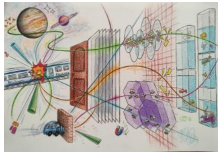

Paths of present silicon sensor R&D

DRD3

Monolithic devices
(WG1/WP1-CMOS)
55-180 nm processes

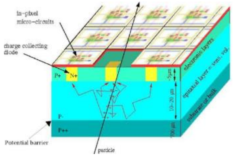

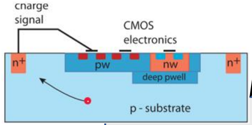

Small electrode device

MAPS

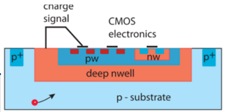

Large electrode device

with gain

Depleted MAPS wo Gain

Depleted MAPS wo Gain

with gain

Optimized for rates/power/position resolution

Optimized for radiation hardness /timing

Hybrid devices
(WG2/WP2-4D tracking)

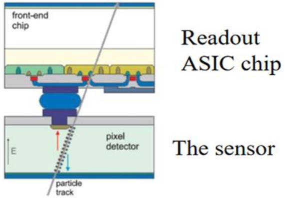

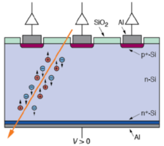

Planar

3D devices

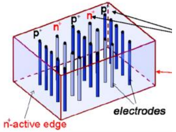

Large area passive devices (strips)

With Gain (LGADs)

Trench 3D

Column 3D

With Gain

(red)	proof of concept ongoing
(orange)	recent research (working prototype)
(green)	proven/demonstrated

https://indico.cern.ch/event/1552124/

WG3,6/WP3 extreme fluence and WBS

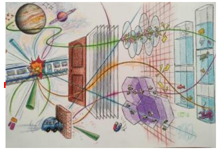

Improve the radiation hardness of the semiconductor detectors and exploitation of the benefits of WGS for particle physics

Projects **running**, **proposal draft submitted (work ongoing)**, **proposals in preparation (work ongoing):**

- Understanding silicon at extreme fluences (**devices developed with in WP2**)
  - Radiation damage in Si PiN and LGAD sensors
  - Many RD50 projects running on the radiation hardness
- Wide-Bandgap-Semiconductors
  - SiC LGAD Detector (one running one in preparation)
  - Development of radiation-hard GaN devices for MIP detection
  - Radiation hardness of 25um 3D diamond detectors
  - Graphene/SiC Detector

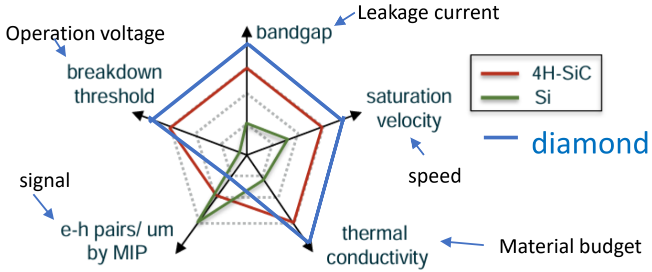

Main challenges and developments:

Silicon at extreme fluences:

- understanding material properties (impact ionization, mobility, trapping…)
- understanding the operation

SiC/GaN

- understanding the material properties – defects formation
- processing of large device SiC-LGADs

Diamond:

- scalability of 3D column processing
- availability of high quality large diameter wafers

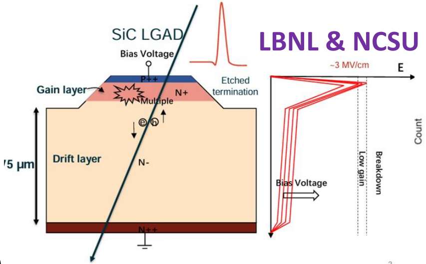

LBNL & NCSU

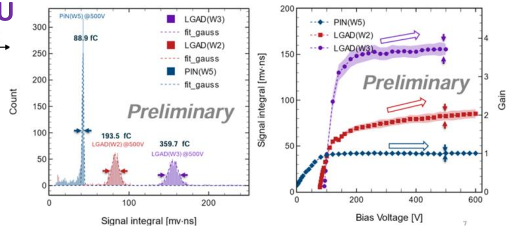

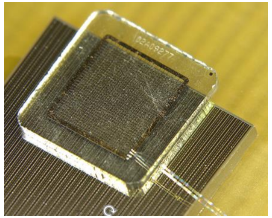

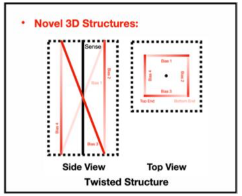

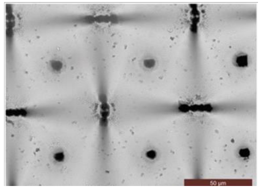

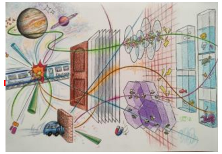

https://indico.cern.ch/event/1552124/

WG 4: Simulations

DRD3

Simulations are essential for planning, understanding the performance and designing of devices. Aim to develop tools that could be (easily) implemented to simulate any specific detector or measurement.

“Monte Carlo”
(predicting the performance of complex detector assemblies)

GEANT4

TCAD
(understanding the sensors)

Synopsis, Silvaco …

AllPix2 / Garfield++ as the main tool complement by other ones (also RASER, KDetSim…)

GOALS:

- Implementation of improved semiconductor models (e.g. mobility, impact ionization, trapping …)
- Adaptation of WBS sensors
- Adaptation of dynamic /adaptive E,E_w
- Implementation of common electronics/digitization

E,E_w

GOALS:

- Developing and verification of damage models (effective and defect based)
- Establish how to benchmark/evaluate the models against the measured properties (important milestone)
- Improving the TCAD with new findings (WBS, extreme fluences)
- Develop a flexible framework to simulate performance of different processes (CMOS)

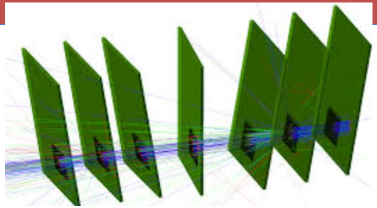

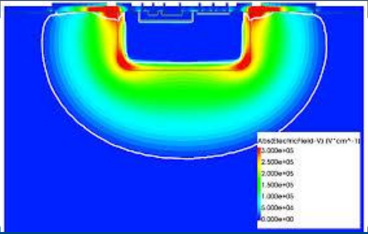

WP1: Solid-State Photodetectors

Examples of ongoing activities

Backside illuminated (BSI) SiPMs: potential for an enhanced PDE and a better radiation tolerance.

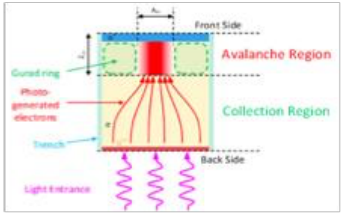

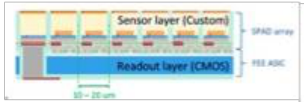

The first results of the FBK IBIS Run samples

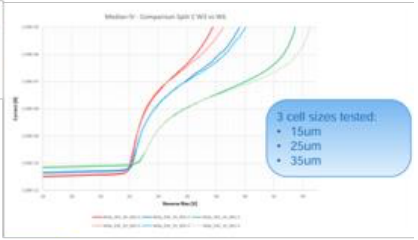

Timing of SSPD & Developing ultra-granular SiPM that integrates with the readout electronics

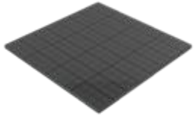

3x3mm2 SiPM Array

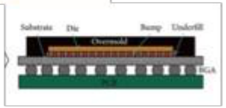

FastIC+
(collab. CERN ICCUB)
Low power Chip

2024 Produced and evaluated

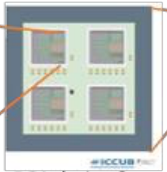

BGA design & production end of June 2025

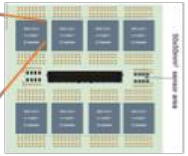

256 Ch 5x5cm2 Module proposal

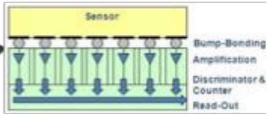

Ultra granular SiPMs

Long term goal 1x1mm2 SiPM array

- Study and **improve the timing of SiPMs**.
- **Optimised, reliable, cost-effective integration** and packaging with integrated cooling.
- **Vertical integration of SiPM arrays to FEE:** optimise timing by reducing the interconnections' parasitic inductances and capacitances.

https://indico.cern.ch/event/1552124/

Take home message

- Semiconductors are excellent for tracking and spectroscopy
- Energy to create charge carrier is 10x lower than gas

  ⟶ large signals without amplification and

  ⟶ less material hence better vertex/tracking resolution
- No need for container
- μ-electronics development helped to have finest segmentation and electronics readout
- Fast signal collection is possible ⟶ timing applications
- Main limitations are cost and ageing (radiation damage)
- Towards 5D measurements (no time to talk about calorimetry…)

THANK YOU FOR YOUR ATTENTION!

Backup

Signal from uniform deposition in a real diode

more realistic treatment: E-field depends on x

simple ansatz: $|\vec{E}| = \dfrac{e\,N_A}{\epsilon\epsilon_0} \cdot x$

and with $\sigma = \dfrac{1}{\rho} = e\,N_A\,\mu_+$ and $\tau = \dfrac{\epsilon\epsilon_0}{\sigma}$

$$|\vec{E}| = \frac{x}{\mu_+\tau} \qquad (\tau \cong 1 \text{ ns})$$

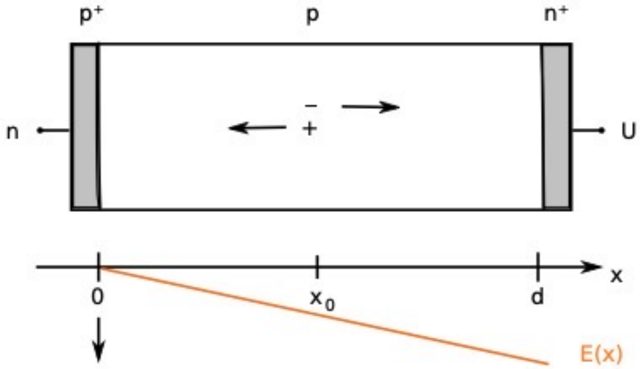

for an electron generated at location x inside depletion zone and mobilities independent of E:

$$v_- = -\mu_- E = \frac{\mu_-}{\mu_+}\frac{x}{\tau} \quad \Rightarrow \quad x = x_0 \exp\left(\frac{\mu_- t}{\mu_+\tau}\right)$$

total drift time of electrons:

$$t_d = \tau\frac{\mu_+}{\mu_-}\ln\left(\frac{d}{x_0}\right)$$

charge signal for $t < t_d$

$$Q_-(t) = -\frac{e}{d}\int\frac{dx}{dt}dt = \frac{e}{d}x_0\left(1 - \exp\left(\frac{\mu_- t}{\mu_+\tau}\right)\right)$$

analogously for hole

$$v_+ = \mu_+ E = -\frac{x}{\tau} \quad \Rightarrow \quad x = x_0 \exp\left(-t/\tau\right)$$

$$Q_+(t) = -\tfrac{e}{d}x_0\left(1 - \exp\left(-t/\tau\right)\right)$$

Total charge

Total charge signal:

$$Q_-(t_d) + Q_+(t \to \infty) = -e$$

signal rise time essentially determined by

$$\tau = \rho \cdot \epsilon \cdot \epsilon_0$$

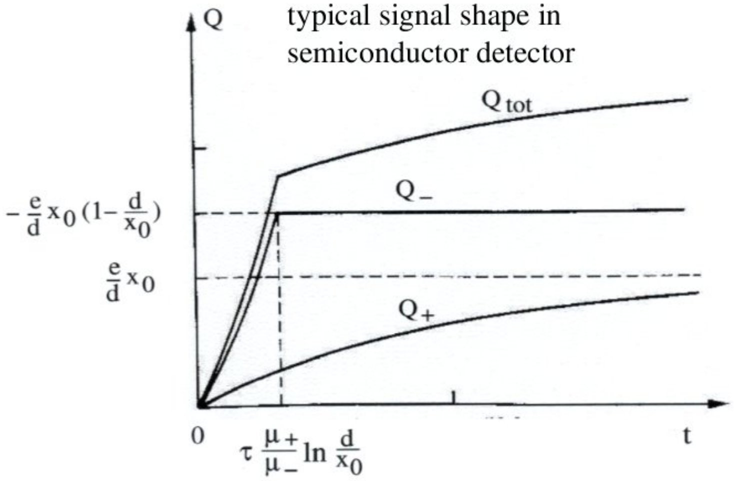

in reality a bit more complicated:

- track not exactly a line charge (distributed over typically 50 μm width)
- $\mu_\pm \neq$ constant
- some loss of charges due to recombination at impurities

  for Si $\quad \tau = \rho \cdot 10^{-12}$ s (ρ in Ωcm), $\rho = 1000\ \Omega$cm $\to \tau = 1$ ns

Absorption coefficient

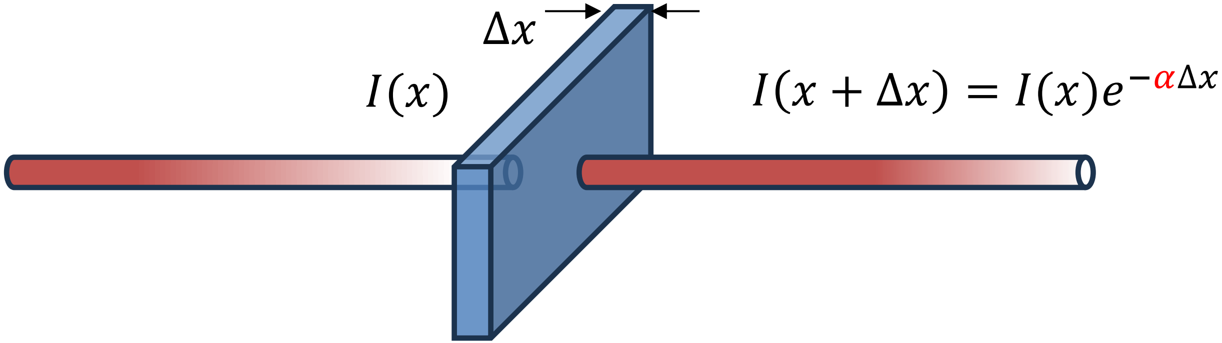

Silicon PIN photodiode

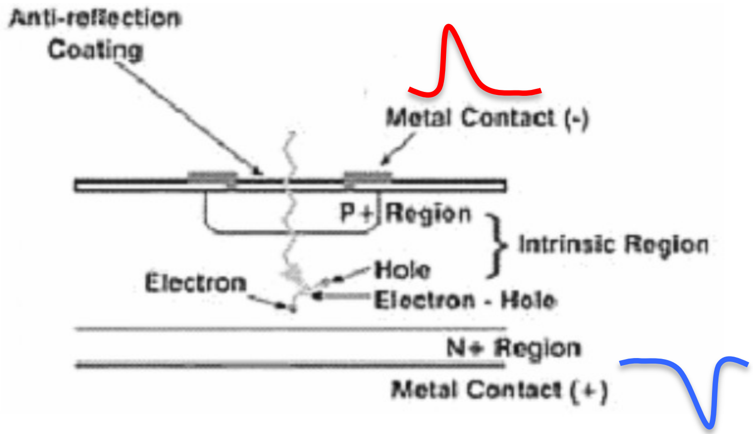

A piece of intrinsic high-ohmic silicon
Sandwiched between two heavily doped n+ and p+ regions

✓ Thick bulk: low capacitance (less noise) + sensible to longer wavelengths
✓ Undoped bulk: low depletion voltage; longer generation/recombination lifetime ➔ small charge losses, low leakage current

HPGe

4.5.4 High purity or intrinsic Ge detectors

from late 1970ies

similar to Li doped Ge or Si detectors, but dark current is kept low not by compensating impurities, but by making material very clean itself

by repeating the purification process (zone melting), extremely pure Ge can be obtained ($\leq 10^9$ impurity atoms per cm^3)
intrinsic layer like compensated zone in Ge(Li), similar sizes possible
advantage: cooling only needed during use to reduce noise

other applications

- low energy electrons
- strongly ionizing particles
- $\mathrm{d}E/\mathrm{d}x$ for particle identification

useful energy range determined by range of particle vs. size of detector

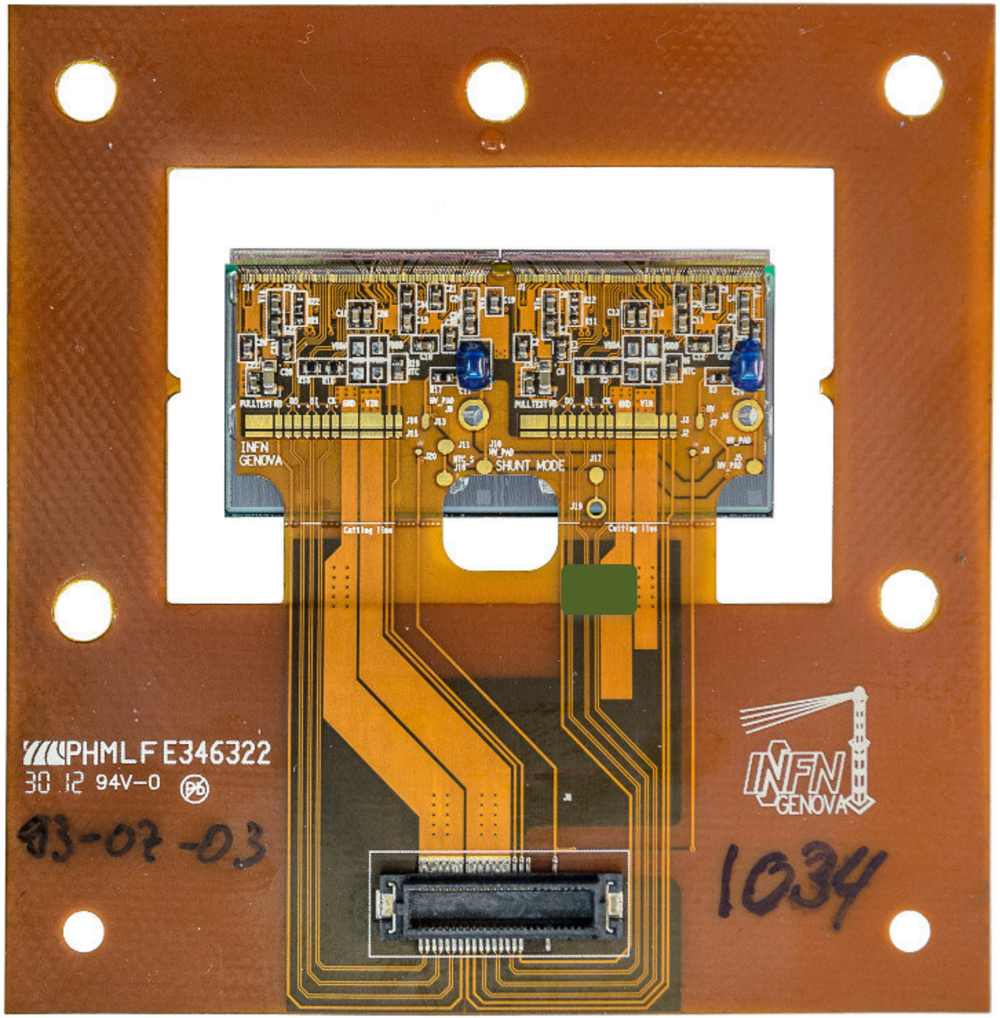
INFN
GENOVA
SHUNT MODE
PHMLF E346322
30 12 94V-0
03-07-03
INFN
GENOVA
1034

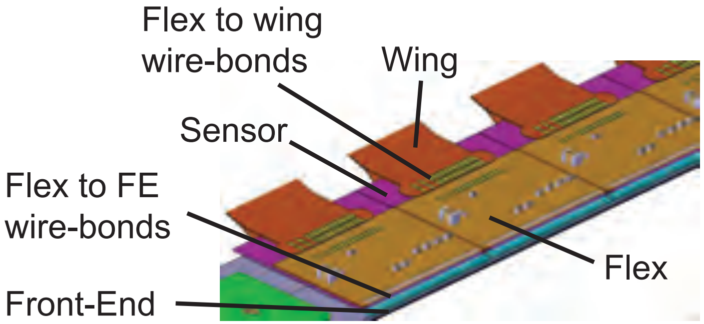
Flex to wing
wire-bonds
Wing
Sensor
Flex to FE
wire-bonds
Flex
Front-End

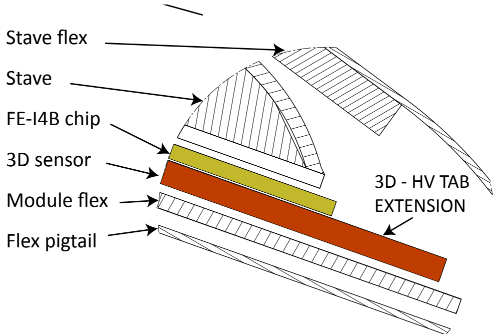
Stave flex
Stave
FE-I4B chip
3D sensor
Module flex
Flex pigtail
3D - HV TAB
EXTENSION

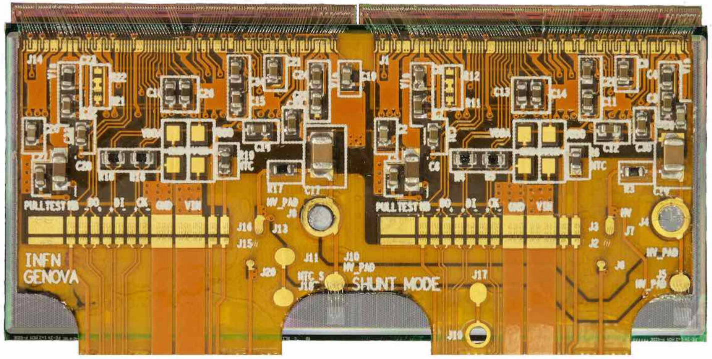

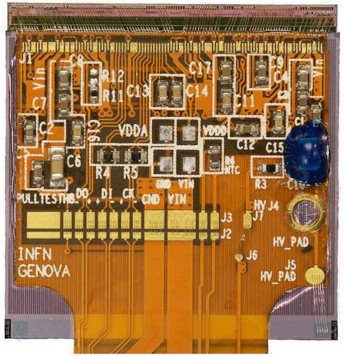

PLANAR

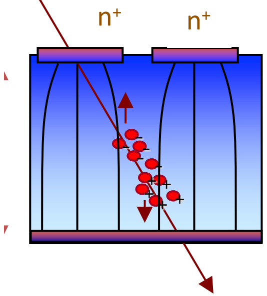

3D

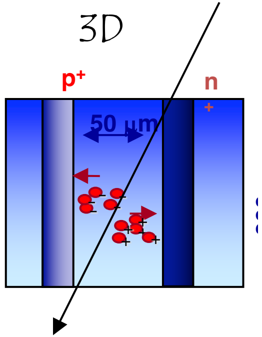

Biasing circuits

For an AC-coupled a DC path must be provided for the strip leakage currents

Two possible methods: via a resistor or by the punch-through method

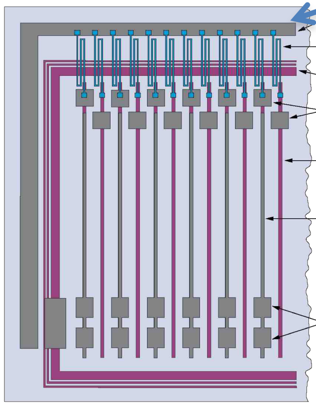

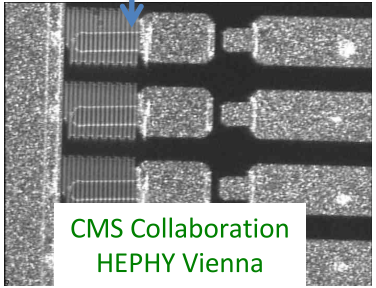

CMS Collaboration
HEPHY Vienna

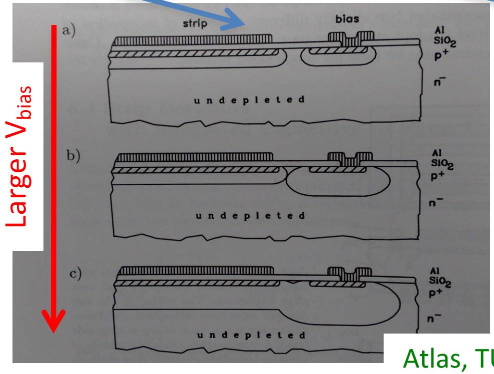

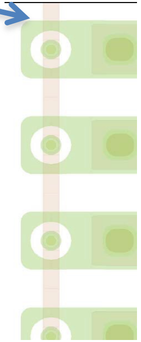

Atlas, TU Dortmund &
MPI-HLL

Deposition of polycristalline silicon between p+ implants and a common bias line

Drawback: Additional production steps and photo lithographic masks required.

Small potential difference between strip implant and the bias dot

This solution allows avoiding the technological steps required for polysilicon deposition in the detector processing; same technology DC and AC strips

Radiation damage?

Microstrip detectors with AC-coupled readout

AC-coupling the detector with the electronics allows to avoid the DC detector leakage current to offset the working point of the preamplifier. Coupling capacitors of suitable value could be integrated in the detector itself (another benefit of the planar process)

DC-coupled detector

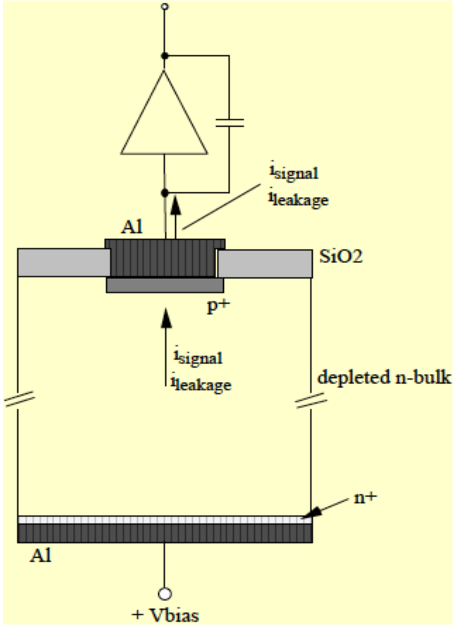

$C_C >> C_{S,tot}$

AC-coupled detector
with integrated coupling capacitance

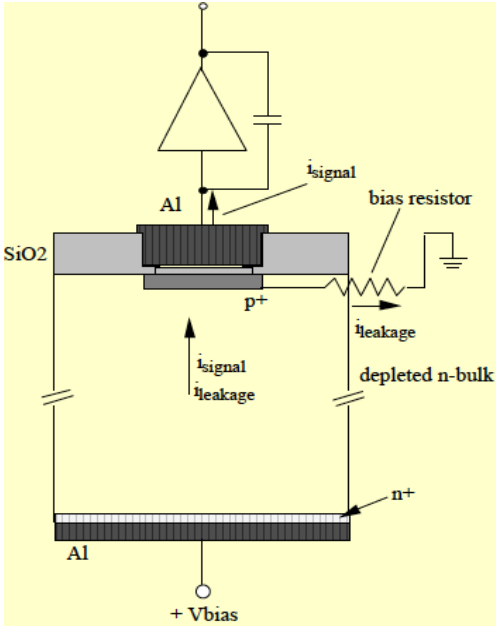

Historical development

silicon sensors

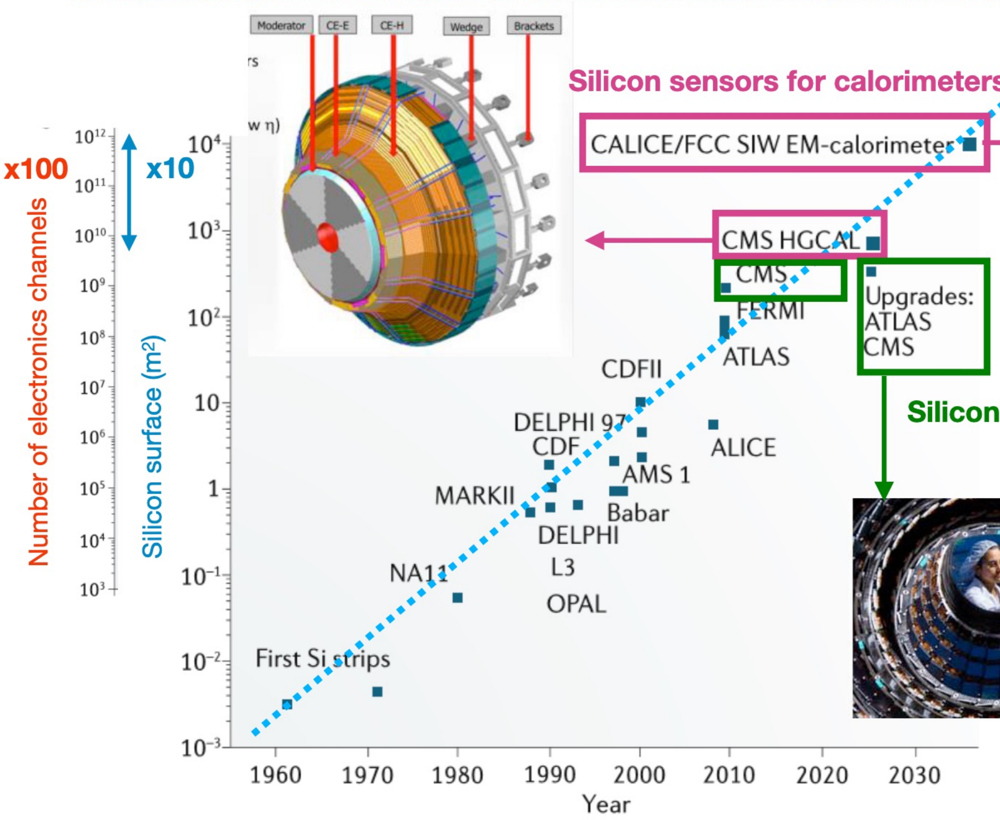

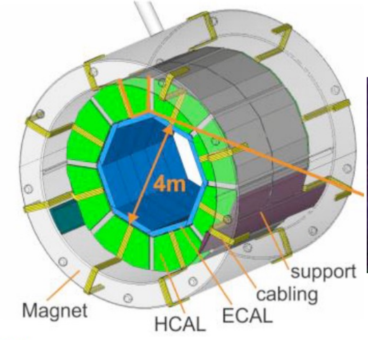

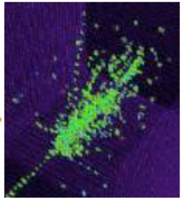

Remarkable: every decade the instrumented areas have increased by a factor of 10 while the numbers of channels in the largest arrays have increased by a factor of 100

Silicon detectors

a continuous growth

Tremendous technological improvements

- The silicon **wafer size** increased from 2” to 12”
- The size of **bump bonds** decreased to < 10 µm and other technologies for hybridisation
- **Technology node** decreasing steadily, 65 nm in HEP

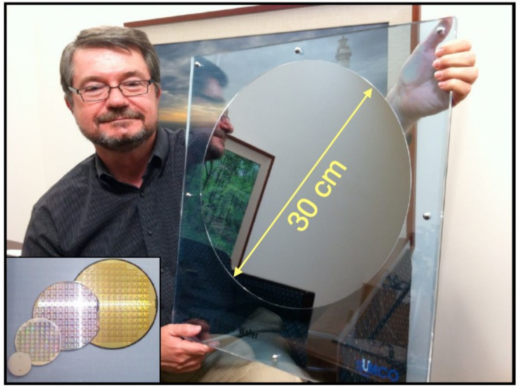

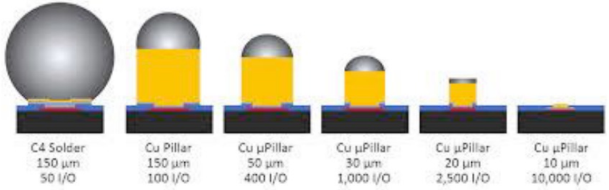

From metal solder sphere to micro-pillars

From solder bonding to bonding without Solder:
Gold µ-pillar Thermo-Compression Bonding

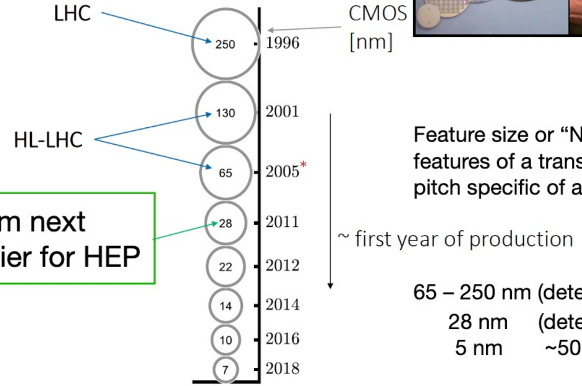

28 nm next frontier for HEP

Feature size or “Node” refers to the size of different features of a transistor including gate length and half-pitch specific of a semiconductor manufacturing process

65 – 250 nm (detector electronics in production in HEP)
28 nm (detector electronics under preparation)
5 nm ~50 atom digital electronics of smart phones

After 28 nm → FinFETs have a completely different geometry, do not seem so promising in terms of radiation hardness

Momentum resolution

Momentum measurement uncertainty:

$$\frac{\sigma_p}{p} = \frac{L^2}{8Rs} \cdot \frac{\sigma_s}{s} = \frac{L^2}{8R} \cdot \frac{\sigma_s}{L^4/64R^2} = \frac{\sigma_s}{L^2} \cdot 8R = \frac{\sigma_s}{L^2} \cdot \frac{8p}{eB} \sim p \cdot \frac{\sigma_s}{BL^2}$$

[Garutti]

Uncertainty σ_s depends on number and spacing of track point measurements; for equal spacing and large N:

$$\sigma_s = \frac{\sigma_{r\phi}}{8}\sqrt{\frac{720}{N+5}}$$

see: Glückstern, NIM 24 (1963) 381 or
Blum & Rolandi, Particle Detection ...

Good momentum resolution:

- large path length L
- large magnetic field B
- good Sagitta measurement

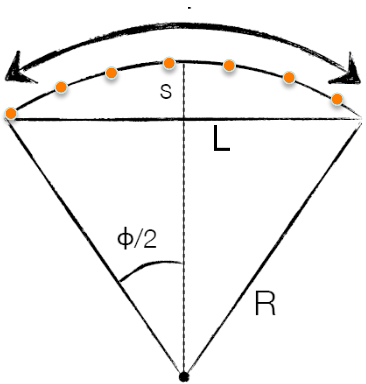

For momentum p: generally in experiment measure p_t

$$\left(\frac{\sigma_p}{p}\right)^2 = \left(\frac{\sigma_{p_t}}{p_t}\right)^2 + \left(\frac{\sigma_\theta}{\sin\theta}\right)^2$$

multiple scattering term conts. in p_t

using $p = \frac{p_t}{\tan\theta}$

Examples:

track uncertainty ≈ p_t

Argus: $\sigma_{pt}/p_t = \boxed{0.009^2} + \boxed{(0.009\ p_t)^2}$

ATLAS: $\sigma_{pt}/p_t = \boxed{0.001^2} + \boxed{(0.0005\ p_t)^2}$

[ATLAS nominal; TDR]

Momentum resolution

Charged particles: circular motion transverse to uniform B field

p_T [GeV/c] = 0.3 x B [T] x R [m]

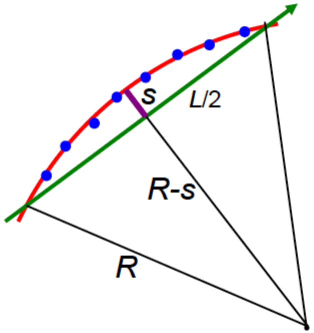

R=$L^2/2s$

Measuring the sagitta s we can measure the transverse momentum p_T

Transverse momentum resolution → $\boxed{\dfrac{\sigma_{p_T}}{p_T} = \dfrac{8p_T}{0.3BL^2}\sigma_s}$

Need strong B, long path length L and excellent sagitta resolution σ_s

The sagitta resolution σ_s depends on the position resolution $\sigma_{\phi r}$ which depends on the sensor intrinsic resolution; $\sigma_{\phi r}$ is limited by multiple scattering

$$\boxed{\sigma_{r\phi} = \sigma_{int} \oplus \sigma_{MS}}$$

Requirement: best possible space point resolution, material at minimum

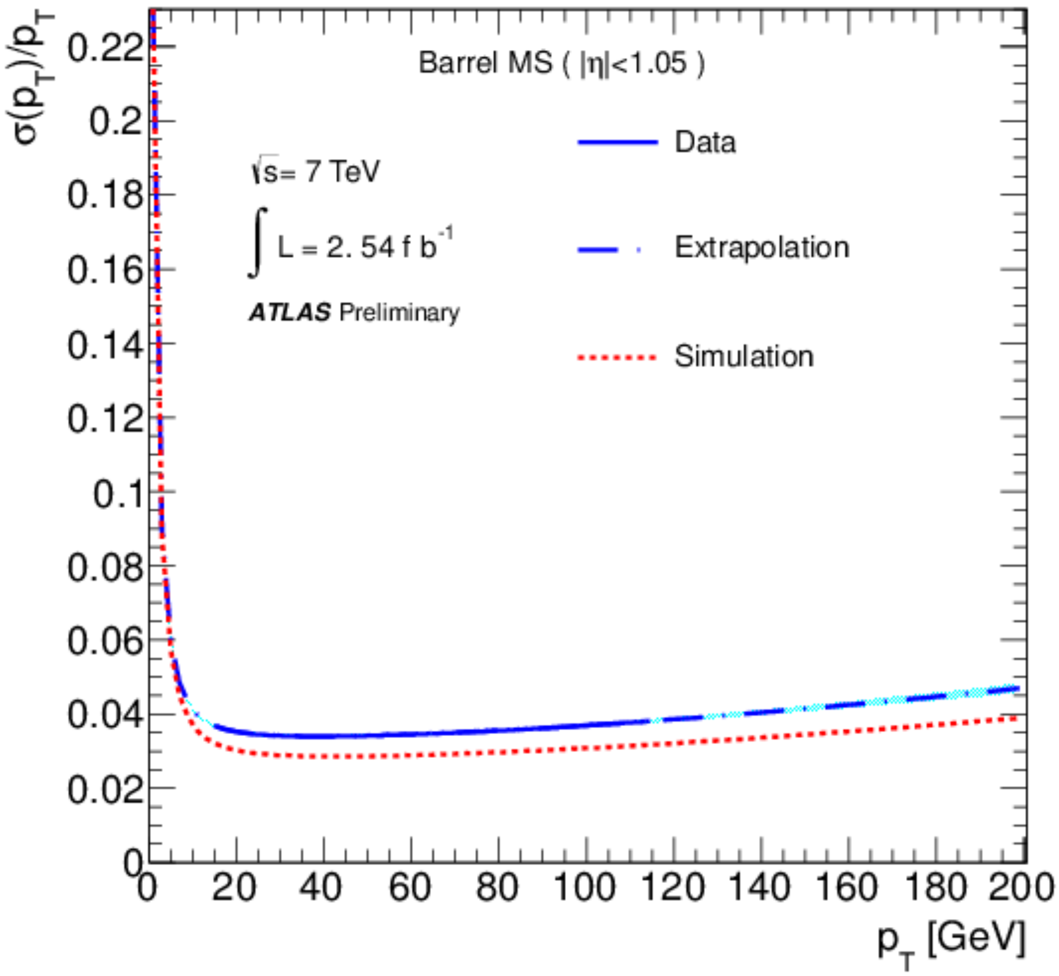

Barrel MS (|η|<1.05)
√s= 7 TeV
∫ L = 2. 54 f b-1
ATLAS Preliminary
Data
Extrapolation
Simulation
σ(pT)/pT
pT [GeV]
0.22
0.2
0.18
0.16
0.14
0.12
0.1
0.08
0.06
0.04
0.02
0
0
20
40
60
80
100
120
140
160
180
200

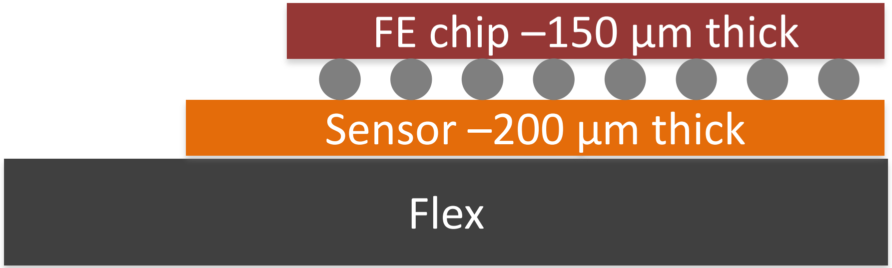
FE chip –150 µm thick
Sensor –200 µm thick
Flex

Vertex Resolution

$x1, x2 =$ measurement planes

$y1\ , y2 =$ measured points, with errors δy

$y = a + bx$

$$b = \text{slope} = \frac{y1 - y2}{x1 - x2} = \frac{y1 - y2}{\Delta x}$$

$$a = \text{intercept} = \frac{1}{2}(y1 + y2) - \frac{1}{2}(y1 - y2)\left(\frac{x1 + x2}{\Delta x}\right) = \bar{y} - b\bar{x}$$

$$(\delta b)^2 = \left(\frac{\partial b}{\partial y1}\right)^2 (\delta y)^2 + \left(\frac{\partial b}{\partial y2}\right)^2 (\delta y)^2 \Rightarrow \delta b = \frac{\sqrt{2}\delta y}{\Delta x}$$

$$\delta a = \frac{\delta y}{2}\sqrt{1 + \frac{8\bar{x}}{\Delta x}}$$

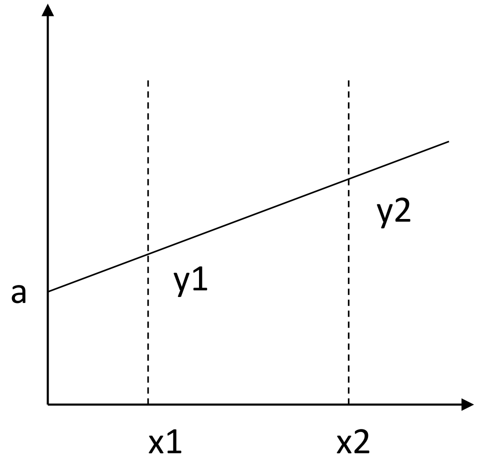

for good resolution on angles (f and q) and intercepts (d, z_0)

- Precision track point measurements
- Maximize separation between planes for good resolution on intercepts
- Minimize extrapolation - first point close to interaction

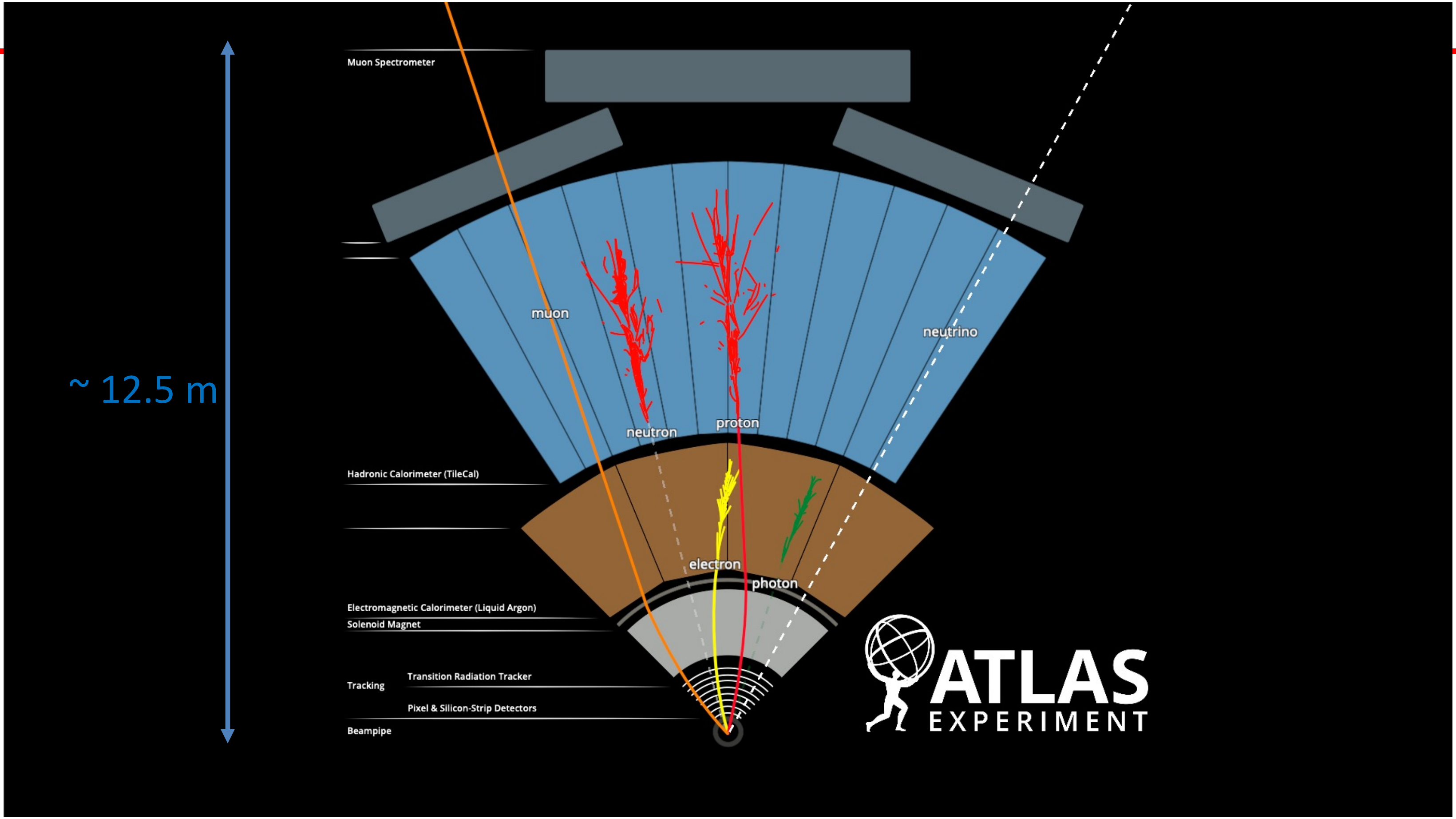

~ 12.5 m
Muon Spectrometer
muon
neutrino
neutron
proton
Hadronic Calorimeter (TileCal)
electron
photon
Electromagnetic Calorimeter (Liquid Argon)
Solenoid Magnet
Tracking
Transition Radiation Tracker
Pixel & Silicon-Strip Detectors
Beampipe
ATLAS
EXPERIMENT

CCD cameras for astronomy

SDSS Photometric Camera –
30 2k x 2k, (24 μm)^2-pixel
Sloan Digital Sky Survey Telescope
2000 – 2008

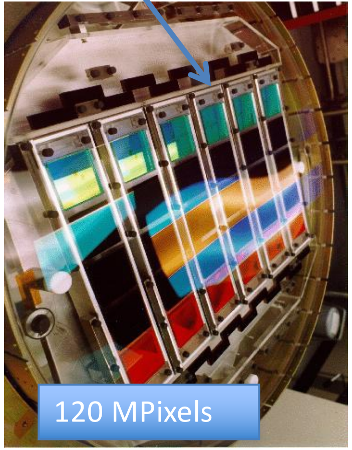

120 MPixels

CCD: Thinned (10-20μm) partially depleted

64 MPixels

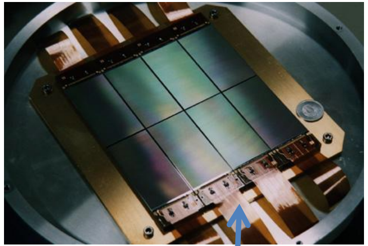

SuprimeCam – 8 2k x 4k, (15 μm)^2-pixel CCDs
Subaru 8-m Telescope
(1998)

CCD: 40 μm thick, partially depleted

PS1 camera
60 4.8k x 4.8k, (10 μm)^2-pixel
Pan-STARRS telescope (2010)

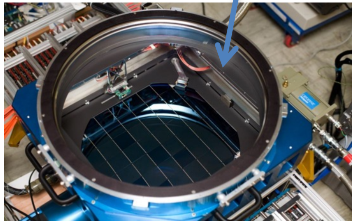

1.4 GPixels

CCD: 75 μm thick, fully depleted

870 MPixels

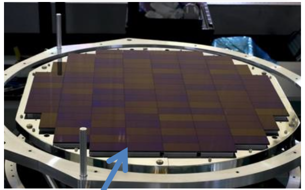

HyperSuprimeCam
116 2k x 4k, (15 μm)^2-pixel
Subaru 8-m Telescope
1st light achieved
28Aug2012

CCD: 200 μm thick, fully depleted

Trend: thick, full depleted CCDs

Thick, fully depleted CCDs

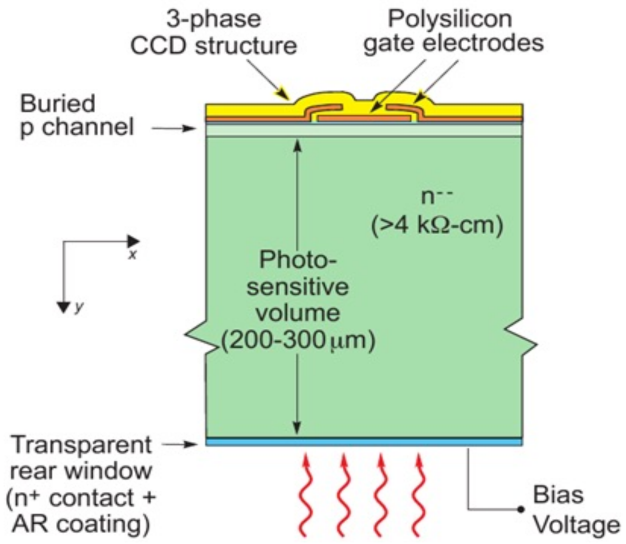

Fully Depleted, Back-Illuminated Charge-Coupled Devices Fabricated on High-Resistivity Silicon
Stephen E. Holland et al., IEEE TRANSACTIONS ON ELECTRON DEVICESVOL. 50, NO. 1 (2003) 225

Merging of p-i-n and CCD technology:
A conventional CCD on a thick, high-resistivity Si substrate (> 4 kΩ-cm), fully depleted

The large thickness results in high near-infrared QE
The fully depleted operation results in the ability to control the spatial resolution

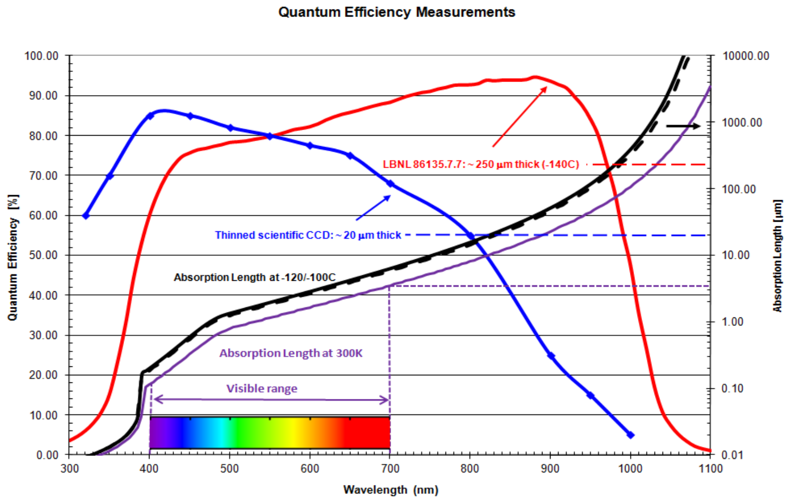

Drawbacks of thick, fully depleted CCDs

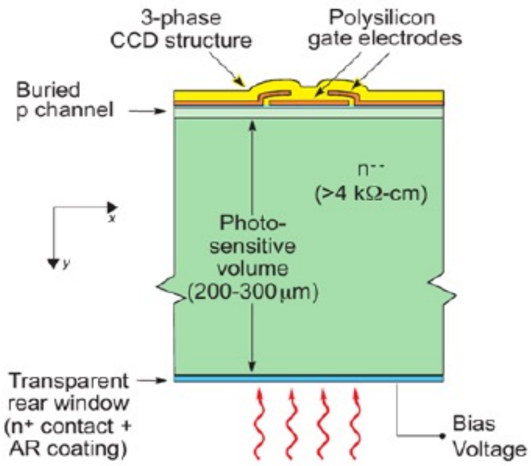

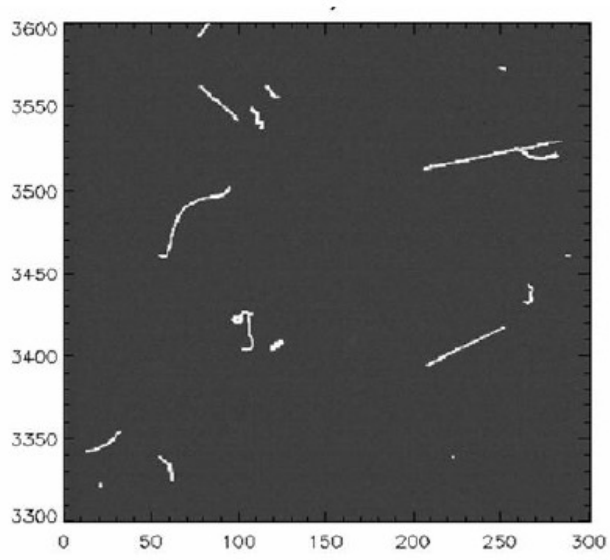

Cosmic rays and Compton electrons from background radiation leave long tracks

30 minute dark
200 μm thick CCD
Small sub-image

LSST sensor specifications

High quantum effciency from 320 to 1080 nm thanks to a large depletion depth (100 μm) and implementation of the sensor in a back-illuminated configuration

To reduce charge diffusion the sensor is fully depleted, and a high internal field is maintained within the depletion region. This is made possible by the use of high resistivity substrates and high applied voltages.

High Fill factor. A total of 189 4 K x 4 K sensors are required to cover the 3200 cm^2 focal plane. To maintain high throughput, the sensors are mounted in four-side buttable packages and are positioned in close proximity to one another with gaps of less than a few hundred μm. The resulting fill factor, *i.e.*, the fraction of the focal plane covered by pixels, is 93%.

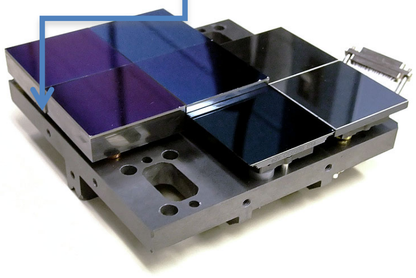

Prototype sensors mounted on a raft baseplate - http://www.lsst.org/News/enews/focal-plane-201101.html

Caméras CCD vs CMOS

Les capteurs CCD présentent encore des avantages significatifs pour l'imagerie haute performance à faible niveau de lumière, mais la technologie CMOS a rattrapé le retard.

Paramètre	CCD	CMOS	Gagnant
Disponibilité	Certaines grandes lignes de capteurs CCD deviennent obsolètes. Capteurs spécialisés coûteux.	Les entreprises investissent massivement, et la technologie s'améliore rapidement.	Le CMOS est l'avenir pour la plupart des applications. Le CCD continue à servir des niches spécialisées.
Coût	Les grands capteurs CCD sont coûteux, et l'électronique est complexe.	Les grands capteurs CMOS sont également coûteux. l'électronique est plus complexe.	CMOS
Efficacité Quantique	60 % - 95 %, bien que les capteurs à haute QE soient très coûteux.	75 % - 95 %	Le CMOS a un meilleur rapport qualité-prix.
Vitesse en mégapixels par second (MPS)	1 à 40 MPS	100 à 400 MPS	CMOS
Bruit de Lecture	5-10 électrons pour les CCD standards, 1 électron pour les dispositifs de multiplication d'électrons complexes (EMCCD).	1-3 électrons sont courants pour les capteurs CMOS modernes, et cela continue de s'améliorer.	CMOS / EMCCD
Refroidissement	Un refroidissement élevé est relativement facile à obtenir.	Les capteurs génèrent une grande quantité de chaleur et ne peuvent pas être refroidi à des températures trop baisses.	CCD
Taille des Pixels	3 à 25 microns	2 à 9 microns	CCD/CMOS
Well-Depth (Capacité)	40,000 à 200,000	30,000 à 75,000. Compensé par empilement grâce au faible bruit de lecture.	CCD / CMOS
Binning	Facilement réalisé au niveau analogique avec zéro bruit ajouté.	Le binage analogique sur puce est limité; la plupart des capteurs disponibles ne peuvent effectuer que du binage 2×2.	CCD
Imagerie Infrarouge	Les capteurs à peuvent atteindre une efficacité quantique élevée entre 650 et 1000 nm.	Actuellement quasi-impossible avec les capteurs CMOS basés sur le silicium.	CCD
Qualité de l'image	Les techniques pour les CCD sont bien établies et efficaces.	Peut être plus complexe, comme les modes HDR.	CCD

The T2K ND280 MultiPixel Photon Counter

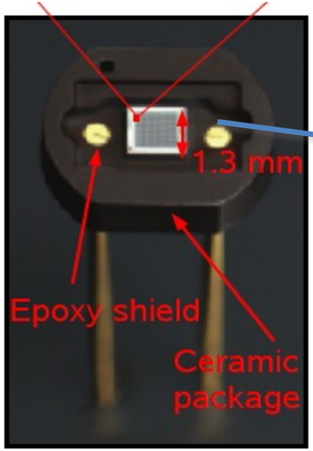

R. Sacco, TIPP2011

Number of pixels	667
Active area	1.3×1.3 mm²
Pixel size	50×50 μm²
Operational voltage	68 – 71 V
Gain	~ 10^6

M. Haigh 2010

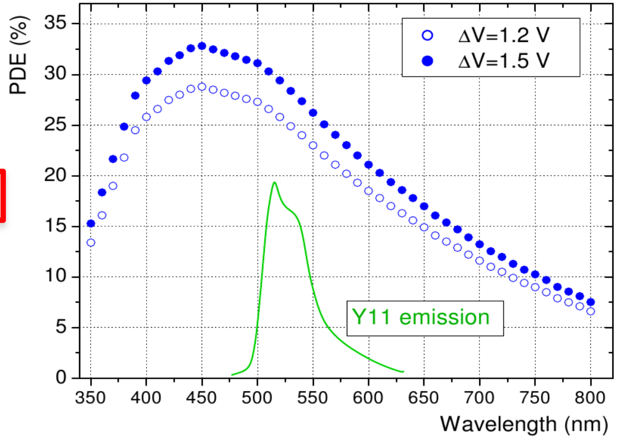

Total number of SiPMs in T2K = 56000
First large experiment to use this type of sensor.

System	Channels	Bad channels	Fraction
ECAL (DSECAL)	22336 (3400)	35 (11)	0.16% (0.32%)
SMRD	4016	7	0.17%
P0D	10400	7	0.07%
FGD	8448	20	0.24 %
INGRID	10796	18	0.17 %
Total	**55996**	**87**	**0.16 %**

Tonyplot – Transient currents

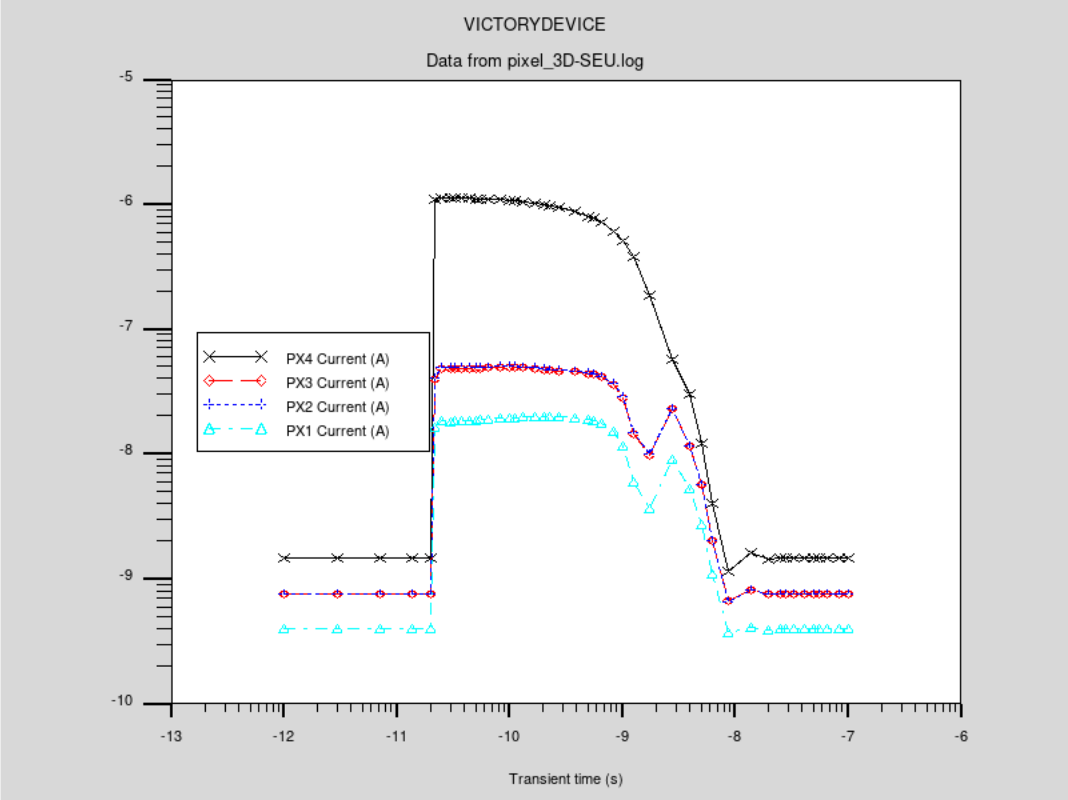

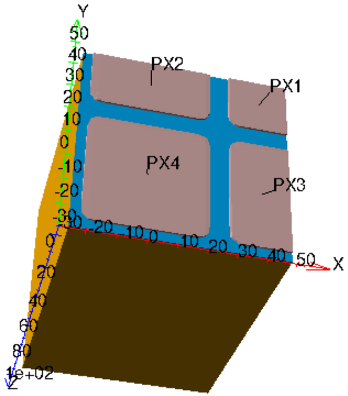

Particle striking in the middle of PX4

Tonyplot – Transient currents

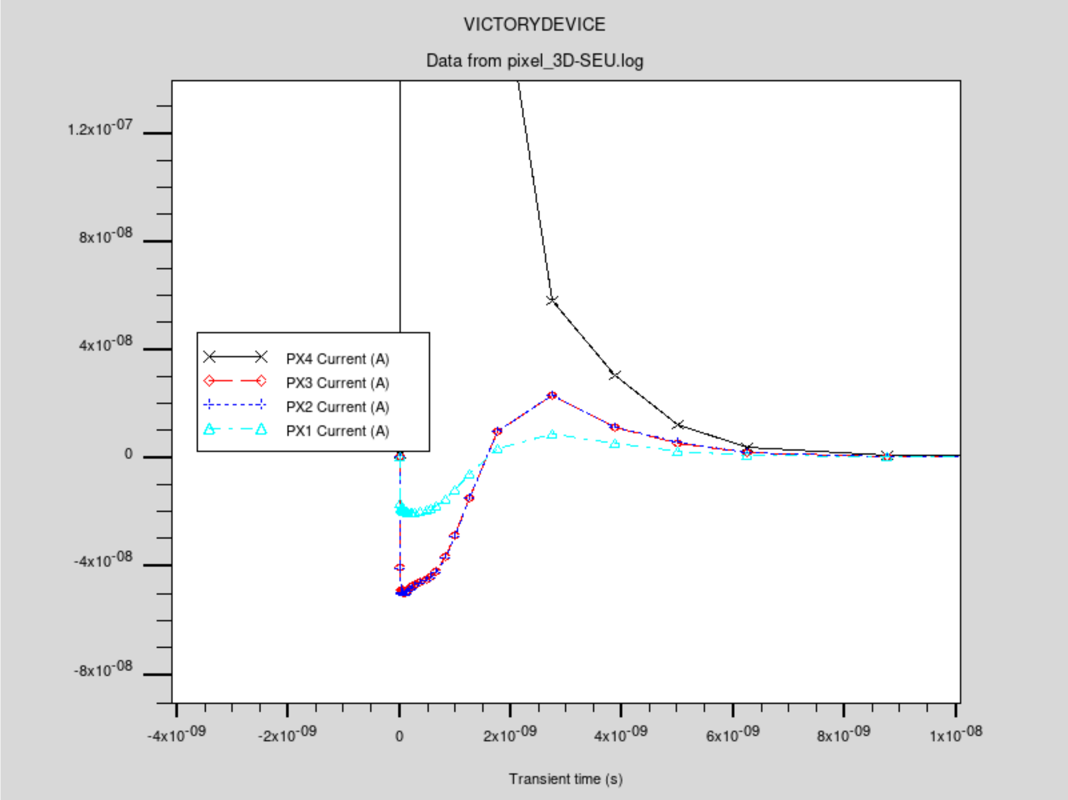

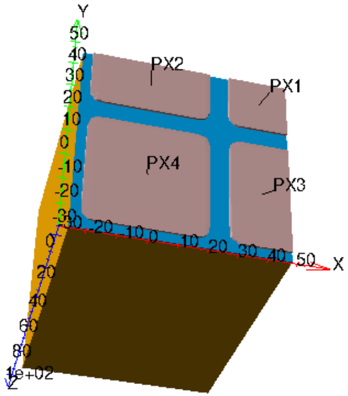

Opposite signal induced on neighbours

Tonyplot – Transient currents

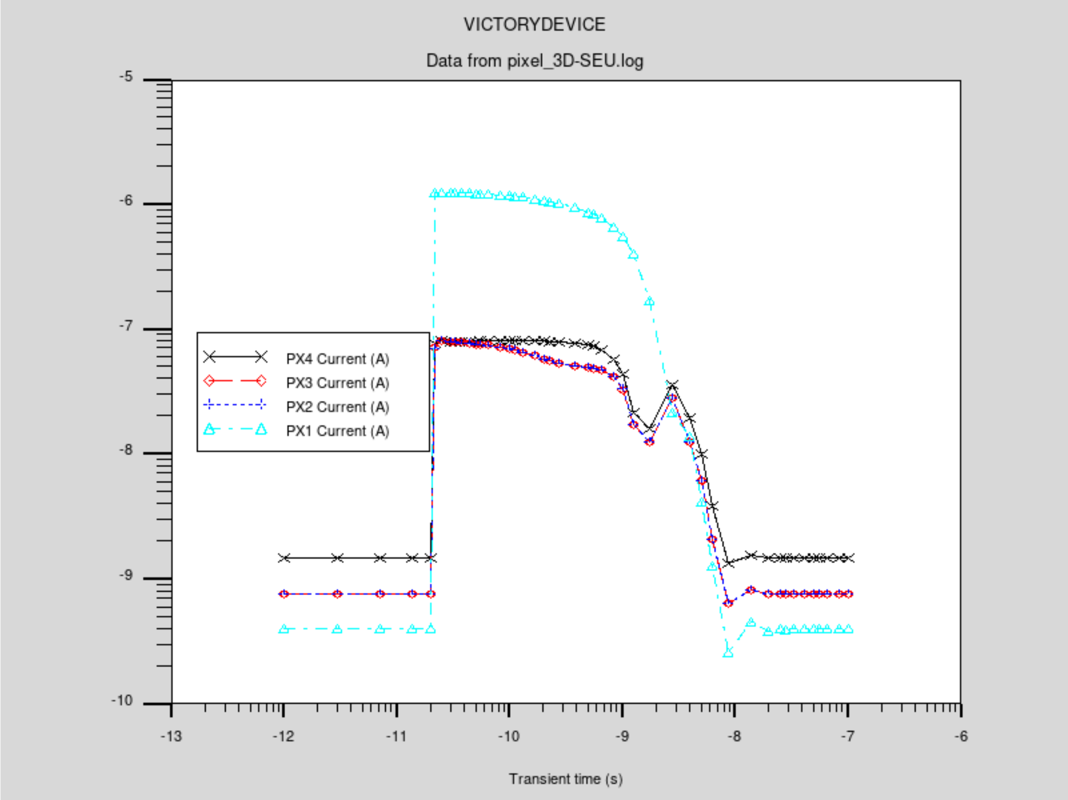

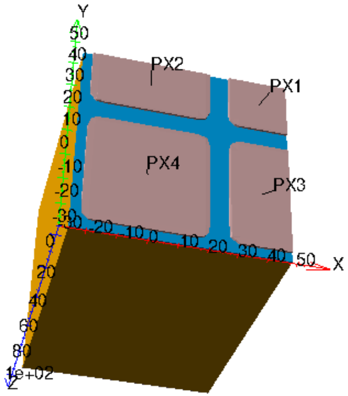

Particle striking in the middle of PX1

Tonyplot – Transient currents

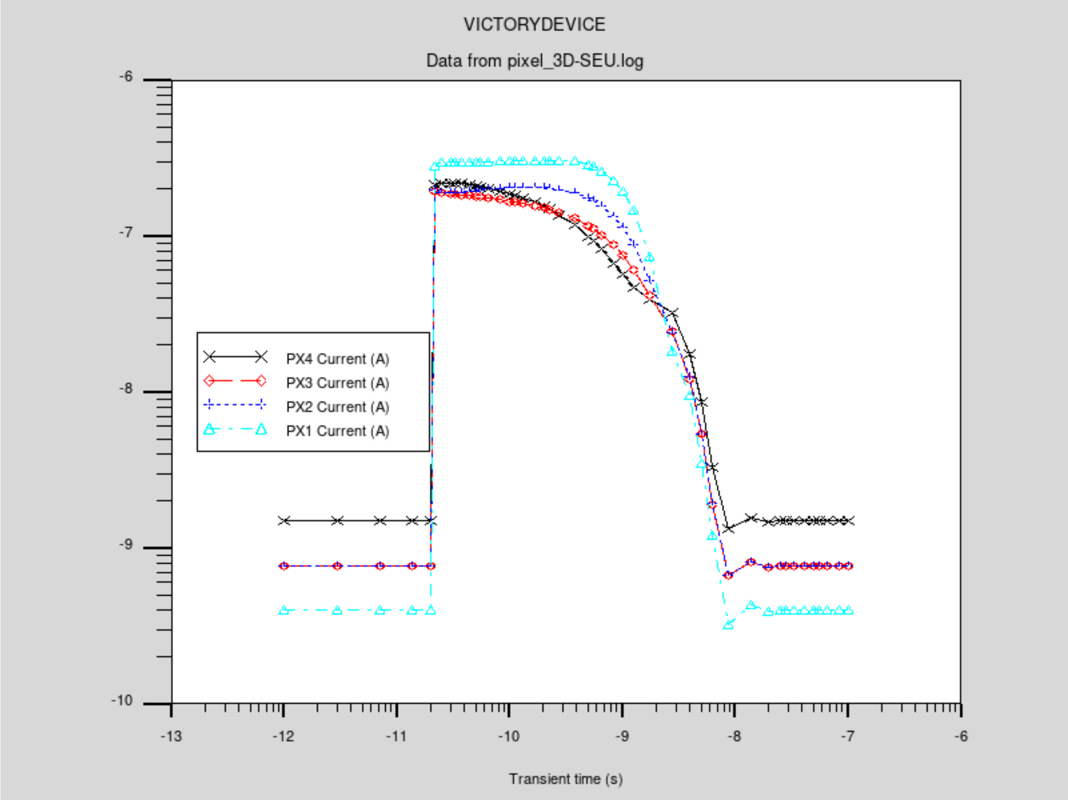

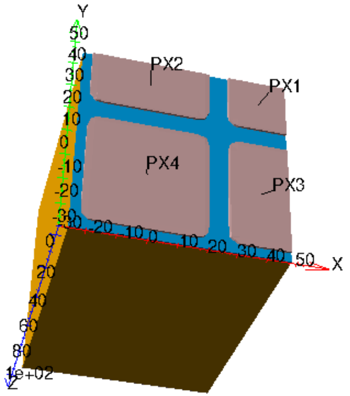

Particle striking in between pixels

Tonyplot – Transient currents

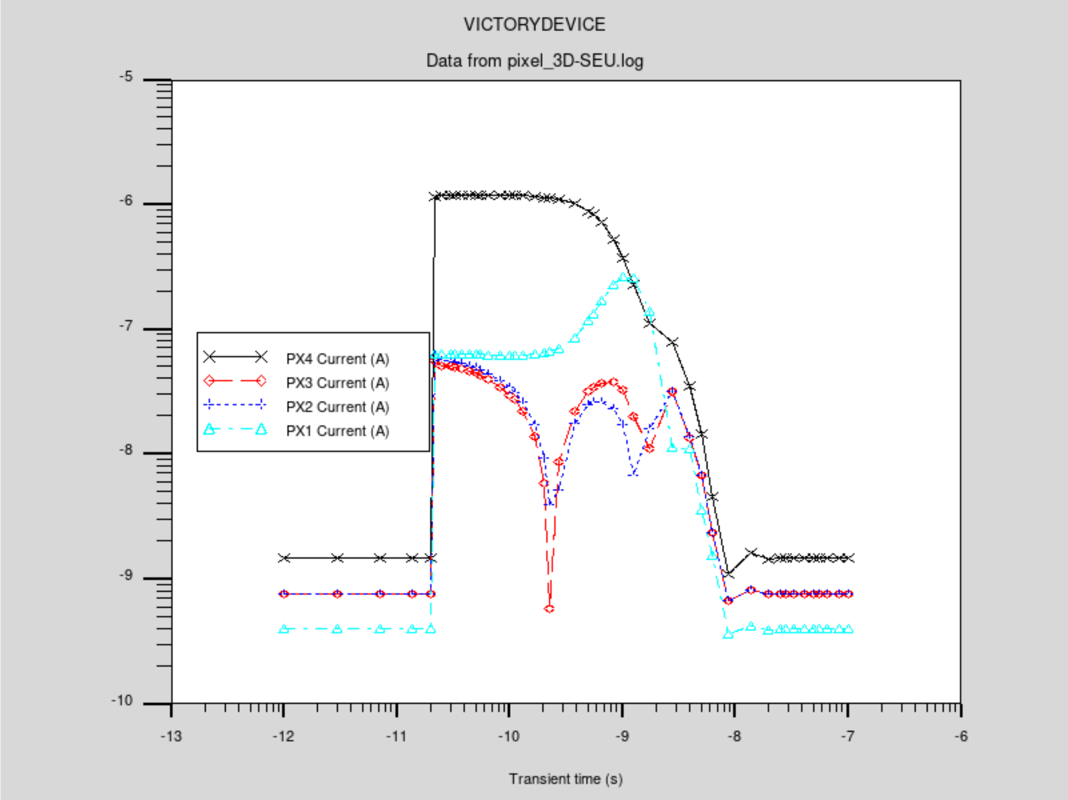

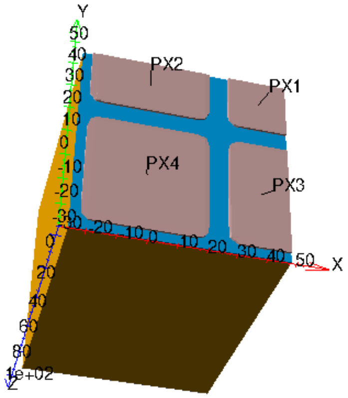

Particle striking diagonally

Tonyplot – Current densities

e- 1.5 ps after particle strike h+

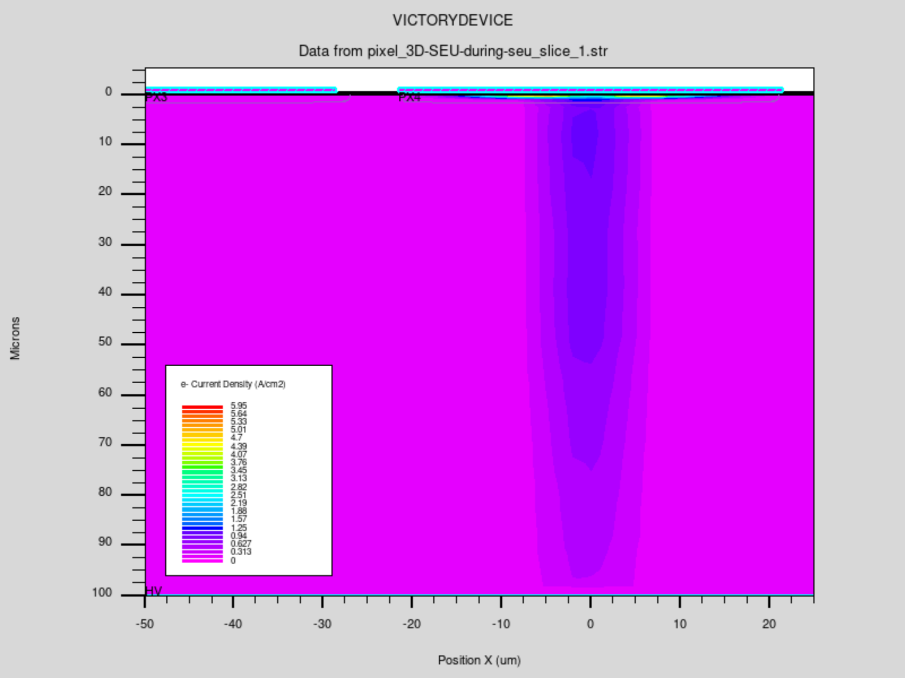

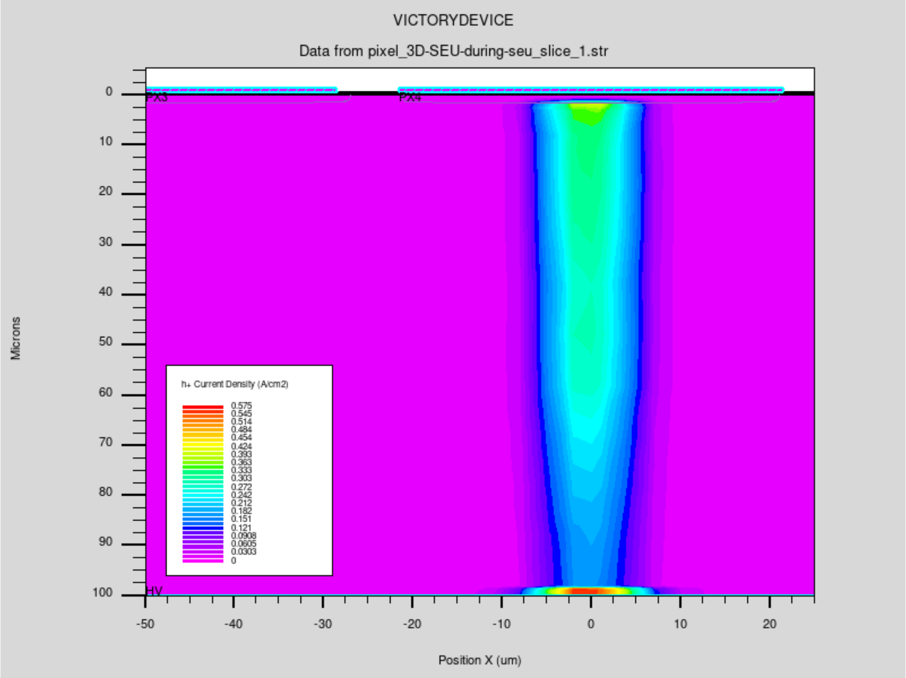

Tonyplot – Current densities

e- 100 ps after particle strike h+

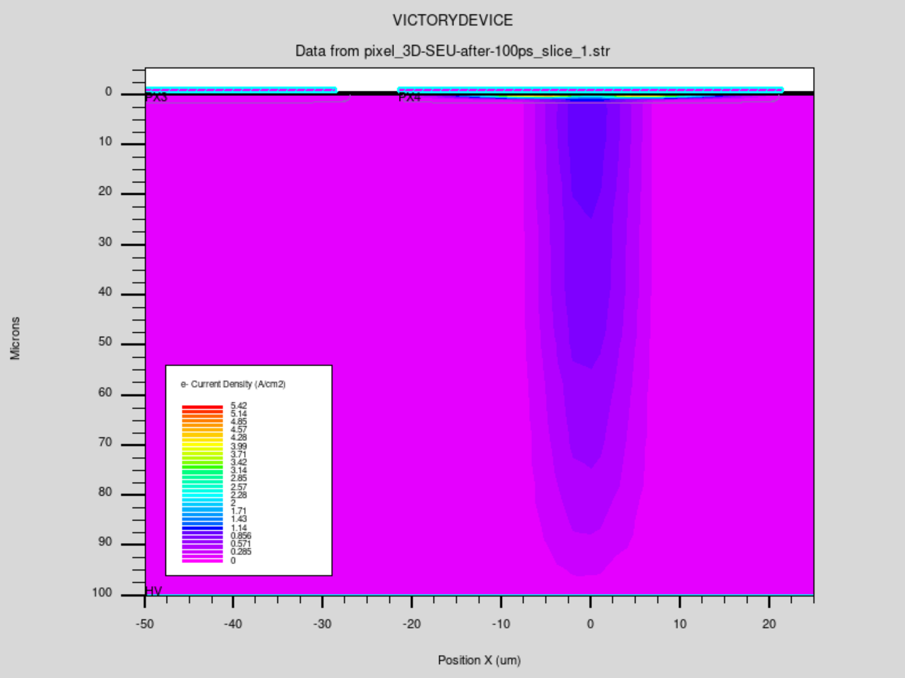

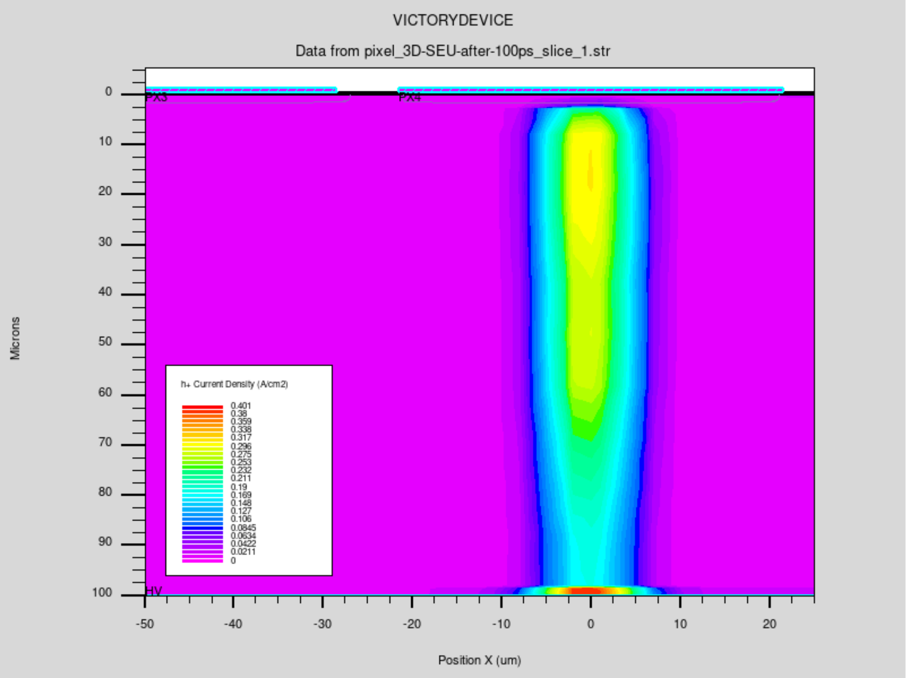

Tonyplot – Current densities

500 ps after particle strike

e-

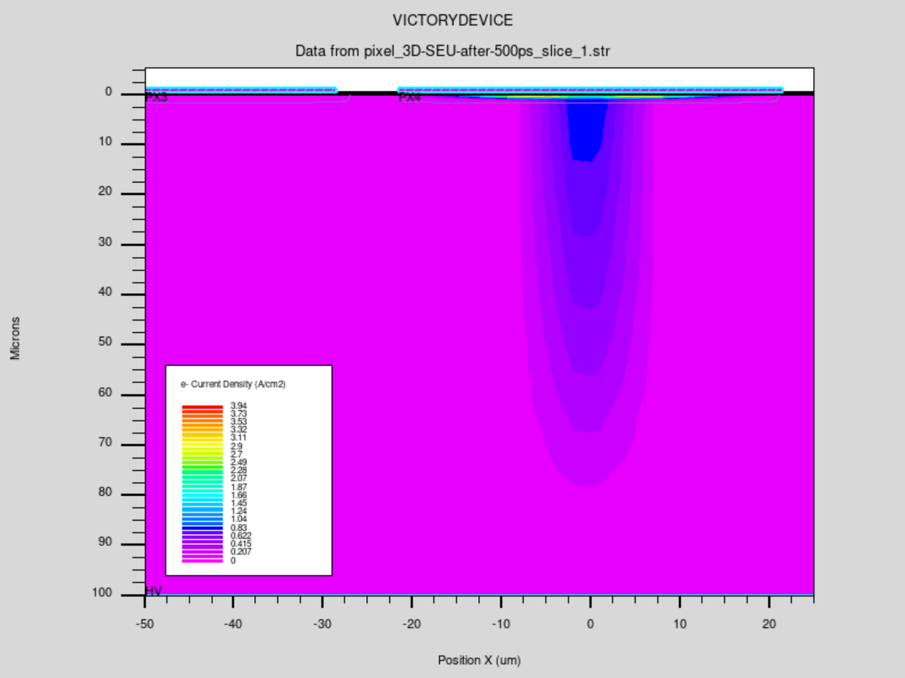

h+

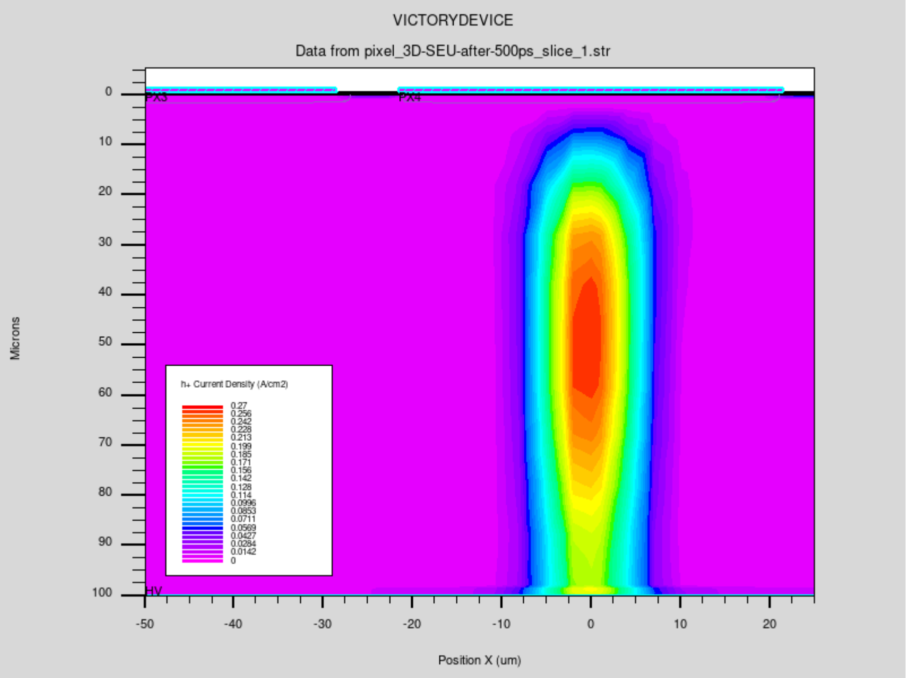

Tonyplot – Current densities

1 ns after particle strike

e-

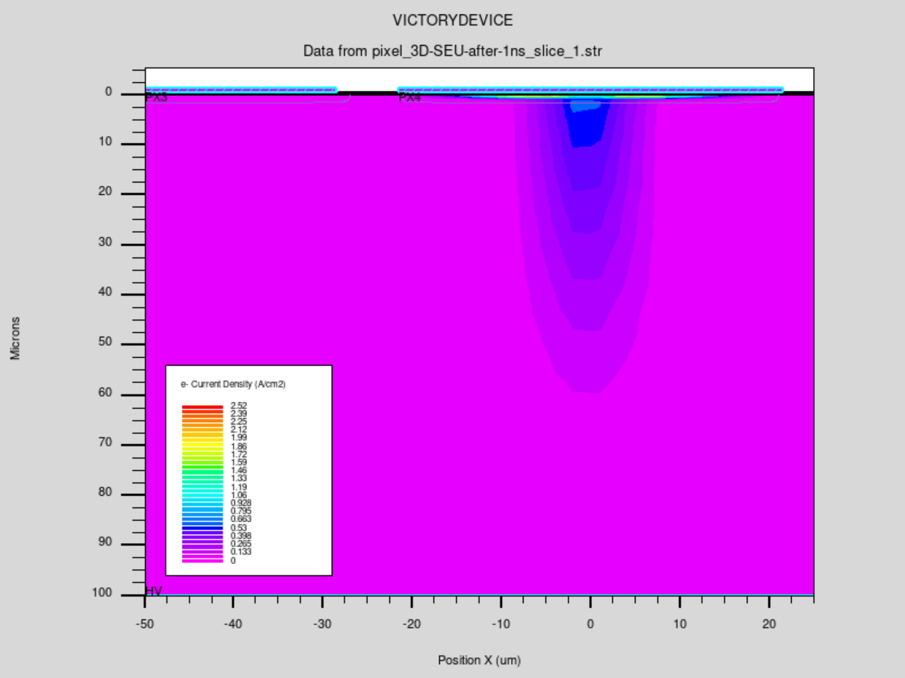

h+

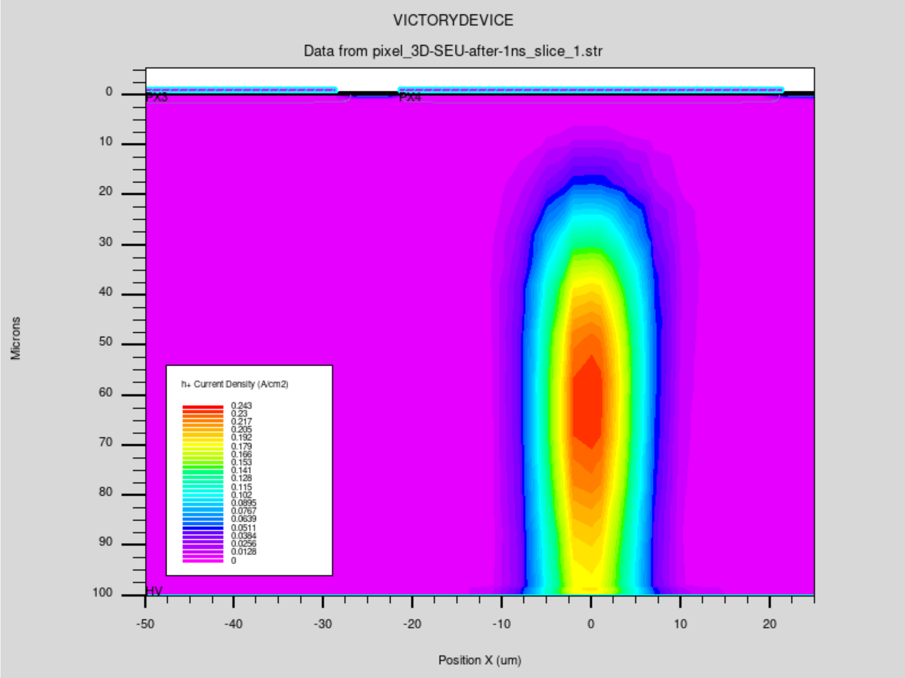

Tonyplot – Current densities

e- 5 ns after particle strike h+

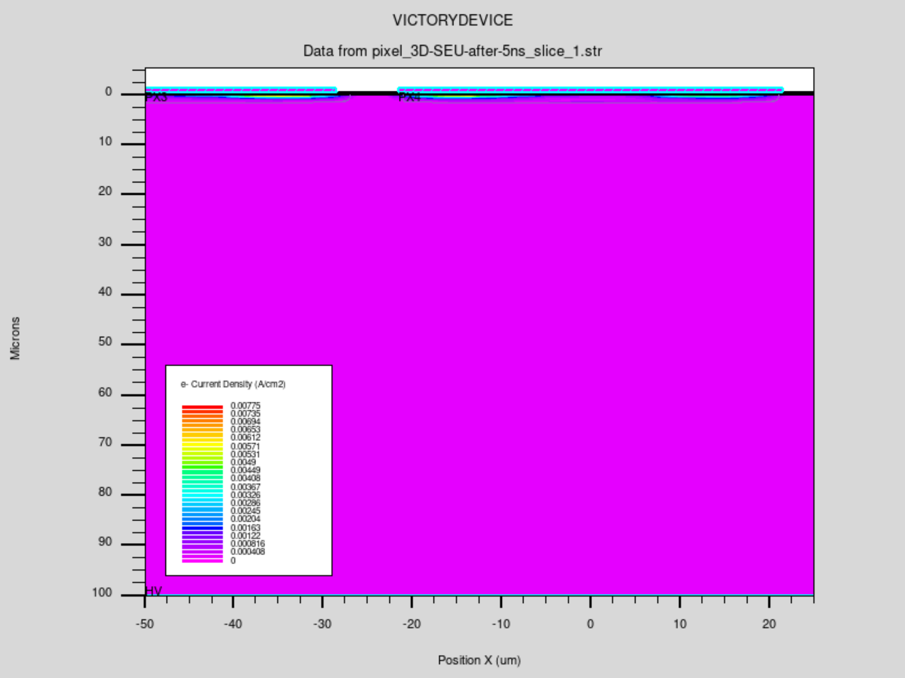

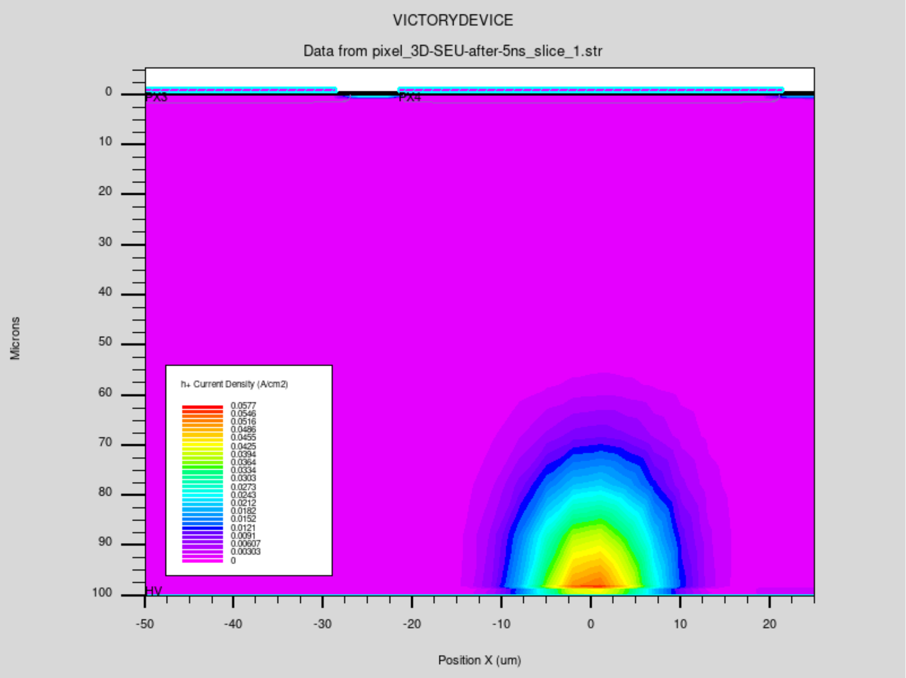

Noise

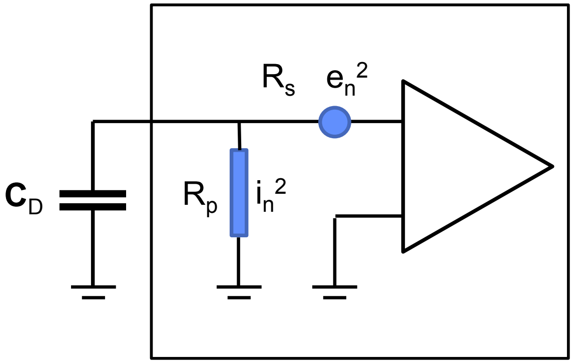

For a sensor that is represented by a capacitance, the noise is determined by the amplifier only. The amplifier noise can be characterized by the parallel and series noise power spectrum.

In case the parallel and series noise power spectra are 'white' we can formulate this as noise resistance R_s and R_p.

The level of this noise is a specification of the amplifier, there is no intrinsic noise in the sensor.

This noise level is very specific to the technology, but in general, lower noise requires more power (current through the input transistor etc.).

This places practical limits on the achievable noise level in systems with high granularity i.e. many channels on a small surface.

W. Riegler, CERN seminar

Optimum filter for best timing

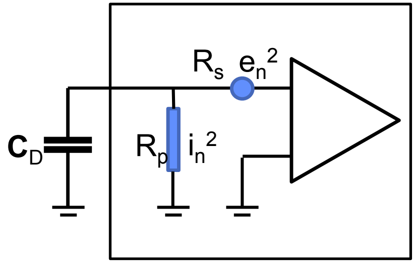

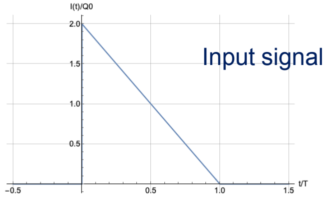

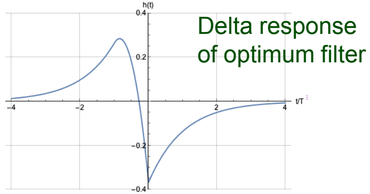

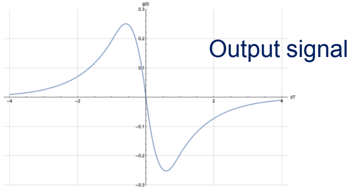

Assuming a silicon sensor with negligible depletion voltage and saturated drift-velocity, the signal shape is a triangle:

$$f(t) = \frac{2Q_0}{T}\left(1-\frac{t}{T}\right) \qquad F(i\omega) = \frac{2Q_0}{\omega^2 T^2}\left(1-e^{-i\omega T}-i\omega T\right)$$

For the noise we assume series noise and parallel noise together with a detector capacitance C_D

$$w(\omega) = \frac{4kT}{R_p} + 4kTR_sC_D^2\omega^2 = a^2 + b^2\omega^2 \qquad e_n^2(\omega) = 4kTR_s \qquad i_n^2(\omega) = \frac{4kT}{R_p}$$

The maximum slope to noise ratio is

$$\left(\frac{k}{\sigma}\right)^2 \le \frac{4Q_0^2}{a^3T^4}\left(2e^{-aT/b}(b+aT) + \frac{a^2T^2}{b} - 2b\right)$$

If we neglect parallel noise we have

$$\left(\frac{k}{\sigma}\right)^2 \le \frac{8Q_0^2}{3b^2T}$$

This filter is a-causal and can only be approximated in practise.

W. Riegler, Detector Signals 21

W. Riegler, CERN seminar

FASTPIX: a monolithic CMOS Sensor with <200ps timing

Sensor Optimization for FASTPIX

- Hexagonal design reduces the number of neighbors and charge sharing → higher efficiency
- Hexagonal design minimizes the edge regions while maintaining area for circuitry → faster charge collection
- Other optimised parameters include opening of p-wells, size of collection electrode, deep n-implant… to optimise charge collection and capacitance

Simulated hexagonal unit cell – electrostatic potential:

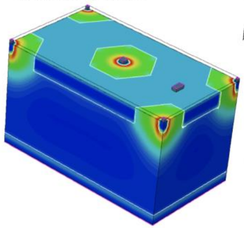

Comparison hexagonal to square pixel cell charge vs. time for particle incident at pixel corner:

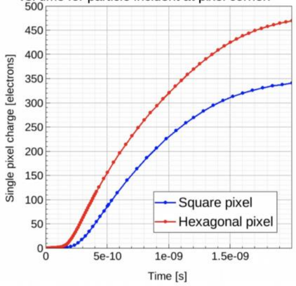

→see M. Munker at iWoRiD 2021 for details on sensor optimisation

- Optimisations important not only for timing, but also for efficiency and radiation tolerance

Test-beam Measurements

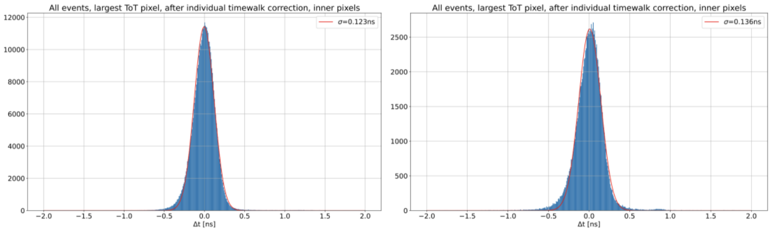

Wafer 18
-6V/-6V pwell/ backside

20x20 µm² matrix (left)
70e threshold

10x10 µm² matrix (right)
50e threshold

- Timing after timewalk correction on 20µm (left) and 10µm (right) matrix
- Pixel-by-pixel correction for best results, reaching below 200ps resolution
- 10µm matrix is operated at lower threshold with a few Hz noise rate
- Larger cluster sizes for 10µm leads to lower average seed charge and thereby more time walk and makes decoding more difficult

< 200ps achieved with a MAPS sensor !

WORKSHOP ON PICO-SECOND TIMING DETECTORS FOR PHYSICS
9–11 Sep 2021
University of Zurich

Eric Buschmann
https://indico.cern.ch/event/861104/contributions/4503032/

W. Riegler, CERN seminar

Silicon modules

- Hexagon-shaped modules tiling the electromagnetic calorimeter and partially the hadronic section
  - Hexagonal sensor shape to maximise area on wafer, partial sensors at borders
- **High Density** (HD) sensors: 0.6 cm^2 cells; **Low Density** (LD) sensors: 1.2 cm^2 cells

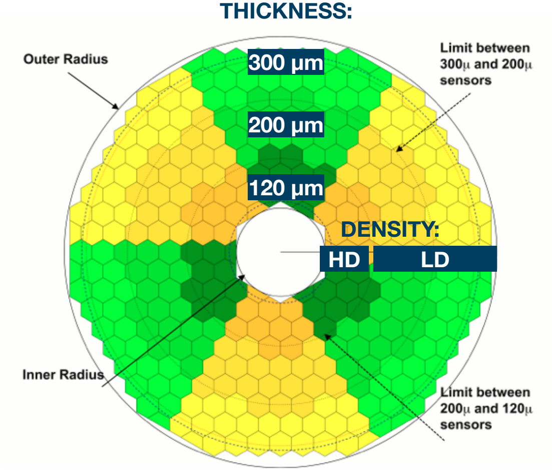

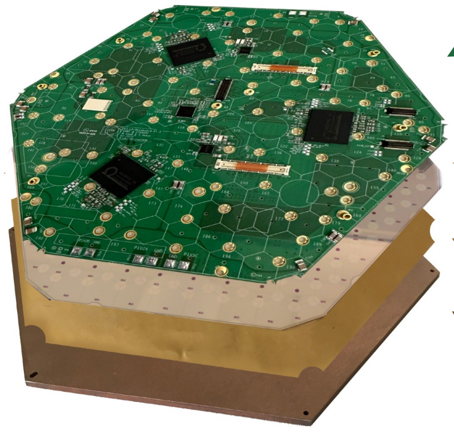

Hexaboard
- Readout of sensor cells with HGCROC custom ASICs and connection to electronics for data transfer
- Bias and low voltage distribution

Silicon sensor
- 8-inch wafers
- Planar, DC-coupled, p-type sensors

Cu-in-kapton isolation
- Grounded for electric noise reduction

CuW baseplate (CE-E) or titanium (CE-H)
- Contributes to absorber material in CE-E
- Gives mechanical stability

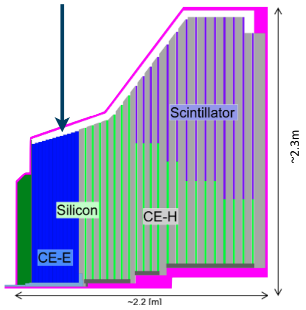

https://indico.cern.ch/event/1596761/

Reconstruction with the Iterative Clustering (TICL) framework

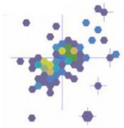

Reconstructed hits

↓

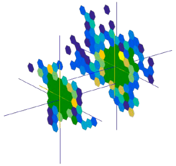

Layer-clusters (2D)

↓

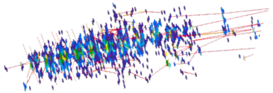

Tracksters (3D)

↓

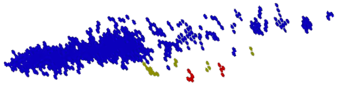

Particles (5D)

CLUE - clustering through **energy density**
- Reduce by 10x the dimensionality and remove noise
- Fast operations (300 events/s) on parallel GPUs

CLUE 3D
- Re-cluster with longitudinal dimension
- Over 200 events/s on parallel GPUs

Particle flow
- Geometrical linking of layer-clusters with timing and energy compatibility
- Build showers/particles and assign properties and probabilities

Several developments ongoing within the framework:
DNN superclustering, energy regressions, tracking tools, ML-based particle ID, …

https://indico.cern.ch/event/1596761/

ATLAS ITk, Q vs fluence - simulations

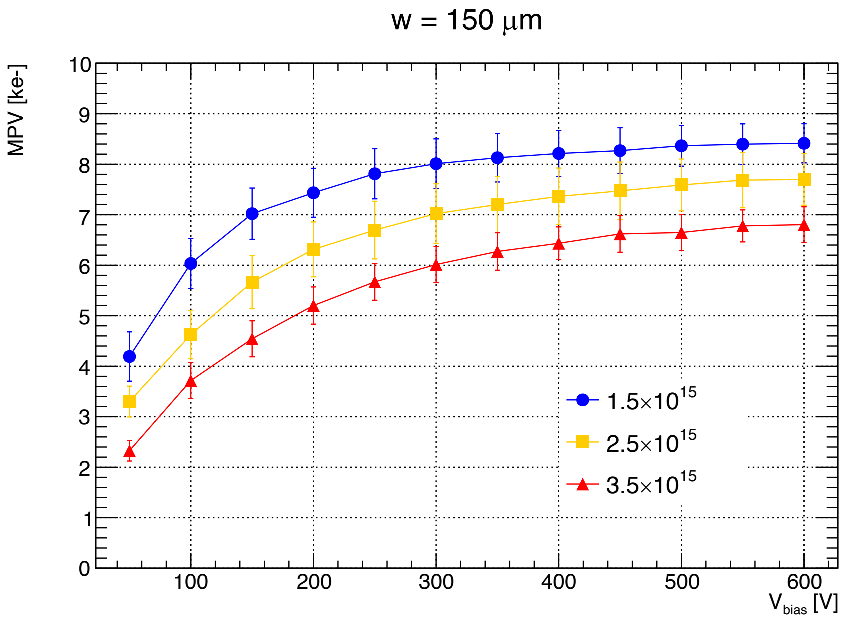

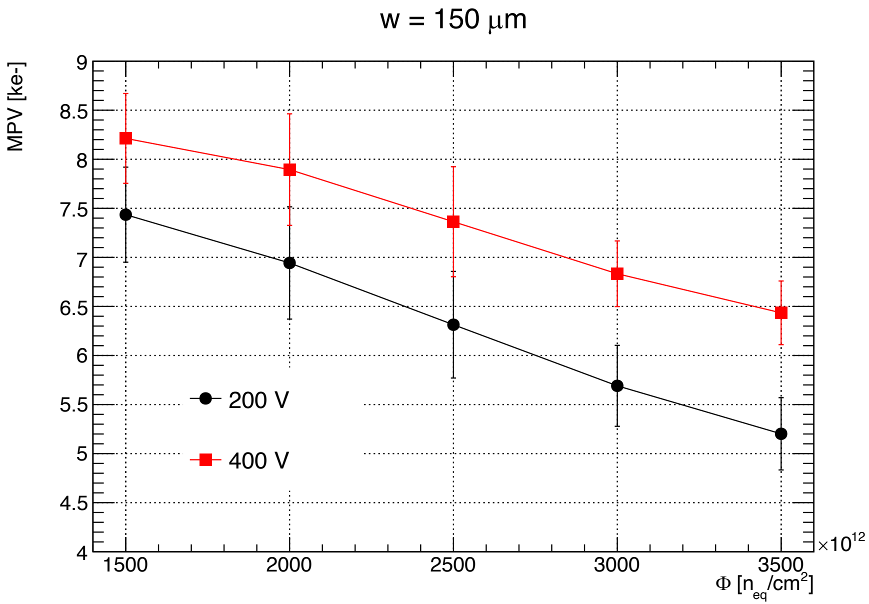

(before irr. Q ~ 10 ke-)

https://doi.org/10.1016/j.nima.2025.171000